

Miocene humid intervals and establishment of drainage networks by 23 Ma in the Central Sahara, Southern Libya

Mark W. Hounslow^{*a}, Helena E. White^b, Nick A. Drake^c, Mustafa J. Salem^d, Ahmed El-Hawat^e, Sue J. McLaren^b, Vassil Karloukovski^a, Stephen R. Noble^f, Osama Hlal^d.

^a Lancaster Environment Centre, Lancaster University, Bailrigg, Lancaster, LA1 4YW, UK (m.hounslow@lancaster.ac.uk)

^b Department of Geography, University of Leicester, University Road, Leicester LE1 7RH, UK (hew12@leicester.ac.uk and sjm11@leicester.ac.uk)

^c Department of Geography, Kings College, London WC2R 2LS, UK (nick.drake@kcl.ac.uk)

^d Department of Geology, Faculty of Science, University of Tripoli, P.O. Box 13040 and 13258, Tripoli, Libya (southlibya@gmail.com and osama.hlal@gmail.com)

^e Earth Sciences Department, University of Garyounis, P.O. Box 1308, Benghazi, Libya (ashawat@hotmail.com)

^f NERC Isotope Geosciences Laboratory, British Geological Survey, Keyworth, Nottingham, NG12 5GG, UK (srn@bgs.ac.uk)

*Corresponding author

Abstract

Terrestrial and lacustrine Neogene and Quaternary sediments in the Libyan Fezzan provide key evidence for paleoclimate changes in the central Sahara, associated with Lake Megafezzan. Understanding of Holocene and late Pleistocene deposits is resolved, but the age of older sediments is not. We provide the first high resolution chronology and stratigraphy of the Neogene deposits in the Fezzan Basin, and so the central Sahara. The sediments are divided into three unconformity-bounded units, the oldest unit, comprising the Shabirinah and Brak formations, is dated using magnetostratigraphy. The Shabirinah Formation is a succession of lacustrine and fluvial units, locally with humid and arid paleosols, which progressively show evidence of increasing aridity up through the succession. The overlying Brak Formation is a pedogenically modified palustrine limestone at basin margin locations. All these units are dated to the early Aquitanian to late Serravallian in the early to mid-Miocene, having formed prior to major volcanic fields to the east. During the mid-late Aquitanian widespread stromatolitic lake sediments developed in SE Fezzan. In the late Burdigalian palustrine carbonate units developed that typically pass laterally into mixed clastic-paleosol-carbonate units that characterise basin margin situations. The Serravallian-aged Brak Formation is a highstand deposit developed during maximum

1 lake extent, which formed due to restriction of basin drainage to the north and east, due to
2 growth of the Jabal as Sawda volcanic centre and uplift of the SW shoulder of the Sirte
3 Basin. Gradual aridification of the central Sahara occurred from the early Miocene, but this
4 trend was periodically interrupted by humid phases during which Lake MegaFazzan
5 developed. The hyperaridity of the central Sahara must have developed after 11 Ma and the
6 main drainage networks from the Fezzan Basin were established before 23 Ma, in the
7 Oligocene indicating the great antiquity of major central Saharan river basins.
8
9

10 11 12 **1. Introduction**

13
14
15 Lake Megafazzan is hypothesised as a giant paleolake that periodically existed in
16 south-west Libya during past Saharan humid phases (Theidig et al., 2000; Drake et al.,
17 2008). This lake has been proposed as important evidence for the greening of the Sahara,
18 allowing early hominins to migrate northwards out of east Africa (Drake et al., 2011a, 2013;
19 Larrasoaña et al., 2013). Our understanding of climate change in the Sahara during the
20 Holocene is reasonably well understood (Lézine et al., 2011; Drake et al., 2011a), and we
21 are beginning to gain an understanding of the Middle to Upper Pleistocene climate change
22 (Pachur and Hoelzmann, 2000; Larrasoaña et al., 2013; Drake et al., 2013). However, for
23 earlier age intervals knowledge is limited and often controversial, particularly the onset of the
24 Sahara Desert, where late Miocene dune systems are thought to be preserved in northern
25 Chad (Schuster et al., 2006), in contrast to the supposed wetter and warmer late Miocene
26 climate based on fossil evidence (Wanas et al., 2009; Stoetzel, 2013). Addressing this issue,
27 climate models have been proposed for the late Miocene, often with conflicting results
28 (Bradshaw et al., 2012; Zhang et al., 2014), but crucially with little solid data to validate them
29 against well-dated sedimentary successions in the central Sahara.
30

31
32
33 Based on interfluvial height assessments from digital elevation models, Lake
34 Megafazzan had a maximum potential size of ca. 135,000 km² (Drake et al., 2008); but its
35 area likely depended on the intensity of humid phases, and the nature of its connection to
36 drainage channels east and north-eastwards into the Sirte Basin. The paleolake deposits
37 since ca. 400 ka have been well studied and dated (Petit-Maire et al., 1980; Thiedig and
38 Geyh 2004; Armitage et al., 2007; Geyh and Thiedig 2008). In addition, channel networks
39 draining southern Libya and its surroundings, have been proposed for various time intervals
40 since the late Miocene (Drake et al., 2008; 2011a; Paillou et al., 2009). Those thought to be
41 the most important drainage systems from the Fezzan Basin (Drake et al., 2008; 2011a), are
42 directed through NE and eastern routes along Wadi Nashu and Wadi Barjuj (Fig.1),
43 ultimately outflowing into the Gulf of Sirte.
44

45
46
47 However, detailed data about the lacustrine and fluvial sediments for the age interval
48 prior to the Upper Pleistocene has not been described. This is in part due to a lack of a
49
50
51
52
53
54
55
56
57
58
59
60
61
62
63
64
65

1 detailed chronology and understanding of regional relationships for these older units; even
2 though widespread limestone and clastic units have been mapped (e.g. Koráb, 1984;
3 Parizek et al., 1984; Seidl and Röhlich 1984; Fig. 1). During fieldwork in the Fezzan between
4 2005 and 2011 we recognised extensive sedimentary sequences exposed beneath deposits
5 dated to the Middle Pleistocene by Geyh and Thiedig (2008), that could potentially help fill
6 this gap (Fig. 1). We here outline a new regional lithostratigraphic framework for these
7 deposits.
8
9

10 In North Africa the chronology of late Cenozoic terrestrial successions is largely based
11 on vertebrate fossils, which are rather rare and appear to be largely restricted to localities off
12 the Sahara platform (Stoetzel, 2013), with scant occurrences from the central Sahara (Boaz
13 et al., 2008). Our new lithostratigraphic framework is securely tied to a detailed chronology,
14 using magnetostratigraphy, which so far in studies of the late Cenozoic of the central
15 Sahara, has yielded only ambiguous evidence of age (Beyer, 2008); although
16 magnetostratigraphic dating of Moroccan Miocene successions has resolved high-resolution
17 ages in parallel with biochronology (Benammi & Jaeger, 2001).
18
19

20 With the new detailed chronology we evaluate the regional stratigraphic relationships
21 of these Lake Megafezzan sediments, re-assess the relationships between the sediment
22 successions and the volcanic centres to the north and east, that have been inferred to
23 restrict basin drainage. We assess the implications of this chronology on the north-Saharan
24 paleoclimate and proposed paleohydrology before the beginning of the hyperarid Sahara.
25
26
27
28
29
30
31
32
33

34 **2. Geological setting and stratigraphic framework**

35 The Fezzan Basin is a broad post-Paleogene depression bounded by uplifted
36 shoulders of the Sirte Basin to the east and the Al Hamadah al Hamra escarpment to the
37 north (Fig. 1), along with older uplifted Paleozoic successions to the northeast (Qarqaf), SE
38 (Dur al Qussah) and SW (Jabal Akakus). Neogene and younger sediments are scattered
39 across the Fezzan, broadly on the fringes of the Awbari and Murzuq Sand seas, since these
40 sediments also underlie the modern dune systems (Fig. 1).
41
42
43
44
45
46

47 Sediments of Lake Megafezzan have been called the Al Mahruqah 'formation' by
48 Theidig et al. (2000) and Geyh and Thiedig (2008). However, a new lithostratigraphy of
49 these units is needed for the following four reasons. First, we have examined a wide variety
50 of units over a large part of the Fezzan Basin, and none of the existing member designations
51 for units of the Al Mahruqah 'formation' (Thiedig et al., 2000; Geyh and Thiedig, 2008) can
52 be adequately applied to our sections. Secondly, in the mapping of the Fezzan Basin, the
53 naming and usage of this unit is inconsistent. The same units have been given different
54 names in different geological maps, ranging from the Al Mahruqah 'formation' in the Al
55 Fuqaha, Al Haruj al Abyad and Sabha maps (Korab, 1984; Seidl and Röhlich, 1984; Woller,
56
57
58
59
60
61
62
63
64
65

1984) to 'continental deposits' in the Awbari and Hamādat Tanghirt maps (Roncovic, 1984; Berendeyv, 1985; Gundobin, 1985; Grubic et al., 1991), to both these units on the Tmassah and Idri geological maps (Koráb, 1984; Parizek et al., 1984). Thirdly, originally Seidl and Röhlich (1984), and later Domaci et al. (1991) and El Ebaidi and Abdulsamad, (2005) applied the Al Mahruqah 'formation' to the carbonate unit (termed the Brak Formation here) exposed on the north side of Wadi ash Shati, when in fact the major thickness of these post-Oligocene sediments in Wadi ash Shati are clastic deposits, with minor carbonates. Finally, Thiedig et al. (2000) expanded the Al Mahruqah 'formation' to include all the 'Pleistocene' to Holocene carbonate units, whereas our work shows some of these units are much older than Pleistocene, and range into the Miocene, as inferred by earlier mapping (Collomb, 1962; Goudarzi, 1970). The new lithostratigraphic framework fits existing and new data into a more detailed stratigraphic sub-division, and allows our new descriptions, and age assignments to be tied into the findings of prior research.

This new framework upgrades the Al Mahruqah formation to group status, the Al Mahruqah Group, that includes all the clastic units, not just the carbonates (Figs. 2, 3). The Al Mahruqah Group includes two major unconformities bounding different sediment packages, thus the expansion to Group status allows a more detailed lithostratigraphic designation of these units. Lithostratigraphic boundaries imply no age information, just the stratigraphic order of the successions in the Fezzan Basin, based on evidence described. This lithostratigraphy applies to all previously mapped Neogene and Quaternary deposits, from those found on the fringes of the Awbari Sand Sea and east towards the western edges of the Paleocene and Eocene outcrops in the SW fringes of the Sirte Basin in Sarir al Qattusah, and south towards Tmassah turning east along Wadi ash Shabirinah (Fig. 1). Neogene and younger deposits exist on the fringes of the Murzuq Sand Sea, but these have not been investigated by us.

Three new formations are proposed; the Shabirinah Formation, the Zarzur Formation and the Shati Formation (Figs. 2, 3). This is in addition to the Brak Formation, which is upgraded from the Brak member, used previously by Thiedig et al. (2000) and Geyh and Thiedig (2008). The units of the Al Mahruqah Group all unconformably overly various older strata ranging in age from the Cretaceous to the Cambrian. The lithostratigraphy is illustrated with detailed section logs, coded into three regions (Fig. 1): SK for the Wadi ash Shati to Wadi Kunayr region (Fig. 4); NU for the northern Awbari Sand Sea area (Fig. 3 and Supplementary Data Fig. S3) and TS for the Tmassah- Wadi ash Shabirinah region (Figs. 3, 5). A brief description of these new formations is provided below, whilst a formal lithostratigraphic description of the formations and their members is detailed in the Supplementary Data. Our on-going chronology work on the younger Zarzur Formation will be published elsewhere.

2.1. Lithostratigraphy of the Al Mahruqah Group

2.1.1. Shabirinah Formation

The Shabirinah Formation underlies the Brak Formation, and its lower parts are dominated by the Tmassah Member of clear fluvial-origin with down-cutting channels, which show paleocurrents and channel systems directed to the ESE to SE (Fig. 6). These channels cut into the red mudstones forming the upper part of the Stromatolite Member (sections TS2 and TS3, Fig. 6 and Supplementary Data). The Tmassah Member is overlain by the Kunayr Member which typically shows (but not always) an upwards increase in calcretisation often within a predominantly clastic succession. This bipartite-facies association (i.e. fluvial siliciclastics, below calcretised clastics) can be recognised throughout the Fezzan, even at basin margin locations, where the lower fluvial dominated part of the Shabirinah Formation may be channel conglomerates. At some locations lateral to the channels rootleted aeolian facies probably occur, but still retaining the overlying carbonate-rich Kunayr Member (section TS6, Fig. 6). In the north side of Wadi ash Shabirinah lacustrine limestones (in sections TS2, TS3) in the base of the Kunayr Member pass laterally eastwards (at sections TS4, TS5, TS6) into nodular calcretes and calcretised palustrine limestones, indicating the basin centre of the Kunayr Member was to the west or SW of section TS2 and TS3. The oldest two members of the Shabirinah Formation occur along the northern fringe of Wadi ash Shabirinah, along Wadi Maharshim and in the 'Qattusah corridor' to the north (Figs. 1, 3, 5).

Near Tmassah, Thiedig et al. (2000) has also illustrated stromatolitic beds which probably belong to our Stromatolite Member (but they assigned them to their Bir az Zallaf Member- i.e their plates 1e,1f, 3h,5c). This distinctive bed can be traced westwards along the north side of Wadi ash Shabirinah towards Tmassah. It can be found again in the outcrops north and NW of Tmassah (Fig. 5). This same distinctive bed has been seen by us some 118 km north of Tmassah at 27°26'2.8"N; 15°34'15.6"E. The overlying Kunayr Member was also seen 4 km to the west at 27°25'7.2"N; 15°32'4.2"E. The Stromatolite Member in Wadi ash Shabirinah appears to pass eastwards into clastic-rich units of the Tmassah Member (Fig. 6), making it distinctly different from palustrine carbonates in the Kunayr Member, which pass eastwards into palustrine limestones, more pedogenically- modified.

Where we have seen the base of the Shabirinah Formation, it rests on Mesozoic or Paleozoic formations, and to our knowledge has no other intervening clastic or carbonate units (Figs. 3, 6). The NE rim of the basin in which the Shabirinah Formation developed was Cretaceous to Eocene sediments of the Sarir al Qattusah and Dur al Msid (Figs. 1, 5), uplifted in the late Oligocene when clastic supply to the western Sirte basin increased (Abouessa et al., 2012) and gentle folding developed in the Zallah Trough (Abdunaser and McCaffrey, 2015; Fig. 1).

2.1.2. Brak Formation

The Brak Formation consists of various Fe-poor dolomitic and micritic limestones. The sediments are highly indurated, showing multiple cementation phases and are typically extensively mottled and brecciated. Abdullah (2010) previously classed the Brak Formation sediments in Wadi ash Shati as groundwater calcretes, however the limestones do not have chalky, nodular or laminated textures of other calcretes (Alonso-Zarza, 2003). A groundwater calcrete origin also seems less-likely, in that the boundaries of the limestone are diffuse, and the formation is also very thick compared to most other groundwater calcretes (cf. Alonso-Zarza, 2003). The Brak Formation instead shares most characteristics with modified palustrine limestones (Wright and Platt, 1995; Freydet and Verrechia, 2002) and thus likely indicates the formation is a basin-margin palustrine limestone, with the main Brak basin centre somewhere to the southwest of the Qattusah corridor and south of Brak (Fig. 1, 3).

In Wadi ash Shati the Brak Formation oversteps and on-laps the basement to the north, showing that it represents an expression of the maximum fill of the 'Brak-basin', with the Brak Formation representing the high-stand unit of its underlying successions.

Seidl and Röhlich (1984) and Domaci et al. (1991), report ostracods, gastropod and bivalves from this unit, but the more extensive studies of Abdullah (2010) from the Brak area do not record such findings, concurring with our observations. It may be these earlier studies confused Brak Formation carbonates with the Bir az Zallaf carbonate units (which can be locally calcretised), or it could be they identified more basinal correlatives of the Brak Formation, which might be expected more centrally in the Fezzan.

The Brak Formation in its type area in Wadi ash Shati occupies heights which range from 390 m (at SK-3 section, Figs. 4, 7) to ca. 438 m on the southern flanks of the Qarqaf uplift, on the northern fringes of Wadi ash Shati (Figs. 1, 7). ENE of Ashkidah the base of the Brak Formation rises to ca. 435 m, with the top of the Brak Formation to the NE of this area, around 457 m, at Geyh and Theidig (2008) Brak 'member' site 8 (Fig. 7). These E-W differences in elevation reflect some tilting (or faulting) after deposition of the Brak Formation. In most of the outcrops in Wadi ash Shati the Brak Formation rests directly on a heavily calcretised basement breccia between two and 5 m thick, sometimes having the appearance of cemented scree (Abdullah, 2010). In one southerly outcrop (section SK-3) in Wadi ash Shati the lower parts of the formation overlies and grades into siliciclastics and red mudstones that we assign to the underlying Shabirinah Formation (Fig. 7).

Basalt fragments (from the Jabal as Sawda volcanics?) have been reported from the basal breccias in the Brak Formation in Wadi ash Shati (Goudarzi, 1970). This indicates the Brak Formation there is younger, or its early parts are coeval, with the Jabal as Sawda volcanic field to the NE. Similarly, north of Wadi Kunayr, map evidence (Woller, 1984) shows

basalts of the Jabal as Sawda volcanic centre interbedded in the boundary interval between the Shabirinah Formation and the overlying Brak Formation (Fig. 8). On the north side of Wadi Kunayr the underlying Shabirinah Formation fills a paleo-wadi, since the Paleozoic and Mesozoic basement rises to the north and south (Fig. 8).

We have not documented the transition between the Brak Formation and the top of the underlying Shabirinah Formation in the Wadi Kunayr area (Fig. 4), but infer that the Brak Formation terminates the upwards increase in calcretisation we see through the underlying Shabirinah Formation, so the transition is inferred to be conformable to the north of Wadi Kunayr (Fig. 7). In the outcrops east of Tmassah (Figs. 1, 5, 6) the contact between the Brak and Shabirinah formation appears to be conformable or there is a south-westwards (i.e. towards basin centre) lateral transitional from heavily calcretised palustrine limestones and clastics at basin margins to more clastic-rich units in the upper parts of the Shabirinah Formation. In the south of the Sarir al Qattusah (Fig. 1), the thickest carbonates (the Brak Formation) appear to be restricted to the NE margin of the outcrops (Fig. 5). In the area north of Tmassah, El Ebaidi and Abdulsamad (2005) and Domaci et al. (1991) also record the possible(?) conformable transition between the Brak Formation (their Al Mahruqah) and the underlying clastic continental deposits (our Shabirinah Formation).

2.1.3. Zarzur Formation

The Zarzur Formation largely consists of green to tan-coloured siliciclastic units, of coarse-silt to coarse-sand, often heavily rootleted (and poorly consolidated), but occasionally containing cross-bedded intervals. This formation includes the unit attributed to the Bir az Zallaf Member of Geyh and Thiedig (2008). From their lithostratigraphic description, it is clear their Bir az Zallaf unit largely relates to the two to three limestone beds of the Bir az Zallaf Member at the top of our Zarzur Formation, and not the ca. 60 m of underlying clastics found at Bir az Zallaf (Fig. 9 and Supplementary Data). The inverted stratigraphic elevation in Wadi ash Shati, and unconformable relationships with the overlying Shati Formation clearly shows the Zarzur Formation is much older than the Shati Formation (Figs. 3, 4, 9). This is also borne-out by saturated and near saturated OSL dates (> 420 ka) from the top of the Zarzur Formation (Armitage et al., 2007).

The base of the Zarzur Formation is marked by a major erosional unconformity, which in Wadi ash Shati cuts down into the underlying Paleozoic (Fig. 9). Similar relationships are seen in the Qarārat al Marār area in the northern Awbari Sand Sea (Figs. 1, 3 and supplementary Figs. S3, S4). This lower elevation of the earliest Zarzur Formation with respect to the Brak Formation (Fig. 9), signifies a major interval of erosion of the Brak Formation and older units, prior to Zarzur Formation deposition. However, we have not seen any location where the Zarzur Formation rests on the Brak Formation. Only in the northern

1 Awbari Sand Sea area, do we see the Zarzur Formation resting on what we interpret as the
 2 Shabirinah Formation (section NU2-b, Supplementary Data Fig. S4). However, like Geyh
 3 and Thiedig (2008), we consider the Brak Formation to be an older unit of the Al Mahruqah
 4 Group, because of the inverted stratigraphy clearly seen in Wadi ash Shati (Fig. 9). In Wadi
 5 ash Shati the youngest units of the Zarzur Formation range up to ca. 379 m elevation. In the
 6 Qarārat al Marār area (Fig. 1) the youngest units of the Zarzur Formation range up to an
 7 elevation of 400 m, and in Wadi Tanarat up to 577m (Supplementary Data Figs. S3, S4).
 8 Hence, elevations as used by Geyh and Thiedig (2008) to infer relative age, is an erroneous
 9 assumption. Equivalents of the Zarzur Formation occur on the northern fringes of the Murzuq
 10 Sand Sea, but we have not investigated these in detail, however our reconnaissance
 11 observations share similarities with those of Geyh and Thiedig (2008).
 12

13 The Zarzur Formation locally contains an impoverished, often poorly preserved fauna
 14 of ostracods, gastropods and rare bivalves and charophytes (Domaci et al., 1991; Abdullah,
 15 2010). Basin-margin representatives of the Zarzur Formation are known from the Qarārat al
 16 Marār area, where the clastic units are replaced by fluvial conglomerates (section NU2-
 17 c, NU2-b, Supplementary Data Figs. S3, S4) and the carbonate units can be laterally
 18 substituted by several metres of calcretised limestone resting on basement (section NU3-e;
 19 Supplementary Data Fig. S4).
 20

21 **2.1.4. Shati Formation**

22 The Shati Formation consists of a wide variety of lacustrine sediments deposited since the
 23 Upper Pleistocene. This includes the coquinas of the Aqar Member with ages around 100-
 24 125 ka (Petit-Maire et al., 1980; Armitage et al., 2007; Geyh and Thiedig 2008). Various
 25 fossiliferous late Pleistocene to middle Holocene poorly cemented silts and muds, have also
 26 been widely investigated (White et al., 2000; Armitage et al., 2007; Drake et al., 2008;
 27 Cremaschi and Zerboni 2009), which are here assigned to the Bir al Hasy Member (Figs. 2,
 28 3). These units give OSL and radiocarbon, dates from 12-3 ka. The base of the Shati
 29 Formation is marked by a major erosional unconformity everywhere in the Fezzan. In Wadi
 30 ash Shati this unconformity cuts down into the underlying Zarzur Formation and other older
 31 units of the Al Mahruqah Formation, so the top of the Shati Formation occupies similar
 32 elevations to the lower parts of the Zarzur Formation (Fig. 9). Similar relationships are seen
 33 in the Qarārat al Marār area (Fig. 1) in the Northern Awbari Sand Sea and in Wadi al Ajal
 34 (west-northwest of the Murzuq Sand Sea).
 35
 36
 37
 38
 39
 40
 41
 42
 43
 44
 45
 46
 47
 48
 49
 50
 51
 52
 53
 54
 55

56 **3. Sampling for chronology**

57 Three sections were sampled in 2009 for magnetostratigraphy to investigate the age of
 58 the Brak and Shabirinah formations (Table 1 and Fig. 10). Section SK8 is exposed along a
 59
 60
 61
 62
 63
 64
 65

1 trackway into Wadi Kunayr, through south and SW facing bluffs below the Areal Agricultural
2 Station on the plateau top (Figs. 4, 7). The SK8 section represents the Kunayr Member and
3 the underlying parts of the Shabirinah Formation. The lower few metres of this succession
4 are composed of reddish mudstones and sandstone, overlain by black to maroon silty
5 paleosols, capping fining-up channel sandstones (Fig. 10). The channels of the sandstone
6 units are well exposed 3.7 km to east of section SK8 (at 27°39',50.3"N;15°10',18.2"E),
7 where they are oriented towards 135°, with shallow channels up to ca. 200 m wide. The
8 Kunayr Member consists of mottled and rootleted sandstones, locally with nodular calcrete
9 development, some within paleosol horizons. The documented section ends with
10 paleochannels that show complex down-cutting relationships that make stratigraphic
11 correlations with respect to overlying units unclear. This carbonate-rich upper-most unit is
12 exposed extensively on the plateau to the N and NE of the section and is probably
13 transitional into the Brak Formation, since Geyh and Thiedig (2008) identified the Brak
14 Formation some 33 km to the NE (Fig. 8), some 15-20 m stratigraphically above the top of
15 the measured section.
16

17 The lower boundary of the Kunayr Member can be traced westwards along the bluffs
18 for around 7 km, with the basement elevation rising to the NW (Figs. 4, 6, 7). The extent of
19 the Shabirinah Formation outcrops to the east was not fully investigated, but satellite
20 imagery suggests it may extend 20 - 40 km eastwards, and then rest on the Maastrichtian
21 (Woller, 1984).
22

23 Section TS3 is the proposed type section of the Tmassah and Stromatolite Members
24 of the Shabirinah Formation (Figs. 6,10). The section is dominated by clastic units, but
25 contains well-developed lacustrine limestone beds towards the base (lower part of
26 Stromatolite Member) and in the basal and lower parts of the Kunayr Member. The red
27 mudstones of the upper part of the Stromatolite Member thicken considerably a little to the
28 south and west (e.g. section TS2; Fig. 6), indicating the Tmassah Member here is an incised
29 channel (i.e. there is a hiatus at the base of this member). The Stromatolite Member
30 continues for at least another 3 km to the east (to 26°30',55.3"N;16°31',57.6"E), and was
31 seen 9.3 km to the west (at 26°31',47.9"N;16°24',31.7"E) in this area. In the TS3 section
32 the upper part of the Kunayr Member is exposed in a hillside (at
33 26°30',47.9"N;16°30',6.6"E), which is capped by a rootleted silica-cemented sandstone.
34 The same sandstone bed was seen capping plateaus 11 km to the east (at
35 26°30',32.8"N;16°36',43.8"E). Samples from the carbonate bed in the Stromatolite
36 Member in sections TS2 and TS3 were sampled for U-Th and U-Pb dating (Supplementary
37 Data Table S2).
38

39 The SK3 section was exposed in a working quarry in central Wadi ash Shati (Figs. 1,4,
40 7). This section is the type location of the Al Mahruqah 'formation' of Seidl and Röhlich
41 (1984), and of our Brak Formation. The lower part of the section is composed of red
42
43
44
45
46
47
48
49
50
51
52
53
54
55
56
57
58
59
60
61
62
63
64
65

1 mudstones with green mottling, passing up into a calcareous sandstone- sandy limestone,
2 which in turn grades up into the main limestone rich part of the Brak Formation (Fig. 10).

3 In total 127 paleomagnetic samples were collected from these three sections, and
4 located onto sedimentary logs (Fig. 10). The samples were oriented using a compass. About
5 60% of the samples (other than the well-cemented limestones) were poorly consolidated,
6 and were impregnated with a 2:1 mix of Na- silicate and water (Kostadinova et al., 2004) to
7 consolidate them prior to cutting into specimens. For some of these samples, this
8 impregnation process started in the field, and was left to dry and harden overnight before
9 orientating and packing for transport. After further consolidation in the laboratory, cubic
10 specimens were cut from the hand samples using a circular saw, often re-treating the more
11 friable specimen slices several times during this process to consolidate them for final
12 specimen preparation.
13
14
15
16
17
18
19
20

21 ***3.1. Laboratory Methodology***

22
23 Low field magnetic susceptibility (K_{if}) was measured using a Bartington MS2B sensor.
24 Measurements of Natural Remanent Magnetisation (NRM) were made using a CCL 3-axis
25 cryogenic magnetometer (noise level ca.0.002 mA/m), using multiple specimen positions,
26 from which the magnetisation variance was determined. Generally 2 to 3 specimens from
27 each sample were subjected to stepwise thermal demagnetisation, using a Magnetic
28 Measurements Ltd thermal demagnetiser, in 100°C steps up to 400°C, followed by 30°C
29 steps until around 630°C, sometimes 650°C, or until instability set-in or the specimen
30 demagnetised down to the magnetometer noise. Alternating field (AF) demagnetisation was
31 used on a few samples from the SK8 section, after heating to 350°C, but proved ineffective.
32 K_{if} was monitored after heating stages to monitor mineralogical change. Specimens were
33 kept in mu-metal boxes (residual field <20 nT) between demagnetisation and measurements
34 steps.
35
36
37
38
39
40
41
42

43 In total 28 and 247 paleomagnetic specimens were demagnetised from the Brak and
44 Shabirinah Formations respectively. The bedding dip in all these units was zero so a fold test
45 was not possible.
46
47

48 Characteristic remanence (ChRM) directions were isolated using principle component-
49 based statistical procedures implemented in LINEFIND, which uses the measurement
50 variance along with statistical procedures for identifying linear and planar structure in the
51 demagnetisation data (Kent et al., 1983). Both linear trajectory fits and great circle
52 (remagnetisation circle) data were used in defining the paleomagnetic behaviour, guided by
53 objective and qualitative selection of the excess standard deviation parameter (ρ), which
54 governs how closely the model variance, used for analysis, matches the data measurement
55 variance (Kent et al., 1983). The PMAGTOOL software (<http://www.lancaster.ac.uk/staff/>)
56
57
58
59
60
61
62
63
64
65

hounslow/resources/software.htm) was used for the analysis of mean directions and virtual geomagnetic poles.

Backfield isothermal remnant magnetisation (IRM) up to 1.75 T was applied to a representative sub-set of specimens, to investigate the magnetic mineralogy. Anhysteretic magnetisations were applied to investigate the granulometry of the iron oxides. Anisotropy of magnetic susceptibility (AMS) (Liu et al., 2001 and references therein) was evaluated on selected specimens from section SK8, to assess grain fabrics and paleoflow information (Supplementary Data Fig. S5).

U-Pb isotope reconnaissance by laser ablation ICP mass spectrometry (LA-ICP-MS) and solution-mode U-Th chronology by multicollector ICP mass spectrometry (MC-ICP-MS) was attempted on six samples from the Stromatolite Member in the TS2 and TS3 sections. Sample selection was guided by thin section petrography to screen samples for minimum possible silicate detritus contents. U-Th data were obtained on samples subjected to total dissolution with HF-HNO₃-HClO₄. Analytical procedures, including ion exchange chemistry and mass spectrometry followed Douarin et al. (2013), with details given in the Supplementary Data. Data were obtained on a Thermo Scientific Neptune Plus MC-ICP-MS and calculation of activity ratios and ages used the decay constants of Cheng et al. (2013).

4. Results

4.1. Magnetic Mineralogy Results

The NRM intensity and magnetic susceptibility (MS) are broadly related to each other (see Supplementary Data Fig. S5a), with carbonate-rich samples having weak (sometimes diamagnetic) susceptibilities, and red or mud-rich samples (e.g. in paleosols) having the largest NRM intensity or magnetic susceptibility. Some clustering of these magnetic data into the various lithostratigraphic units, is related in part to the often higher carbonate content of the Brak Formation and Kunayr Member samples, compared to those of the Tmassah Member (Supplementary Data Fig. S5a).

Red mudstones and sandstones from the SK3 and TS3 sections, and all non-red samples from the SK8 section do not saturate in IRM fields of 1.75T, indicating substantial amounts of haematite (or goethite) in these types of samples. Other lithologies in the SK3 and TS3 sections saturate by ca. 1T, but still have 10-35% of IRM acquisition above 300 mT probably indicating a substantial haematite contribution to the IRM, as well as a more dominant low coercivity phase, possibly magnetite, or Ti-magnetite (Supplementary Data Fig. S6). Remanent coercivity of non-red samples from the TS3 section are between 109-253 mT, in comparison to non-red samples from other sections, which range between 44-98 mT, indicating a substantial difference in the relative contributions of low coercivity (magnetite) and haematite between the southerly (near Tmassah) and northerly sections (Wadi ash Shati to Wadi Kunayr). The large contributions from haematite (or goethite) tally

1 with the ineffective application of AF demagnetisation on the NRM. Early and mid Miocene
2 clastic and carbonate rocks from the western Desert in Egypt, share similar magnetic
3 properties (Abdeldayem, 1996). The AMS data displays depositional fabrics (Supplementary
4 Data Fig. S5b), with Kmax axes showing approximate E-W alignment, generally consistent
5 with the trend of fluvial channels to the east of section SK8. There is also evidence of a
6 weaker lateral transport direction, reflected also in paleocurrent data from the SK7 section
7 (Fig. 7; Supplementary Data Fig. S5c).
8
9

10 11 12 **4.2. Paleomagnetic Results** 13

14
15 During demagnetisation specimens generally have stable MS values until ca.450°C,
16 when the majority show either a small increase (up to 2x initial value) or decrease in MS,
17 indicating initiation of some mineralogical alteration (Van Velzen and Zijdeveld, 1992).
18 Reddened samples tend to show less changes in MS values. In non-red specimens, this
19 alteration sometimes obscured the recovery of the remanence at higher demagnetisation
20 temperatures. Unblocking temperatures of the NRM are generally distributed throughout the
21 demagnetisation range up to ca. 600-650°C (demagnetisation is often complete by 600-
22 650°C), with most often more than half of the NRM removed by around 300-450°C, after
23 which the rate of unblocking decreased. Reddened samples tend to have a more rapid drop
24 in NRM intensity at <200°C, possibly suggestive of goethite (or pigmentary haematite;
25 Marton et al., 1980) partly carrying the NRM.
26
27

28
29 Of the 275 specimens measured, some 88% give data that can be confidently
30 interpreted as containing a ChRM component. Low stability components between room
31 temperature and up to 300 to 450°C, appear to be composed of two groups. Firstly, in 70%
32 of specimens (regardless of if they are interpreted as having reverse and normal polarity) the
33 low stability component is a Brunhes-like magnetisation with mean direction of 002°/42°
34 (Supplementary Data Fig. S7). The remainder appear to have a variety of 'mixed directions'
35 somewhat scattered, either northerly directed negative inclination components or southerly
36 directed positive inclination components. These mixed directions are interpreted as
37 composite components, mostly mixes between the Brunhes overprint, and the primary
38 reverse direction, since 68% of them have interpreted reverse polarity (see Supplementary
39 Data). Random viscous components also probably contribute to the large scatter in these
40 low stability components. Intermediate stability components seem to be entirely random
41 (Supplementary Data Fig. S7).
42
43

44
45 High stability components inferred to be the ChRM are difficult to extract from most
46 specimens, with only 25% of the specimens giving suitable line-fits to the demagnetisation
47 data (here called S-class data). These are largely at demagnetisation temperatures
48 beginning around 350 to 400°C, either to the origin or until around 600°C (Figs. 11a,e). Often
49
50
51
52
53
54
55
56
57
58
59
60
61
62
63
64
65

1 above 600°C, the directional scatter is large, or the specimen demagnetised. The remaining,
2 75% of specimens display greater circle trends towards interpreted normal or reverse
3 polarity (here called T-class data, Figs. 11b,c,d,f). The low to moderate success rate in
4 obtaining line-fits may reflect the often sandy, well sorted, silt and clay-poor nature of most
5 samples; as such sediments tend to be rather poor paleomagnetic field recorders. Silt-rich or
6 reddened lithologies generally display the best paleomagnetic behaviour, but are few in
7 number. The 75% of specimens with great circle trends reflects the difficulty in isolating the
8 ChRM from the low and intermediate stability components during demagnetisation (e.g. Fig.
9 11f).

14 **4.2.1. Mean Directions and Paleopoles**

16 Mean directions were determined using specimen-based means, by combining the
17 great circle paths with those specimens with line-fit ChRM (Table 2), to produce combined
18 means using the method of McFadden and McElhinny (1988). This method determines a
19 mean direction, by including the 'fixed-point' ChRM directions, and those points on the
20 projected great circles, which maximise the resultant length (i.e. in effect those calculated
21 points on the great circle which are closest to the combined mean direction). The great-circle
22 combined means pass the reversal test for the TS3 and SK3 sections, but marginally fail for
23 the SK8 section, with $<10^\circ$ between antipodal directions (Table 2).

29 The confidence intervals on our paleopoles overlap with the apparent polar wander
30 path (APWP) for the 0-30 Ma interval for Africa (Torsvik et al., 2012), showing the reliability
31 of the mean directions (Supplementary Data Fig. S8). The limited number of Miocene to
32 recent age poles from Africa, tend to show a general displacement to the east of the APWP,
33 whereas the poles from the Jabal as Sawda volcanic rocks tend to have lower latitudes, due
34 to shallower mean inclinations than our data. This discrepancy is not due to inclination
35 shallowing in our sediment sections, which if corrected for tends to move the poles
36 northwards to steeper poles (see Supplementary Data Fig. S8).

45 **4.2.2. Magnetostratigraphic Interpretation**

47 The line-fit ChRM directions from the sections were converted to virtual geomagnetic
48 pole (VGP) latitude (Opdyke and Channel, 1996) using the great circle ChRM means in
49 Table 2 (Fig. 12). For those specimens that had no line-fit, the point on their great circle
50 nearest this mean, was used for calculating the VGP latitude. All specimens were also
51 assigned a 'polarity quality' based on the quality of demagnetisation behaviour and, if from T-
52 class specimens, the length and end-position of the great circle trend (similar to the
53 procedures used by Ogg and Steiner, 1991; Hounslow and McIntosh, 2003). One specimen
54 of good-quality polarity (i.e. S-Type) was sufficient to define the horizon polarity, whereas
55 with specimens of poorer quality at least two are required (Fig. 12). Some 11% of all
56
57
58
59
60
61
62
63
64
65

specimens failed to yield data which could be used to determine specimen polarity, but no horizons failed to yield specimens which could be reliably used to determine magnetic polarity (Fig. 12).

The SK8 and TS3 sections can be correlated together using the base of the Kunayr Member, where the underlying part of the Tmassah Member is reverse polarity dominated. The youngest parts of the Shabirinah Formation in all three sampled sections have dominantly normal polarity, which allows us to construct a composite magnetostratigraphy using the three sections (Fig. 13). The composite magnetostratigraphy is generated using the numerical optimisation techniques described in Hounslow (2016). For this data the optimisation shifts the SK3 section (without a metre-scale change), but has both a shift and a scale change for the data in the TS3 section. The optimised composites are in the metre scale of the SK8 section, whose data remain unscaled.

From the TS2 and TS3 section logs and field evidence it is clear that at least ca. 3 m of red mudstones are missing from the upper part of the Stromatolite Member at sampled section TS3 (Figs. 6, 10). This is due to down-cutting of the channel sandstone in the base of the Tmassah Member at section TS3. We therefore break the TS3 section into two subdivisions, with the youngest normal polarity sample in the Tmassah Member correlating to the base of the normal polarity interval at SK8 with its lower boundary at 11.4 m (Fig. 13). This broadly correlates the red-black (humid) paleosols seen in the SK8 section with the fluvial lower part of the Tmassah Member at section TS3 (Figs. 10, 13). A slightly lower position of the Stromatolite Member at TS3 was considered, which correlated the interval of red mudstones in the TS3 and SK8 sections (Fig. 10). This gave a projected missing thickness for the upper part of the Stromatolite Member of 9.7 m, which appears too large based on the field evidence, so was rejected as a possibility.

We derive two likely composite magnetostratigraphies (Fig. 13), because of ambiguity in how to correlate the SK3 section to the upper parts of the SK8 and TS3 sections. The differences between composites A and B relate to the position of the SK3 section, which is correlated to a younger magnetozone in the TS3 section in the composite B (Fig. 13). Composite-B better correlates the sandstone bed in the uppermost part of the TS3 section with the clastic interval (with red mudstones) at section SK3. Composites A and B both give a projected missing 2.9 m and 2.5 m of section respectively, from the top of the Stromatolite Member at TS3, similar to the estimated amount based on field data and nearby sections such as TS2 (Fig. 10). Normal polarity magnetozone Sb6r.1n was not detected at section TS3, which may relate to a potentially missing part in section TS3, due to some uncertainty in exactly how to correlate sampled sub-sections in the field, which join at this level.

4.3. U-Pb and U-Th chronology results

1 The samples from the TS3 section have U contents of ca. 1-1.5 ppm while the
2 samples from the TS2 section have a wider range of U contents from 0.5 to ca.5.4 ppm.
3 Both groups of samples have variable and significant amounts of Th with resultant low
4 $^{230}\text{Th}/^{232}\text{Th}$ activity ratios ($[\text{Th}]$) ranging from ca.1 to 18 (Supplementary Data Table
5 S2). Detritus-corrected age uncertainties are large and significantly limit the utility of the
6 dataset. Nevertheless, the data are sufficient to indicate that most of the carbonates
7 analysed are at or close to U-Th secular equilibrium, and are thus > ca. 500 ka old
8 (Supplementary Data Table S2, Fig. S9). The exception, and only apparently 'reliable' date
9 obtained, was sample TM6 at 242 ± 24 ka. Given that this date is not in stratigraphic order
10 and there is evidence of a much older age from other chronometers, it is interpreted as
11 reflecting a post-depositional disturbance of the carbonate mineralogy. In oxidizing
12 environments uranium is very mobile and recrystallisation or major disturbance of the
13 carbonate at any time can cause uranium to be redistributed. This is clearly an issue with
14 these sediments, since oxidising sediment systems are the norm. One other sample
15 nominally records a <500 ka age, but as $[\text{Th}]$ is ca. 1.3, the calculated age is
16 strongly controlled by the assumed initial Th isotope composition and is therefore not
17 interpreted here. Overall, the data obtained indicate these carbonates are unsuitable for U-
18 Th or U-Pb chronology (see Supplementary Data for further discussion).

30 5. Discussion

33 5.1. Other chronological controls

34 The basalt fragments in the basal Brak Formation in Wadi ash Shati, and basalt flows
35 inferred in the basal Brak Formation in mapped outcrops to the north of Wadi Kunayr (Fig.
36 8), are probably derived from the Jabal as Sawda lava field to the north (but may be from the
37 older al Hasawinah lava fields). The Jabal as Sawda lavas are dated to 12.3 - 10.5 Ma (Ade-
38 Hall et al., 1975; Liégeois et al., 2005) using the K/Ar method. This implies the Brak
39 Formation is younger than ca. 12-10 Ma, and the Shabirinah Formation is older than this.

40 The SE and E flowing paleocurrents in the Shabirinah Formation, indicate the
41 formation pre-dates the bulk of the Haruj al Aswad volcanic field, otherwise the volcanic field
42 would have been an effective barrier to eastwards fluvial transfer into the Sirte Basin. The
43 Haruj al Aswad volcanic field, has mean K/Ar ages of 2.8 ± 2.0 Ma (range 8.1 ± 0.11 Ma to
44 0.5 ± 0.1 Ma; Cvetkovic' et al., 2010; Bardintzeff et al., 2012; uncertainty as 1 SD), indicating
45 the Tmassah Member is older than ca. 8 Ma. However, both Cvetkovic et al. (2010) and
46 Drake et al. (2008) report outlier K/Ar dates of 11.8 ± 0.4 Ma and 10.2 ± 1.3 Ma respectively, so
47 minor earlier phases of the Haruj al Aswad seem possible. This is consistent with radiometric
48 dating from the Jabal Eghei volcanic centre, illustrating the long-lived nature of the Libyan
49
50
51
52
53
54
55
56
57
58
59
60
61
62
63
64
65

volcanic centres (Radivojević et al., 2015). It is not clear if these minor early phases of the Haruj al Aswad volcanic field could have blocked fluvial access into the Sirte Basin.

Hence, together the volcanic field radiometric dating, and stratigraphic relationships indicate the Shabirinah Formation is older than about 11 - 8 Ma , with the Brak Formation younger than 10-12 Ma, placing these formations in the Miocene to Pliocene.

Between the Brunhes chron until the mid-Oligocene (chron C11) the mean duration between geomagnetic field reversals was 0.248 Ma (Lowrie and Kent, 2004). Since we have 33 to 37 magnetozones in our two composites, this implies the minimum duration of our composite magnetostratigraphy is of the order of 8-9 Ma, so the oldest parts of the Shabirinah Formation likely range down to 19-16 Ma, as a minimum age estimate (ca.20 Ma as an older estimate). However, it is unlikely our sampling of this 55-60 m succession has detected every magnetochron, since using these duration estimates and the average sample spacing (ca. 1 sample per 0.75 m) indicates a mean duration between sampling levels of ca. 70 kyrs, indicating that chrons <ca. 40 kyrs are unlikely to have been detected. This suggests the age duration of our composites may be closer to ca. 9 Ma, and the age of the oldest parts of the Shabirinah Formation to lie between 20 - 17 Ma.

Geyh and Thiedig (2008) have dated the Brak Formation and the Bir az Zallaf Member using the $^{230}\text{Th}/\text{U}$ method. The Brak Formation gives a median age of 353 ± 31 ka (1 SD) while the Bir az Zallaf Member has a median age of 223 ± 26 ka (excluding open system samples). These $^{230}\text{Th}/\text{U}$ dates seem highly implausible, based on the stratigraphic relationships in Wadi ash Shati, since a major unconformity, followed by ca. 90 m of erosion (Fig. 9), with a subsequent ca. 30 m of clastic sediment deposition of the Sifar and Sayl members, separate the Brak Formation and Bir az Zallaf Member , with an apparent ca.130 ka age difference.

In the Sarir al Qattusah, west of the Haruj al Aswad (Fig. 1) Schlüter et al. (2002) estimate an erosion rate on carbonate dominated hamada surfaces of 1-2 m/Ma. In the hyperarid (1-10 mm/year of rainfall), low elevation parts of the Atacama Desert, cosmogenic isotope determined erosion rates of bedrock are 0.4 to 10 m/Ma (Fujioka and Chappell, 2011). In the Namib Desert erosion rates of sediment basins are of the order of 5-16 m/Ma, higher than bed rock erosion rates (3-5 m/Ma) in the same region, and both are consistent with fission track estimates (Fujioka and Chappell, 2011). Using the maximum of these erosion rate estimates suggests the ca. 90 m of erosion in Wadi ash Shati took at least ca. 5 Ma to produce rather than the ca. 130 ka suggested by $^{230}\text{Th}/\text{U}$ dating.

Hence, the $^{230}\text{Th}/\text{U}$ dates are grossly out of step with both the regional stratigraphic relationships of these units, our magnetostratigraphy and likely erosion rates, which instead suggest a 130 ka time difference, should occupy around 1.5 m in our sediment successions. However, like our attempted U-Th dating, the $^{230}\text{Th}/\text{U}$ dates themselves likely relate to late Pleistocene surface weathering, with groundwater mobilisation of uranium prior to deposition

of the earliest parts of the Shati Formation (i.e. the Aqar Member), starting at around 100-136 ka. The consistent positive relationship between elevation and age (and negative relationship between inferred age and $\delta^{13}\text{O}$) in the $^{230}\text{Th}/\text{U}$ dates (Geyh and Thiedig, 2008) may relate to the characteristics of the groundwater modification process, with the U-system fixed-in slightly earlier at higher elevation sites. Intervals of Quaternary pluvial mobilisation of U are also known from the Egyptian deserts between 240-80 ka (Osmond and Dabous, 2004).

5.2. Magnetostratigraphic age model

Without firm age tie points for the magnetostratigraphy, we use quantitative correlation methods to correlate to the geomagnetic polarity timescale (GPTS) to date objectively these successions. Three main methods have been previously used. Firstly, cross-correlation using either magnetozone lengths, L_i (and GPTS chron durations; Lowrie and Alvarez, 1984), or \log_e of the ratio (r_i) of lengths of the underlying magnetozone (i.e. $r_i=L_i/L_{i-1}$, with L in metres or Ma duration for the GPTS; Man, 2008). Secondly, a likelihood-based method linked to a stochastic model of sediment deposition (Man 2011). Both of these methods are limited by the necessity for a complete recording of all GPTS polarity chrons in the section, which is a problem with our data. The method of Man (2011) is also restricted to a limited number of section magnetozones (8 to 12) due to adherence to a single stochastic sedimentation model. Thirdly, the dynamic time warping method, proposed by Lallier et al. (2013), using r_i values but incorporating potentially missing magnetozones in sections, by considering correlations which minimise the local variation of the accumulation rate.

In all these methods, converting magnetozone height to r_i in effect transforms the GPTS and section data into a consistent dimensionless scale, and reduces the impact of changes in sedimentation rate. However, it does impose non-linear noise on r_i , since shorter magnetozones have the least well-defined heights in the section (due to sample spacing issues), so the intervals with the least uncertainty in r_i are those with r_i ca. 1, and longer magnetozone lengths. Lallier et al. (2013) used a correction factor to account for the biased uncertainty in r_i .

However, in essence all these methods utilise only one characteristic (magnetozone height, or r_i) of the polarity pattern, when the character of the GPTS may be better expressed by multiple parameters which express characteristics like polarity bias around the chron, or relative durations of more than two adjacent chrons (Olson et al., 2014). The advantage of utilising characteristics from the adjacent magnetozones, is some smoothing of the response function to limit impacts of magnetozone thickness uncertainty.

We use the sequence slotting method (Clark 1985; Gordon et al., 1988; Thompson and Clark 1989), as implemented in the CPLSLOT programme (<http://www.lancs.ac.uk/staff/>

hounslow/resources/software/cplslot.htm), an objective method of quantitative correlation that can deal with multivariate datasets (See Supplementary Data). The method seeks a correlation which minimises the dissimilarity (defined by a distance metric) between the two aligned datasets. Sequence slotting is not constrained to have sequential matching of data points across matched successions (e.g. as in cross correlation), so can deal with missing chrons in the GPTS, and variable sedimentation rates. We parameterise each magnetozone with its polarity (-1, or +1), duration (in Ma), $\text{Log}_e(r_i)$, polarity bias (including the two adjacent chrons), and Sherman's ω_2 statistic (using the two adjacent chrons). ω_2 measures the deviation of magnetozone lengths as a proportion of the average length (Olson et al., 2014). The durations of magnetozones in the polarity composites were estimated using section durations based on reversal rates of 0.259 Ma^{-1} , which is the median rate for the last 29 Ma, if chrons <40 ka are excluded from the GPTS of Ogg (2012). All 5 chron parameters also then approximately fall in the numerical range -2 to +2, which allows no parameter scaling to be used in the sequence slotting. A Euclidean distance metric was used (Gary et al., 2005). A blocking constraint of 2 (Thompson and Clark 1989), was used which limits missing chrons in the GPTS to one subchron normal-reverse polarity pair.

The goodness-of-match of the sequence slotting is evaluated in two ways. Firstly, from the conventional slotting parameters, particularly the Δ parameter, which takes values from >0 to ca. 1 (Δ <ca. 0.5 indicates very good similarity; Thompson and Clark, 1989). Secondly, matrix association coefficients (R_c , RV_2 and standardized RV) which evaluate the similarity of the whole configuration of variables between the two datasets (Smilde et al., 2009; Abdi, 2010). The weakness of the Δ parameter is that it is most strongly impacted by data variability proximal to the levels considered, so quite different correlation solutions can give similar Δ , so using Δ alone can be misleading. That is Δ tends to indicate the goodness of the 'local-match' in a simple sense. In contrast, the R_c , RV_2 and standardized RV (matrix association coefficients) tend to respond better to longer-scale structure in the data, are less impacted by local noise, and tend to respond closer to visual similarity when data are plotted side by side. Likely solutions can also be imaged by the H-matrix (Gordon et al., 1988), which is a visual representation of the matching similarity of the two data successions as they are slid past each other (the concept is similar to the similarity matrix of Gary et al., 2005). See the Supplementary Data for further details.

Testing composite-A indicates there are two likely match solutions, one which places the upper part of the composite polarity in the Tortonian (top SB10n.2n=C3Br.2n; base SB1r=C5Cn.2r), and one which places it in the Serravallian (top SB10n.2n=C5An.1n; base SB1r=C6Br, Supplementary Data Fig. S10). The one with the larger matrix association coefficients is the Serravallian solution, whereas the slotting parameter Δ is similar for both age models. Composite-B indicates, like composite-A, that the two most likely solutions place the upper part of the polarity composite in the Tortonian (SB10n.2n=C3Br.2n;

1 SB1r=C5Cn.2r) and Serravallian (SB10n.2n=C5An.1n; SB1r=C6Br). Like composite-A the
 2 Serravallian solution has the larger matrix association coefficients, with the Δ parameter
 3 similar for both age models. The Serravallian composite-B solution also has lower Δ and
 4 larger matrix association coefficients compared to the Serravallian Composite-A solution
 5 (Supplementary Data Figs. S11, S12) and is the final preferred solution (Fig. 13). This places
 6 the base of the Brak Formation at ca. 13 Ma, a little bit older than inferred by the supposedly
 7 interbedded Jabal as Sawda lava's. It could be that the inferred interbedded basalts occur
 8 slightly higher in the Brak succession north of Wadi Kunayr. At section SK3 the Brak
 9 Formation ranges up into chron C5An.1n of age 12.0 to 12.2 Ma, similar to the oldest Ar/K
 10 dates from the Jabal as Sawda lavas. Hence, it is probable the Brak Formation continues to
 11 younger ages than those seen in section SK3, as inferred by its presence at higher
 12 elevations (Fig. 7).

13 The accumulation rates are broadly similar through the Tmassah Member to Brak
 14 Formation, but decline markedly through the underlying Stromatolite Member
 15 (Supplementary Data Fig. S12). This may relate to a regional hiatus (missing interval) at the
 16 base of the Tmassah Member, since the composite polarity does not appear to capture the
 17 dominant reverse polarity well through chrons C6Ar and C6AA. Alternatively, it may relate to
 18 a shut-down in coarse clastic supply in the Stromatolite Member, which is dominated by
 19 micritic lacustrine limestones and mudstones.

30 **5.3. Implications**

31 It is clear the lacustrine humid intervals associated with Al Mahruqah Group are not
 32 only found in the late Quaternary Shati Formation, but also occur in the early and mid
 33 Miocene. Three lacustrine-palustrine phases are present in the Shabirinah and Brak
 34 formations that suggest episodes of greater humidity when Lake Megafezzan developed.
 35 These are separated by clastic sediments and paleosols deposited in less humid intervals in
 36 which we have no direct evidence for lake deposits. The first of these intervals of greater
 37 humidity is during the late Aquitanian and is represented by the limestone bed in the
 38 Stromatolite Member, which is most widespread in the region east and north of Tmassah, to
 39 within 45 km south of Wadi Kunayr. Since in the Wadi ash Shabirinah area the lower parts of
 40 the Shabirinah Formation are dominated by fluvial clastics furthest to the east, it implies we
 41 are dealing with fluvial fringes to a large lake, located further west, which is dominated by
 42 fine-grained red clastics and stromatolitic limestones. In the Wadi ash Shabirinah area in
 43 spite of dominant cross-bedding directions to the SE (Fig. 6), some clastic material was also
 44 supplied from the NNE, since the units pinch out in this direction. We also have evidence of
 45 proximal channels supplying material southwards (section TS7, Fig. 6). These imply the
 46 paleotopography during this interval was a valley-like fluvial transport system (with some
 47
 48
 49
 50
 51
 52
 53
 54
 55
 56
 57
 58
 59
 60
 61
 62
 63
 64
 65

1 lateral supply), likely flowing eastwards through a low in the Paleozoic basement ridge north
2 of Dur al Qussah into the Abu Tumayan Trough (Fig. 1). A similar situation may have existed
3 in the Wadi Kunayr area, where a secondary mode in the AMS K_{max} axes, and paleocurrent
4 data suggest lateral flow (Supplementary Data Fig. S5c).

5 The part of the Shabirinah Formation below the Kunayr Member equates in time to
6 Aquitanian-Burdigalian fluvial (or part fluvial) units seen in the Sirt Basin (Qarat Janannam
7 Member). Equivalent age units in the Egyptian western Desert are the Al Moghra Formation
8 and the Messioua and Sehib formations in Tunisia (Fig. 14). Dating of these other North
9 African fluvial or estuarine (Hassan, 2013) units is either by lithostratigraphic correlation in
10 Tunisia (Mannai-Tayech, 2009) or their vertebrate faunas (Fig. 14). The vertebrates in these
11 Aquitanian-Burdigalian deposits in Egypt and Libya are large vertebrates such a
12 hippopotamus and land carnivores together with micro-vertebrate remains, such as rodents
13 (Morlo et al., 2007) along with fossilised tree logs and fish (Cook et al., 2010). Vertebrates
14 from the Marada Formation in Libya are diverse and include large land and water mammals
15 and reptiles together with small vertebrates such as rodents, bats and rabbits/hares (
16 Wessels, et al., 2003; Llinás -Agrasar, 2004). These together indicate the tropical and
17 savanna climatic conditions along the Tunisian-Libyan- Egyptian coastline during the
18 Aquitanian-Burdigalian.

19 The second palustrine interval is found in the lower part of the Kunayr Member,
20 restricted so far to the area east of Tmassah. It dates to the latest Burdigalian (chron C5Cn)
21 through into the early Langhian. These limestones laterally grade north-eastwards and
22 eastwards into interbedded calcreted clastic units. Such lateral relationships follow the model
23 outlined by Alonso-Zarza (2003) for palustrine-calcrete units in semi-arid settings, indicating
24 that the central part of the Kunayr Member paleolake basin was to the west or SW of the
25 current outcrops, a region where the deepest part of the southern sub-basin of the Fezzan
26 topographic low is found today (Drake et al., 2008). Compared to the underlying Tmassah,
27 Stromatolite and Maharshim members calcretisation and pedogenically modified clastics and
28 palustrine limestones are significant components of the Kunayr Member. Calcrete occurs in
29 regions that experience an annual soil moisture deficit, either from a low annual rainfall or
30 sub-humid regions characterised by a pronounced dry season (Candy et al., 2004). The
31 chron interval C5Cn to C5AC corresponds with the higher temperatures of the mid Miocene
32 Climatic Optimum, covering most of the Langhian (Hilgen et al., 2012). Therefore the
33 calcretisation in the Kunayr Member is likely a response to the increased moisture deficit
34 stimulated by the higher temperatures.

35 The age of the base of the Kunayr Member is closely aligned in time with the
36 transgressive base of the marine Ar Rahlah Member (of the Marada Formation in the Sirt
37 Basin) and the marine Marmarica Formation of the Egyptian Western Desert (Fig. 14).
38 These southward marine incursions in the North African margin seem to record the higher
39
40
41
42
43
44
45
46
47
48
49
50
51
52
53
54
55
56
57
58
59
60
61
62
63
64
65

1 global eustatic sea-levels starting in the late Burdigalian (Chron C5C) and ending before
2 Chron C5AB (Hilgen et al., 2012). Similar aged marine transgressive units are seen in
3 central Tunisia dated to foraminifera zones N7 to N10 (Chron C5C to C5AC; Fig. 14;
4 Mannai-Tayeck, 2009). In the Fezzan Basin this closer proximity to the sea perhaps drove
5 the climate to be less seasonal suggesting the higher temperatures of the mid Miocene
6 climatic optimum, were the primary reason soil moisture deficits driving the calcretisation in
7 the Kunayr Member.
8
9

10 The main palustrine phase of the Fezzan Basin Miocene is represented by the
11 deposition of the Brak Formation during the Serravallian. This limestone may represent the
12 most extensive palustrine deposit in the Fezzan basin, since it oversteps onto basement
13 highs and eastern fringes of the Fezzan Basin, along the foot of the Sarir al Quttasah
14 Paleogene escarpment. Although we have no direct evidence about the nature of the basin-
15 centre equivalent of the Brak Formation, it is assumed to be a more open lacustrine version
16 of the palustrine limestone unit (or a mudstone unit) we see at basin margins. One of the
17 reasons the Brak Formation may be so extensive is that the exits from the Fezzan into the
18 Sirte Basin were restricted by initial growth of the Jabal as Sawda volcanic centre (restricting
19 the NE Wadi Nashu exit?; Fig.1) and uplift of the western side of the Sirte Basin, thus
20 allowing a larger lake to develop.
21
22
23
24
25
26
27
28

29 The best-dated evidence we have for other Serravalian terrestrial sediments in the
30 adjacent countries to Libya is from Tunisia, where the Beglia Formation forms a NE
31 prograding succession above marine and non-marine strata in central and SW Tunisia (Fig.
32 14; Mannai-Tayeck, & Otero 2005). A humid terrestrial climate in North Africa during the
33 Serravalian is indicated by fossil crocodiles and a variety of other large land vertebrates from
34 the Beglia Formation (Serravalian – Tortonian in age; Pickford, 2000; Mannai-Tayeck,
35 2009), which are associated with a large NE flowing river system exiting from the Algerian-
36 Tunisian central Sahara (Mannai-Tayeck & Otero 2005). A larger regional assessment by
37 Swezey (2009) suggested the central Saharan Miocene strata were deposited by fluvial
38 systems that reached a maximum extent during the Langhian–Serravallian. The Brak
39 Formation therefore may be expression of this maximum extent of fluvial-related units in the
40 central Sahara, of which the Beglia Formation may also be an expression.
41
42
43
44
45
46
47
48

49 The uplift of the southwestern shoulder of the Sirte Basin continued after the Brak
50 Formation, since clearly in both the Wadi ash Shati and Wadi Shabirinah regions the units
51 are tilted to the west (or their eastern parts are up-faulted; Figs. 6, 7). The extent of the
52 Shabirinah and Brak formations to the west is unclear, we only have glimpses of these units
53 in the Northern Awbari Sand Sea, it may be lateral equivalents exist beneath the Murzuq and
54 Awbari Sand seas.
55
56
57
58

59 Preliminary magnetostratigraphic results from the upper part of the overlying Zarzur
60 Formation suggest it may be mid Pliocene (ca. 3 Ma) in age (Drake et al., 2011b), and our
61
62
63
64
65

1 results indicate the younger part of the Brak Formation is at least 12 Ma (or younger). This
2 suggests the erosion event and unconformity between these two formations likely started
3 during the late Miocene. Late Miocene unconformities are recognised throughout the Sirt
4 Basin and have been used as a correlation datum for the top of the Marada and Al Khoms
5 formations (Selley, 1968; El Hawat, 1980 & 2008) and their equivalents in western Egypt
6 (Gerdes et al., 2010; Zaki et al., 2013). El Hawat and Salem (1987) also used the
7 unconformity on the top of the Marada Formation to divide the Miocene stratigraphy in
8 northern Cyrenaica (NE Libya) into Middle and Upper Miocene units (Fig. 14). The earlier
9 event probably relates to an interval of karst development on the Marmarica Formation in the
10 Egyptian Western Desert, which is dated to mammal zone MN9 (ca. 10-11 Ma) in the early
11 Tortonian (Wanas et al., 2009; Zaki et al., 2013.). These circum-Mediterranean and North
12 African events are associated with Mediterranean tectonic reorganisation and eustatic lows
13 in global and Mediterranean sea level during the Tortonian-Messinian (Gerdes et al., 2010;
14 Holgen et al., 2012).

22 Evidence for the geometry of the fluvial transport systems in the Shabirinah Formation,
23 suggest axial-drainage networks. This is clearly seen in Wadi Kunayr, where the Shabirinah
24 Formation occupies a linear topographic depression (ca. 50 m deep over ca. 20 km distance;
25 Figs. 1, 8) in the Mesozoic and Paleozoic basement. Such an axial system is also inferred in
26 the Wadi ash Shabirinah region, where we have a ca. 50 m basement elevation difference
27 over some ca. 9 km normal to the axial transport. Thus the Fezzan Basin axial transport
28 systems must be older than the Aquitanian, suggesting that the major drainage systems of
29 the central Sahara were inherited from networks that initially developed over 23 Ma ago,
30 during the Oligocene.

37 The new evidence of the age of these units shows that the Shabirinah and Brak
38 formations are comparable in age to the Marada Formation of the Sirte Basin, which ranges
39 between Aquitanian to Serravallian in age (Mastera, 1985; El Hawat and Pawellek, 2004;
40 Fig. 14). In its type area in the eastern Sirte Basin, the Marada Formation is composed of a
41 lower fluvial clastic unit, the Qarat Jahannam Member of Aquitanian to Burdigalian age
42 (Wessels et al., 2003). This is overlain by a diachronous marine carbonate-clastic unit, the
43 Ar Rahlah Member of Langhian–Serravallian age (El Hawat and Pawellek, 2004; Figs. 4,
44 14). Similar aged fluvial successions dominate in the western Sirte Basin in the Hun Graben
45 and Zallah Trough, laterally transitional to marine units to the NE. Although the dating
46 evidence (mammal fossils for the early-mid Miocene; Wessels et al., 2003) for the Marada
47 Formation may not be quite as precise as the magnetostratigraphy from the Shabirinah-
48 Brak formations, the upwards transition to carbonate-clastic units in the Kunayr Member
49 appear to be synchronous with those of the Ar Rahlah Member of the Marada Formation.
50 This evidence, plus the paleocurrent data from the Shabirinah Formation suggests that these
51 units were connected across what is now the Al Haruj al Aswad volcanic fields, which
52
53
54
55
56
57
58
59
60
61
62
63
64
65

became active later as the Sirte Basin was tilted north-westwards (Abdunaser and McCaffrey, 2015).

6. Conclusions

We provide the first detailed assessment of the lithostratigraphy of the Lake Megafezzan sediments, as represented by the Al Mahruqah Group, dividing them into three unconformity-bound packages. The oldest of these packages, the Shabirinah and Brak formations are a succession of lacustrine and fluvial units locally with humid paleosols in its lower parts, which progressively show evidence of semi-arid paleosol development up through the succession, culminating in the palustrine limestone unit represented by the Brak Formation.

Paleomagnetic data from 124 samples, demonstrate the Shabirinah and Brak formations hold a magnetic polarity stratigraphy, which is carried by a combination of magnetite and haematite. The mean directions obtained concur with the expected paleopoles position for Africa in the Miocene to recent interval. A composite polarity succession has 10 major reverse and normal polarity magnetozone couplets, estimated to span ca. 9 Ma. Sequence slotting methods are used to quantitatively correlate the magnetozone composite to the geomagnetic polarity timescale, demonstrating that these formations are lower to mid Miocene in age, 12 to 23 Ma older than previously implied by $^{230}\text{Th}/\text{U}$ dating. The new dating broadly confers with Ar/K dates from the Jabal as Sawda lavas, which are probably interbedded with the sediment succession around the lower to mid parts of the Brak Formation. Attempts at Th/U dating of these successions are strongly impacted by mid and late Pleistocene U-mobility in ground water, and do not reflect sediment deposition ages.

Three main phases of lacustrine limestones developed. During the late Aquitanian a widespread stromatolitic lake developed in the SE Fezzan, which passes laterally into basin margin fluvial clastic units. During the late Burdigalian palustrine carbonate units typically pass laterally into mixed clastic to more calcretised palustrine units which characterise basin margin situations. The Serravallian age Brak Formation, a palustrine unit is a high-stand deposit showing the maximum likely extent and elevation of lake levels in a more extensive Fezzan Basin, although its basin centre lateral equivalent, is not seen. These formations largely developed prior to the development of the volcanic centres in the western fringes of the Sirte Basin, and suggest the major drainage networks of the Libyan Sahara developed prior to 23 Ma in the Oligocene. Increasing paleosol modification of the lake carbonates develop upwards through these successions and are the response to increasing soil-moisture deficits. The increasing prevalence of lacustrine limestones may be due to the development of a larger topographic basin in the Fezzan with the initial growth of the Jabal

1 as Sawda volcanic centre and associated uplift of the SW shoulder of the Sirte Basin,
2 progressively restricting water into the Fezzan basin. Alternatively, the maximum
3 Serravallian expansion may relate to maximum development of fluvial systems across the
4 whole central Sahara during the mid Miocene. These results show the hyper-aridity of the
5 central Sahara must have developed after about 11 Ma.
6

7 Supplementary data to this article can be found online at <http://dx.doi.org/10.xxx>
8
9

10 **Acknowledgements**

11
12
13 Field work logistics would not have been possible without Toby Savage and Kevin
14 White. Support was from Repsol/REMSA and David Mattingly's field teams (supported from
15 the Society for Libyan Studies Desert Migrations Project) along with logistic and financial
16 support provided by the University of Benghazi Research Centre. The Libyan Dept of
17 Antiquities assisted with desert permits. Some paleomagnetic data was measured by Matt
18 Riding, but most was obtained by HEW during a self-funded PhD. NIGL colleagues Nick
19 Roberts, Neil Boulton and Diana Sahy assisted with the U-Pb and U-Th work which was
20 funded by NIGL project IP-1180-0510 to Sue McLaren.
21
22
23
24
25
26
27

28 **References**

- 29
30
31 Abdeldayem, A. L., 1996. Palaeomagnetism of some Miocene rocks, Qattara depression,
32 Western Desert, Egypt. *Journal of African Earth Science*, 22, 525-533.
33
34
35 Abdi, H., 2010. Congruence: Congruence coefficient, RV -coefficient, and Mantel coefficient.
36 In: Salkind, N. (Ed.), *Encyclopaedia of Research Design*. Thousand Oaks, CA, Sage,
37 pp. 223-230.
38
39
40 Abdullah, M., 2010. Petrography and Facies of the Al- Mahruqah Formation in the Murzuq
41 Basin, SW Libya. (PhD thesis), Universität Hamburg.
42
43
44 Abdunaser, K. M., McCaffrey, K. J., 2015. Tectonic history and structural development of
45 the Zallah-Dur al Abd Sub-basin, western Sirt Basin, Libya. *Journal of Structural*
46 *Geology*, 73, 33-48.
47
48
49 Abouessa A., Pelletier J., Durringer P., Schuster M., Schaeffer P., Métais E., Benammi M.,
50 Salem M., Hlal O., Brunet M., Jaeger J-J., Rubino J-L., 2012. New insight into the
51 sedimentology and stratigraphy of the Dur At Talah tidal-fluvial transition sequence
52 (Eocene–Oligocene, Sirt Basin, Libya). *Journal of African Earth Sciences* 65, 72–90.
53
54
55 Ade-Hall, J.M., Reynolds, P.H., Dagle, P., Mussett, A.E., Hubbard, T.P., 1975. Geophysical
56 studies of North African Cenozoic volcanic areas: II. Jebel Soda, Libya. *Canadian*
57 *Journal of Earth Sciences*, 12, 1257–1263.
58
59
60 Albritton, C. C., Brooks, J. E., Issawi, B., Swedan, A. 1990. Origin of the Qattara depression,
61 Egypt. *Geological Society of America Bulletin*, 102, 952-960.
62
63
64
65

- 1
2
3
4
5
6
7
8
9
10
11
12
13
14
15
16
17
18
19
20
21
22
23
24
25
26
27
28
29
30
31
32
33
34
35
36
37
38
39
40
41
42
43
44
45
46
47
48
49
50
51
52
53
54
55
56
57
58
59
60
61
62
63
64
65
- Alonso-Zarza, A. M., 2003. Palaeoenvironmental significance of palustrine carbonates and calcretes in the geological record. *Earth-Science Reviews*, 60, 261-298.
- Armitage, S.J., Drake, N.A., Stokes, S., El-Hawat, A., Salem, M.J., White, K., Turner, P., McLaren, S.J., 2007 Multiple phases of North African humidity recorded in lacustrine sediments from the Fezzan Basin, Libyan Sahara. *Quaternary Geochronology*, 2, 181–186.
- Bardintzeff, J. M., Deniel, C., Guillou, H., Platevoet, B., Télouk, P., Oun, K. M., 2012. Miocene to recent alkaline volcanism between Al Haruj and Waw an Namous (southern Libya). *International Journal of Earth Sciences*, 101, 1047-1063.
- Benammi, M., Jaeger, J. J. 2001. Magnetostratigraphy and palaeontology of the continental Middle Miocene of the Aït Kandoula Basin, Morocco. *Journal of African Earth Sciences*, 33(2), 335-348.
- Blondel, T. J. A., Gorin, G. E., Jan Du Chene, R., 1993. Sequence stratigraphy in coastal environments: sedimentology and palynofacies of the Miocene in central Tunisia. In: Posamentier, H.W., Summerhayes, C.P., Haq, B.U., Allen, G.P. (Eds.), *Sequence stratigraphy and facies Associations*. Special Publication of the International Association of Sedimentologists, vol. 18, p161-179, Blackwell Publishing, Oxford.
- Stoetzel, E. 2013. Late Cenozoic micromammal biochronology of northwestern Africa. *Palaeogeography, Palaeoclimatology, Palaeoecology*, 392, 359-381.
- Berendeyev, N.S., 1985. Geological map of Libya 1:250,000, Sheet: Hamādat Tanghirt (NH 32-16) Explanatory Booklet. Industrial Research Centre, Tripoli.
- Beyer, C. 2008. Establishment of a chronostratigraphical framework for the As Sahabi sequence in NE Libya. In: Boaz, N.T., El-Arnauti, A. Pavlakis, P. & Salem, M.J. *Circum-Mediterranean Geology and Biotic evolution of the Neogene Period: The perspectives from Libya*. Garyounis University Scientific Bulletin, Special Issue no.5, pp. 59-69.
- Boaz, N. T., El-Arnauti, A., Agustí, J., Bernor, R. L., Pavlakis, P., Rook, L. 2008. Temporal, lithostratigraphic, and biochronologic setting of the Sahabi Formation, North-Central Libya. In: Salem, M.J. (Ed.), *Geology of East Libya: Third Symposium on the Sedimentary Basins of Libya*, Vol. 3, pp. 959-972, Earth Science Society of Libya, Tripoli.
- Bradshaw, C. D., Lunt, D. J. Flecker, R. Salzmann, U., Pound, M. J., Haywood, A. M., Eronen, J. T., 2012. The relative roles of CO₂ and paleogeography in determining Late Miocene climate: results from a terrestrial model-data comparison. *Climates of the Past Discussions* 8, 715–786.
- Candy, I., Black, S., Sellwood, B. W. 2004. Quantifying time scales of pedogenic calcrete formation using U-series disequilibria. *Sedimentary Geology*, 170, 177-187.
- Cheng, H., Edwards, R.L., Shen, C.C., Polyak, V.J., Asmerom, Y., Woodhead, J., Hellstrom, J., Wang, Y., Kong, X., Spötl, C. and Wang, X., 2013. Improvements in ²³⁰Th dating, ²³⁰Th and ²³⁴U half-life values, and U–Th isotopic measurements by multi-collector inductively coupled plasma mass spectrometry. *Earth and Planetary Science Letters*, 371, 82-91.
- Clark, R.M., 1985. A FORTRAN program for constrained sequence-slotting based on minimum combined path length. *Computers & Geosciences*, 11, 605–617.

- 1
2
3
4
5
6
7
8
9
10
11
12
13
14
15
16
17
18
19
20
21
22
23
24
25
26
27
28
29
30
31
32
33
34
35
36
37
38
39
40
41
42
43
44
45
46
47
48
49
50
51
52
53
54
55
56
57
58
59
60
61
62
63
64
65
- Collomb, G.R., 1962. E'tude geologique du Jabal Fezzan et de sa bordure Paléozoïque. Notes Mémoire, Compagnie Française des Pétroles, 1, 35.
- Cook, T. D., Murray, A. M., Simons, E. L., Attia, Y. S., Chatrath, P., 2010. A Miocene selachian fauna from Moghra, Egypt. *Historical Biology*, 22, 78-87.
- Cremaschi, M., Zerboni, A., 2009. Early to Middle Holocene landscape exploitation in a drying environment: two case studies compared from the central Sahara (SW Fezzan, Libya). *Comptes Rendus Geoscience*, 341, 689-702.
- Cvetković, V., Toljić, M., Ammar, N. A., Rundić, L., Trish, K. B., 2010. Petrogenesis of the eastern part of the Al Haruj basalts (Libya). *Journal of African Earth Sciences*, 58, 37-50.
- Domaci, L., Röhlich, P., Bosak, P., 1991. Neogene to Pleistocene continental deposits in the northern Fezzan and central Sirt Basin. In: Salem M.J., Beliad, M.N. (Eds.), *The geology of Libya*, Elsevier, Amsterdam, Vol. 5, pp. 1785-1801.
- Douarin, M., Elliot, M., Noble, S. R., Sinclair, D., Henry, L. A., Long, D., Moreton, S.G., Roberts, J. M. 2013. Growth of north-east Atlantic cold-water coral reefs and mounds during the Holocene: a high resolution U-series and 14 C chronology. *Earth and Planetary Science Letters*, 375, 176-187.
- Drake, N.A., El-Hawat, A.S., Turner, P., Armitage, S.J., Salem, M.J., White, K.H., McLaren, S., 2008. Palaeohydrology of the Fezzan Basin and surrounding regions: the last 7 million years. *Palaeogeography, Palaeoclimatology, Palaeoecology*, 263, 131-145.
- Drake, N.A., Blench, R.,M., Armitage, S.J., Bristow, C.S. White, K.H., 2011a. Ancient watercourses and biogeography of the Sahara explain the peopling of the desert. *Proceedings of the National Academy of Sciences USA*, 108, 458-462.
- Drake, N.A., Salem, M.J., Armitage, S.J., Francke, J., Hounslow, M.W., Hlal, O., White, K.H., El-Hawat, A., 2011b. DMP XV: Palaeohydrology and Palaeoenvironment: Initial results and report of 2010 and 2011 Fieldwork. *Libyan Studies* 42, 139-149.
- Drake, N. A., Breeze, P., Parker, A., 2013. Palaeoclimate in the Saharan and Arabian Deserts during the Middle Palaeolithic and the potential for hominin dispersals. *Quaternary International*, 300, 48-61.
- El Ebaidi S.A, Abdulsamad, E.O., 2005. Petrography and evaluation of some Meso-Cenozoic raw materials deposits in Murzuq Basin, SW Libya: review and contribution. *The Fourth International Conference on the Geology of Africa*, Vol. 2, pp. 255-26. Assiut, Egypt.
- El-Hawat, A.S., 1980. Carbonate-terrigenous cyclic sedimentation and palaeogeography of the Marada Formation (Middle Miocene), Sirt Basin. In: Salem, M.J., Busrewil, M.T. (Eds.), *The Geology of Libya*, Vol. 3. London, Academic Press pp. 427-448.
- El Hawat, A.S., 2008. The Pre-Messinian Miocene stratigraphy and sedimentation in the Marada-Zaltan area, Sirt Basin, Libya. In: Boaz, N.T., El-Arnauti, A. Pavlakis, P., Salem, M.J. (Eds.), *Circum-Mediterranean Geology and Biotic evolution of the Neogene Period: The perspectives from Libya*. Garyounis University Scientific Bulletin, Special Issue no.5, pp. 23-32.
- El- Hawat, A.S., Pawellek, T., 2004. A field guidebook to the geology of Sirt Basin, Libya. *RWE Dea North Africa*, 73p.

- 1
2
3
4
5
6
7
8
9
10
11
12
13
14
15
16
17
18
19
20
21
22
23
24
25
26
27
28
29
30
31
32
33
34
35
36
37
38
39
40
41
42
43
44
45
46
47
48
49
50
51
52
53
54
55
56
57
58
59
60
61
62
63
64
65
- El Hawat, A. S. & Salem, M. J., 1987. A case study of the stratigraphic subdivision of Ar-Rajmah Formation and its implication on the Miocene of Northern Libya. In: Deák, M. (Ed.), VIII'th Congress of the Regional Committee on Mediterranean Neogene Stratigraphy : Symposium on European Late Cenozoic Mineral Resources, Budapest, 15-22 September 1985, Geological Institute Yearbook, Vol. 70, pp173-183, Technical Publishing, Budapest.
- Freytet, P. & Verrecchia, E.P., 2002 Lacustrine and palustrine carbonate petrography: an overview. *Journal of Palaeolimnology*, 27, 221-237
- Fujioka, F., Chappell, J., 2011. Desert landscape processes on a timescale of millions of years, probed by cosmogenic nuclides. *Aeolian Research*, 3, 157-164.
- Gary, A.C., Johnson, G.W. Ekart, D.D., Platon E., Wakefield, M.I., 2005. A method for two-well correlation using multivariate biostratigraphical data. In: Powell, A. J., Riding, J. B. (Eds.), Recent developments in applied biostratigraphy. The Micropalaeontological Society, Special Publications, pp. 205–217.
- Gerdes, K. D. Winefield, P. Simmons M. D., Van Oosterhout, C., 2010. The influence of basin architecture and eustacy on the evolution of Tethyan Mesozoic and Cenozoic carbonate sequences. In: Van Buchem, F. S. P., Gerdes, K. D., Esteban, M. (Eds.), Mesozoic and Cenozoic carbonate systems of the Mediterranean and the Middle East: stratigraphic and diagenetic reference models. Geological Society, London, Special Publications, 329, 9–41.
- Geyh, M.A., Thiedig, F., 2008. The Middle Pleistocene Al Mahruqah Formation in the Murzuq Basin, northern Sahara, Libya evidence for orbitally-forced humid episodes during the last 500,000 years. *Palaeogeography, Palaeoclimatology, Palaeoecology* 257,1-21.
- Gordon, A.D., Clark, R.M., Thompson, R., 1988. The use of constraints in sequence slotting. In: Diday, E. (Ed.), Data analysis and informatics, V. North Holland Publishing, Amsterdam, pp. 353-364.
- Goudarzi, G.H., 1970. Geology and mineral resources of Libya -a reconnaissance. U.S. Geological Survey Professional Paper, 660, 104p.
- Grubic, A., Dimitrijevic, M., Galecic, M., Jakovljevic, Z., Komarnicki, S., Protic, D., Radulovic, P., Roncevic N.S., 1991. Stratigraphy of Western Fezzan (SW Libya). In: Salem, M.J., Belaid, M.N. (Eds.), The geology of Libya. Vol. 4, pp. 1529-1564.
- Gundobin, V.M., 1985. Geological map of Libya 1:250,000, Sheet: Qarārat al Marār (NH 33-13) Explanatory Booklet. Industrial Research Centre, Tripoli.
- Hassan, S. M., 2013. Sequence stratigraphy of the Lower Miocene Moghra Formation in the Qattara Depression, North Western Desert, Egypt. Springer Science & Business Media.
- Hilgen, F.J., Lourens, L.J., Van Dam, J.A., 2012. The Neogene Period. In: Gradstein, F. M., Ogg, J. G., Schmitz, M., Ogg, G. (Eds.), Vol. II, The geologic time scale 2012, Elsevier, pp. 923-978.
- Hounslow, M.W., McIntosh, G., 2003. Magnetostratigraphy of the Sherwood Sandstone Group (Lower and Middle Triassic), south Devon, UK: detailed correlation of the marine and non-marine Anisian. *Palaeogeography, Palaeoclimatology, Palaeoecology* 193, 325-348.

- 1
2
3
4
5
6
7
8
9
10
11
12
13
14
15
16
17
18
19
20
21
22
23
24
25
26
27
28
29
30
31
32
33
34
35
36
37
38
39
40
41
42
43
44
45
46
47
48
49
50
51
52
53
54
55
56
57
58
59
60
61
62
63
64
65
- Hounslow, M.W., 2016. Paleozoic geomagnetic reversal rates following superchrons have a fast re-start mechanism. *Nature Communications*, 7, doi:10.1038/ncomms12507
- IRC, 1985. 1:1,000000 geological map of Libya, Industrial Research Centre, Tripoli.
- Kent, J.T., Briden, J.C., Mardia, K.V., 1983. Linear and planar structure in ordered multivariate data as applied to progressive demagnetisation of palaeomagnetic remanence. *Geophysical Journal Royal Astronomical Society*, 81, 75-87.
- Koráb, T., 1984. Geological Map of Libya 1: 250 000. Sheet: Tmassah NG 33-7. Explanatory Booklet. Industrial Research Centre, Tripoli.
- Kostadinova M., Jordanova N., Jordanova D., Kovacheva M., 2004. Preliminary study on the effect of water glass impregnation on the rock-magnetic properties of baked clay. *Studia Geophysica et Geodaetica*, 48, 637-646.
- Lallier, F., Antoine, C., Charreau, J., Caumon, G., Ruiu, J., 2013. Management of ambiguities in magnetostratigraphic correlation. *Earth and Planetary Science Letters*, 371, 26-36.
- Larrasoaña J.C., Roberts, A.P., Rohling, E.J., 2013. Dynamics of green Sahara periods and their role in hominin evolution. *PLoS one* 8, doi: 10.1371/journal.pone.0076514
- Lézine, A.M., Hély, C., Grenier, C., Braconnot, P., Krinner, G., 2011. Sahara and Sahel vulnerability to climate changes, lessons from Holocene hydrological data. *Quaternary Science Reviews*, 30, 3001-3012.
- Liégeois, J. P., Benhallou, A., Azzouni-Sekkal, A., Yahiaoui, R., Bonin, B., 2005. The Hoggar swell and volcanism: reactivation of the Precambrian Tuareg shield during Alpine convergence and West African Cenozoic volcanism. In: Foulger, G.R., Hatland, J.H. Presnall, D.C., Anderson, D.L. (Eds.), *Plates, plumes and paradigms*. Geological Society of America Special Papers, 388, 379-400.
- Llinás -Agrasar, E. L., 2004. Crocodile remains from the Burdigalian (lower Miocene) of Gebel Zelten (Libya). *Geodiversitas*, 26, 309-321.
- Liu, B., Saito, Y., Yamazaki, T., Abdeldayem, A., Oda, H. Hori, K., Zhao, Q., 2001. Paleocurrent analysis for the Late Pleistocene–Holocene incised-valley fill of the Yangtze delta, China by using anisotropy of magnetic susceptibility data. *Marine Geology*, 176, 175–189.
- Lowrie, W., Alvarez, W., 1984. Lower Cretaceous magnetic stratigraphy in Umbrian pelagic limestone sections. *Earth and Planetary Science Letters* 71, 315–328.
- Lowrie, W., Kent, D.V., 2004. Geomagnetic polarity timescales and reversal frequency regimes, In: Channell, J.E.T., Kent, D.V., Lowrie, W., Meert, J. (Eds.) *Timescales of the paleomagnetic field*, American Geophysical Union, pp. 117-129.
- Man, O., 2008. On the identification of magnetostratigraphic polarity zones. *Studia Geophysica et Geodaetica*, 52, 173–186.
- Man, O., 2011. The maximum likelihood dating of magnetostratigraphic sections. *Geophysical Journal International*, 185, 133-143.

- 1
2
3
4
5
6
7
8
9
10
11
12
13
14
15
16
17
18
19
20
21
22
23
24
25
26
27
28
29
30
31
32
33
34
35
36
37
38
39
40
41
42
43
44
45
46
47
48
49
50
51
52
53
54
55
56
57
58
59
60
61
62
63
64
65
- Mannaï-Tayech, B., 2009. The lithostratigraphy of Miocene series from Tunisia, revisited. *Journal of African Earth Sciences*, 54, 53-61.
- Mannaï-Tayech, B., Otero, O., 2005. Un nouveau gisement miocène à ichthyofaune au sud de la chaîne des Chotts (Tunisie méridionale). *Paléoenvironnement et paléobiogéographie*. *Comptes Rendus Palevol*, 4, 405-412.
- Márton, E., Márton, P., Heller, F., 1980. Remanent magnetization of a Pliensbachian limestone sequence at Bakonycsernye (Hungary). *Earth and Planetary Science Letters*, 48, 218-226.
- Mastera, L., 1985. Geological map of Libya 1:250 000. Sheet Maradah (NH 34–9). Explanatory Booklet. Industrial Research Centre, Tripoli, Libya.
- McFadden, P.L., McElhinny, M.W., 1988. The combined analysis of remagnetisation circles and direct observations in paleomagnetism. *Earth Planetary Science Letters* 87, 161-172.
- McFadden, P.L., McElhinny, M.W., 1990. Classification of the reversal test in paleomagnetism. *Geophysical Journal International*, 103, 725-729.
- Morlo, M., Miller, E. R., & El-Barkooky, A. N. 2007. Creodonta and Carnivora from Wadi Moghra, Egypt. *Journal of Vertebrate Paleontology*, 27, 145-159.
- Ogg, J.G., Steiner, M.B., 1991. Early Triassic polarity time-scale: integration of magnetostratigraphy, ammonite zonation and sequence stratigraphy from stratotype sections (Canadian Arctic Archipelago). *Earth and Planetary Science Letters*, 107, 69-89.
- Ogg, J.G., 2012. Geomagnetic polarity timescale. In: Gradstein, F. M., Ogg, J. G., Schmitz, M., Ogg, G. (Eds.), Vol.1. *The geologic time scale 2012*, Elsevier, pp. 85-114.
- Olson, P., Hinnov, L., Driscoll, P., 2014. Nonrandom geomagnetic reversal times and geodynamo evolution. *Earth and Planetary Science Letters*, 388, 9–17.
- Opdyke, N.D., Channell, J.E., 1996. *Magnetic stratigraphy*. International Geophysical Series Vol. 64, Academic Press, London.
- Osmond, J. K., Dabous, A. A., 2004. Timing and intensity of groundwater movement during Egyptian Sahara pluvial periods by U-series analysis of secondary U in ores and carbonates. *Quaternary Research* 61, 85-94.
- Pachur, H.-J., Hoelzmann, P., 2000 Late Quaternary paleoecology and paleoclimates of the eastern Sahara. *Journal of African Earth Sciences* 30, 929-939.
- Paillou, P., Schuster, M., Tooth, S., Farr, T., Rosenqvist, A., Lopez S., Malezieux, J.M., 2009. Mapping of a major paleodrainage system in eastern Libya using orbital imaging radar: The Kufrah River. *Earth and Planetary Science Letters*, 277, 327–333.
- Parizek, A., Klen, L., Röhlich, P., 1984. Geological map of Libya 1:250,000, Sheet: Idri (NG 33-1), Explanatory Booklet. Industrial Research Centre, Tripoli.
- Pickford, M., 2000. Crocodiles from the Beglia Formation, Middle/Late Miocene boundary, Tunisia, and their significance for Saharan palaeoclimatology. *Annales de Paléontologie*, 86, 59–67.

- Petit-Maire, N., Delibrias, G., Gaven, C., 1980. Pleistocene lakes in the Shati area, Fezzan (27, 30'N). *Paleoecology of Africa*, 12, 289-295.
- 1
2
3
4
5
6
7
8
9
10
11
12
13
14
15
16
17
18
19
20
21
22
23
24
25
26
27
28
29
30
31
32
33
34
35
36
37
38
39
40
41
42
43
44
45
46
47
48
49
50
51
52
53
54
55
56
57
58
59
60
61
62
63
64
65
- Radivojević, M., Toljić, M., Turki, S. M., Bojić, Z., Šarić, K., Cvetković, V., 2015. Neogene to Quaternary basalts of the Jabal Eghei (Nuqay) area (south Libya): Two distinct volcanic events or continuous volcanism with gradual shift in magma composition? *Journal of Volcanology and Geothermal Research*, 293, 57-74.
- Roncevic, N.S., 1984. Geological map of Libya 1:250,000, Sheet: Hasi Anjiwal (NG 32-4) Explanatory Booklet. Industrial Research Centre, Tripoli.
- Selley, R.C., 1968. Nearshore marine and continental sediments of the Sirt Basin, Libya. *Quarterly Journal of the Geological Society, London*. 124, 419-460.
- Schlüter, J. Schultz, L. Thiedig, F., Al-Mahdi, B.O., Abu Aghreb, A.E., 2002. The Dar al Gani meteorite field (Libyan Shara): geological setting, pairing of meteorites and recovery density. *Meteorite and Planetary Science*, 37, 1079-1093.
- Schuster, M., Düringer, P., Ghienne, J.-F., Vignaud, P., Taisso, H., Likius, M.A., Brunet, M., 2006. The Age of the Sahara Desert. *Science*, 311, 821.
- Seidl, K., Röhlich, P., 1984. Geological map of Libya, 1: 250 000. Sheet Sabhá (NG 33-2), Explanatory Booklet, Industrial Research Centre, Tripoli.
- Smilde, A. K., Kiers, H.A.L., Bijlsma S., Rubingh C.M., van Erk, M.J., 2009. Matrix correlations for high-dimensional data: the modified RV-coefficient. *Bioinformatics*, 25, 401–405.
- Stoetzel, E., 2013. Late Cenozoic micromammal biochronology of northwestern Africa. *Palaeogeography, Palaeoclimatology, Palaeoecology*, 392, 359-381.
- Swezey, C.S., 2009. Cenozoic stratigraphy of the Sahara, northern Africa. *Journal of African Earth Sciences*, 53, 89-121.
- Thiedig, F.M., Oezen, D., El-Chair, M., Geyh, M.A., 2000. The absolute age of the Quaternary lacustrine limestone of the Al Mahruqah Formation — Murzuq Basin, Libya. In: Sola, M.A., Worsley, D. (Eds.), *Geological Exploration in the Murzuq Basin*. Elsevier, Amsterdam, pp. 89–116.
- Thiedig, F.M., Geyh, M.A., 2004. Zyklische lakustrine Kalke im abflusslosen Murzuq-Becken (Libyen) als Zeugnisse interglazialer Feuchtphasen in Nordafrika während der letzten 500 ka. *Beitrag zur Regionalen Geographie*, 135, 267-288.
- Thompson, R., Clark, R.M., 1989. Sequence slotting for stratigraphic correlation between cores: theory and practice. *Journal of Paleolimnology* 2, 173–184.
- Torsvik, T. H., Van der Voo, R., Preeden, U., Mac Niocaill, C., Steinberger, B., Doubrovine, P. V., van Hinsbergen D.J.J., Domeiere, M., Gaina, C., Tohver, E. , Meert, J.G., McCausland, P. J.A., Cocks, L. R. M., 2012. Phanerozoic polar wander, paleogeography and dynamics. *Earth-Science Reviews*, 114, 325-368.
- Van Velzen, A. J., Zijdeveld, J. D. A., 1992. A method to study alterations of magnetic minerals during thermal demagnetization applied to a fine-grained marine marl (Trubi formation, Sicily). *Geophysical journal international*, 110, 79-90.

1 Wanas, H.A. Pickford, M. Mein, P., Soliman, H. Segalen, L., 2009. Late Miocene karst
2 system at Sheikh Abdullah, between Bahariya and Farafra, Western Desert, Egypt:
3 implications for palaeoclimate and geomorphology. *Geologica Acta*, 7, 275-287.

4 Wessels, W., Fejfar, O., Peláez-Campomanes, P. van der Meulen, A., de Bruijn, H., 2003.
5 Miocene small mammals from Jebel Zelten, Libya. *Coloquius de Paleontologia*, Vol. 1,
6 699-715.

7 White, K., McLaren, S., Black, S., Parker, A., 2000. Evaporite minerals and organic horizons
8 in sedimentary sequences in the Libyan Fezzan: implications for palaeoenvironmental
9 reconstruction. In: McLaren, S.J., Kniveton, D.R. (Eds.), *Linking climate change to land*
10 *surface change*, Springer, Netherlands, pp. 193-208.

11 Woller, F., 1984. Geological Map of Libya 1: 250 000. Sheet: Al Fuqaha (NG 33-3).
12 Explanatory Booklet. Industrial Research Center, Tripoli.

13 Wright, V.P. & Platt, N.H., 1995 Seasonal wetland carbonate sequences and dynamic
14 catenas: a re-appraisal of palustrine limestones. *Sedimentary Geology*, 99, 65-71

15 Zaki A., Abdel-Fattah, Z. A., Kora, M. A., & Ayyad, S. N., 2013. Facies architecture and
16 depositional development of Middle Miocene carbonate strata at Siwa Oasis,
17 Northwestern Egypt. *Facies*, 59, 505-528.

18 Zhang, Z., Ramstein, G., Schuster, M., Li, C., Contoux, C. Yan, Q., 2014. Aridification of the
19 Sahara desert caused by Tethys Sea shrinkage during the late Miocene. *Nature*, 513,
20 401-404.

31 **Figure and Table Captions.**

32 Fig. 1. Outline geology of the Fezzan with location of map figure inserts indicated. The
33 eastern outcrop edge of the SW fringe of the Sirte Basin is indicated by the
34 Paleogene escarpment, and to the north the southern edge of the Ghadamas Basin
35 is the Al Hamadah al Hamra escarpment (both shown as Paleogene outcrop). The
36 data defined the topographic depression of the Fezzan Basin. Position of this larger
37 map is shown on the Libya in the corner. Important troughs and uplifts shown,
38 indicate by major fault-bounding systems in the SW Sirte Basin. Large grey arrows
39 are hypothesised drainage exists from the Fezzan Basin referred to as the northerly
40 Wadi Nashu, and easterly Wadi Barjuj exits (Drake et al., 2008, 2011a). Locations of
41 detailed maps and cross-sections in Figs. 4,5,7,8,9 also shown. Map simplified and
42 based on IRC (1985).

43 Fig. 2. New lithostratigraphy of the Al Mahruqah Group in the Fezzan, with major events and
44 features indicated. Major erosion/deflation events indicated (in light grey), which sub-
45 divide the new formations.

46 Fig. 3. Regional stratigraphic relationships of the Miocene and younger sediments in the
47 Fezzan study area, based on this work. The Zarzur Formation ages are inferred
48
49
50
51
52
53
54
55
56
57
58
59
60
61
62
63
64
65

based on this work and Armitage et al. (2007). Data for the Sirte Basin from El-Hawat (1980), El Hawat and Pawellek (2004).

1
2
3
4
5
6
7
8
9
10
11
12
13
14
15
16
17
18
19
20
21
22
23
24
25
26
27
28
29
30
31
32
33
34
35
36
37
38
39
40
41
42
43
44
45
46
47
48
49
50
51
52
53
54
55
56
57
58
59
60
61
62
63
64
65

Fig. 4. Locations of sections shown in Fig. 7, along the Wadi ash Shati to Wadi Kunayr depression. The dark coloured Paleozoic formations are clearly shown to the north side of the Wadi ash Shati to Ar Ramish as Saghirah region. The pale-coloured Shabirinah Formation in the east (section SK7, SK8) can clearly be seen overstepping onto the Paleozoic. Image from bing.co.uk. The highest elevation Zarzur Formation is 379 m at Bir az Zallaf, the lowest elevation Shabirinah Formation in the east of this map is at around 395 m, similar to that at the SK3 site (Fig. 7). Line of cross-section shown in Fig. 9 is dashed line.

Fig. 5. The figured sections and locations in the Tmassah- Wadi ash Shabirinah areas. The Stromatolite Member in the Sarir al Qattusah can be traced a further 70 km north of the map boundary, along the bright coloured ground in the satellite image- along the Qattusah corridor. Base image from Bing.co.uk. The solid grey lines are supposed track/roadways. To the north and NW of the map the Brak and Shabirinah formations range up to elevations of 500- 510 m. Some 30 km south of the TS2/TS3 sections the Jurassic-Cretaceous basement of the Dur an Naqah rises (off the map shown) to above 500 m elevation.

Fig. 6. Schematic relationships of sections east of Tmassah, in the area north of Wadi ash Shabirinah. GE= Google Earth elevation on section top or bottom. Log key in Fig. 10. Same vertical scale for all sections, except TS3 and TS3, which are shrunk to fit the Google Earth elevations. Distances (arrows) between sections indicated. Location of sections shown on Fig. 5.

Fig. 7. Schematic section correlations and heights along North side of Wadi ash Shati towards Wadi Kunayr area. See Fig. 4 for locations. Vertical filled bars (grey) show the height ranges of the plateau formed on the top of the Brak Formation, implying the Brak Formation extends to these maximum elevations (tops of bars) at these locations. Those locations with existing logs, have the top of the logs located at the estimated lowest plateau elevation to determine the base of the Brak Formation. Dashed line is the elevation of the Paleozoic basement. All sections with same metre scale, as shown on the right. Heights from Google Earth. Section SK1, SK2 and SK6 logs from Abdullah (2010). Also shown are the equivalent Geyh and Theidig (2008) sites. Log key in Fig. 10.

Fig. 8. Interpreted geological cross-section from the North side of Wadi Kunayr through section SK8 to the NNE. Topography shown as thick solid line. Elevations from Google Earth. Based on our interpretation of the Al Fuqha geological map (Woller, 1984). Woller (1984) wrongly interpret the Mahruqah Group outcrops as the Maastrichtian Bin Affin Member in parts of the Wadi Kunayr area. G&T= Geyh and

Theidig (2008). A photo of the clastic units in the deepest endoreic depression is shown as Plate 5a in Theidig et al. (2000). To the south of section SK8 basement rises again to 480-490 m elevation within 16 km.

Fig. 9. Sketch section through Wadi ash Shati, showing the height arrangement of the formations. The projected 'basin-fill' for the Brak Formation in the Wadi ash Shati basin (at section location) is around 445m. Heights from Google Earth. Location of section on Figs. 1, 4. Current topography is thick black line.

Fig. 10. Section logs and summary horizon magnetic polarity data for the sections. Width of the bar in the polarity boxes indicates the confidence in the polarity information obtained from the two to three specimens from each sample level. Selected positions (ticks on log) of samples illustrated here marked with sample code.

Fig. 11. Representative demagnetisation data from the Al Mahruqah Group. A,B)= section SK8; C,D)= section SK3, E,F)=section TS3. A) Specimen AP2A, normal polarity (N, behaviour S2), showing a ChRM from 400 to 570°C. B) AP46C, reverse polarity (R, behaviour T2), showing low temperature component from NRM to 350°C, above which an erratic trend towards reverse polarity is evident from 500°C. C) BC18A, normal polarity (N?, behaviour T2), showing low temperature component from NRM to 400°C. A ChRM great circle is fitted from 490°C to origin. D) BC22, reverse polarity (R?, behaviour T1), showing component A NRM to 300°C, with ChRM great circle plane fitted from 300°C to origin. E) TM71, reverse polarity (R, behaviour S2), showing a ChRM from 510 °C to the origin. F) TM1A, reverse polarity (R??, behaviour T3), showing a strong low temperature component from 100-460°C, the steps at 520-550°C recovers a reverse component. Great circle plane fitted from 490°C to origin. See Fig. 10 for specimen locations.

Fig. 12. Detailed magnetostratigraphic data for the sections A) SK3, B) SK8 and C) TS3. In each case the columns are: i) Strength of the specimen natural remanent magnetisation (NRM), ii) Specimen demagnetisation behaviour showing categorisation into good (S1) and poor (S3) ChRM line-fits; great circle fit quality range from good (T1) to poor (T3), and specimens with erratic, interpretable magnetisation are indicated in the X column (see text for details). iii) Interpreted specimen polarity quality, with those in the mid-grey column not assigned a polarity. Poorest quality in column headed ???. iv) Specimen VGP latitude, and horizon polarity. Filled symbols= those specimens possessing an S-class ChRM, and unfilled symbols for specimens with T-class, great-circle behaviour. Polarity key in Fig.10.

Fig. 13. The two composite magnetic polarity stratigraphies (composite A (left) and B (right)) discussed in the text, and the basis of these interpretations derived from the section data. The final preferred age model using composite-B is shown on the right, with the

chron correlation lines to the geomagnetic polarity timescale (Ogg, 2012) derived from the sequence slotting (see Supplementary Data for details).

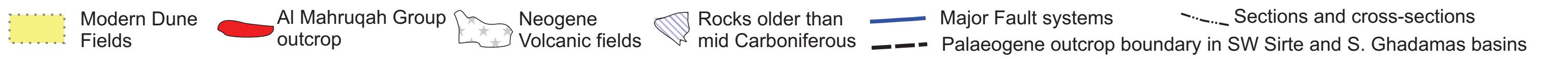
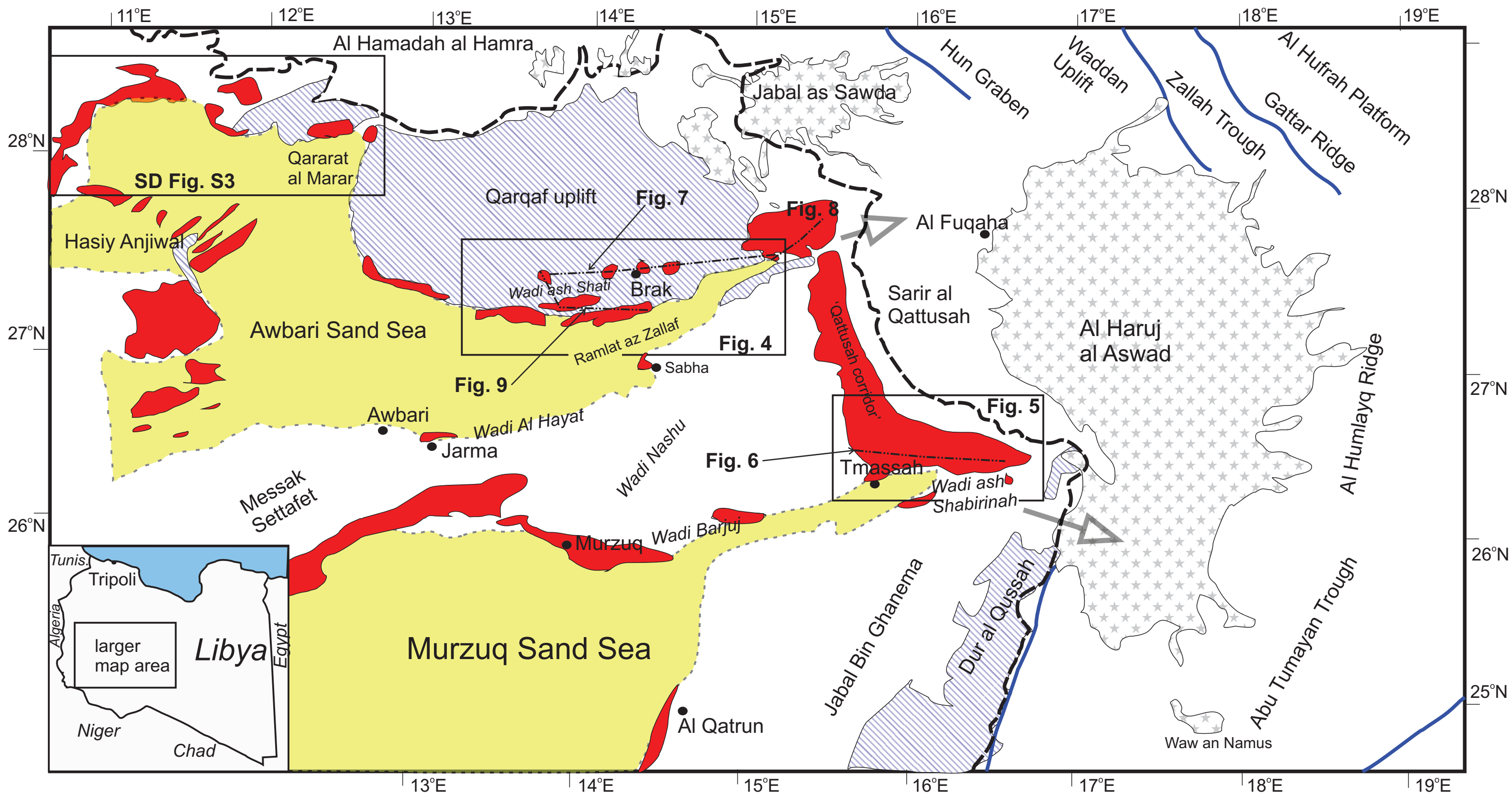
Fig. 14. Comparison of environmental systems in the early and mid Miocene between Libya, Tunisia and western Egypt. Data for Tunisia based on Blondel et al. (1993) and Mannai-Tayech (2009). Egyptian data from Albritton et al. (1990) and Hassan (2013). Sirte Basin data from El-Hawat (2008) and El-Hawat and Pawellek (2004). The chronology of the non-Fezzan Basin formation is mostly secure in the marine units (pelagic foraminifera zones indicated on Tunisia data), and is based on vertebrates in some units and lithostratigraphically inferred in other units.

Section ID	Thickness (m)	No. composite sections	No. Paleomag. samples	Stratigraphic Units
SK-3	18.9	2	25	Brak Fm, Shabirinah Fm
SK-8	39.2	4	59	Kunayr Mbr, Tmassah Mbr
TS-3	27.8	5	43	Kunayr Mbr, Tmassah Mbr, Stromatolite Mbr, Maharshim Mbr

Table 1. Sections sampled for magnetostratigraphy. See Supplementary Table S1 for latitude/longitude location information, and Figs. 4, 5 for map locations. SK sections are in the Wadi ash Shati to Wadi Kunayr area. TS sections are in the Tmassah to Wadi ash Shabirinah area. The TS3 section was also sampled for radiometric dating (Fig. 10).

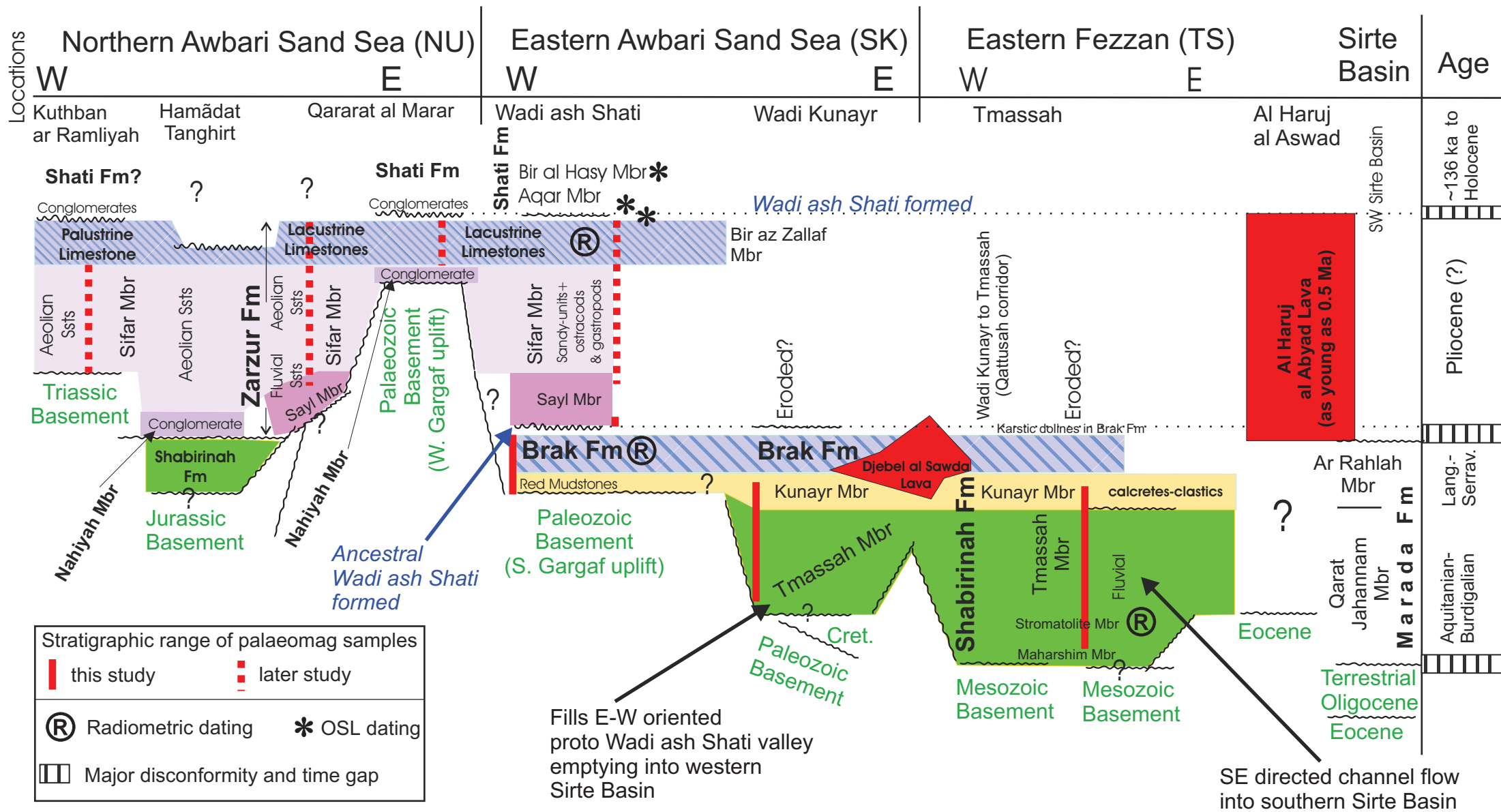
Section [code]	Mean Dec/Inc (°)	α_{95} (°)	$N_T/N_l/N_p$	Reversal Test [γ_o ; γ_c] (°)	VGP Pole Long./Lat. (°)	D_p/D_m (°)
SK3 [BC]	1.2/45.2	5.7	46/9/20	Rc [9.0;12.7]	298/89	4.5/7.2
SK8 [AP]	3.5/42.1	3.1	134/32/72	R- [7.7;6.5]	146/86	2.3/3.8
TS3 [TM]	1.1/42.9	3.8	95/19/58	Rb [1.6;7.6]	153/88	2.9/4.7

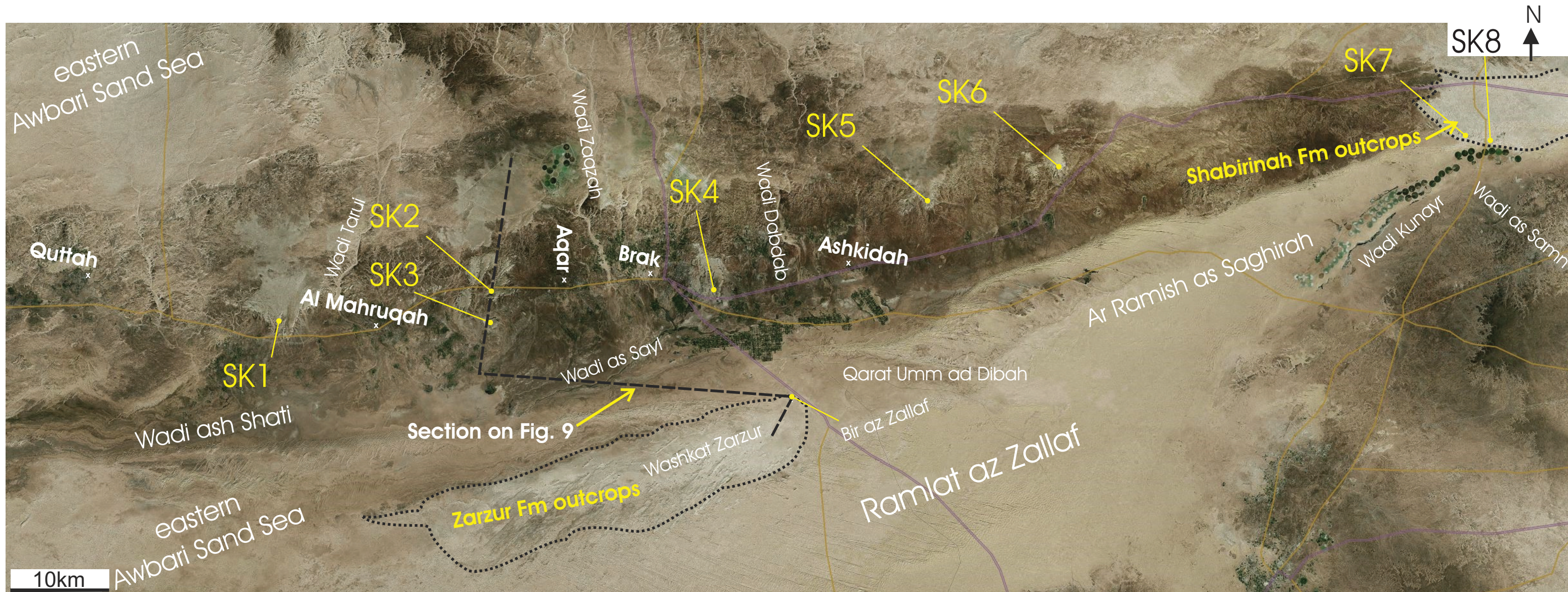
Table 2. Mean paleomagnetic directions for the three sections. Code=sample code. α_{95} =Fisher 95% cone of confidence. N_T =Total specimens measured, N_l =Number of specimens with line-fits, N_p =Number of specimens with great circle fits. For the reversal test (McFadden and McElhinny, 1990), γ_o =observed angle; γ_c =critical angle. Virtual geomagnetic pole (VGP) is the normal pole.

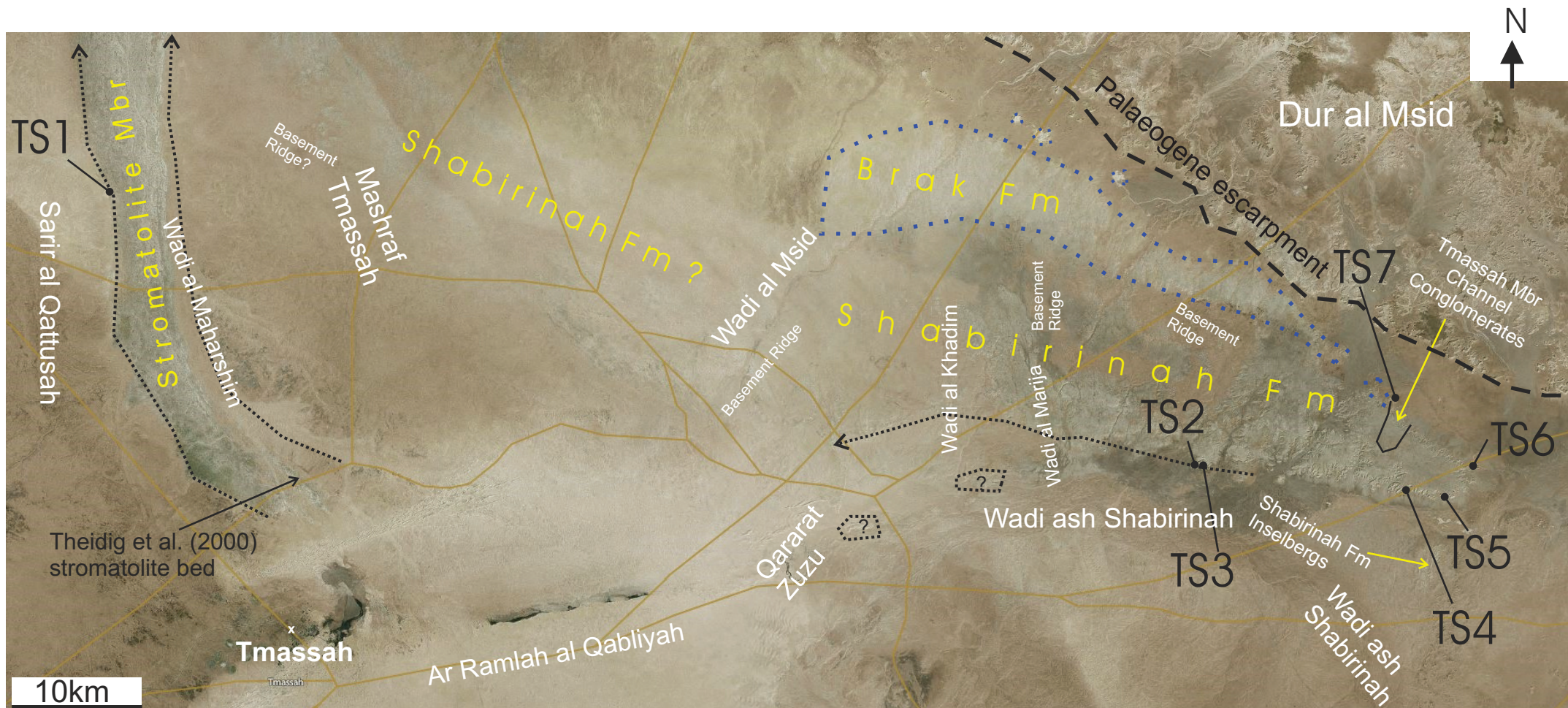


Lithostratigraphy		Key Features
Bir al Hasy Mbr	Shati Fm	Lake muds with <i>Melanoides</i>
Aqar Mbr		Lake shore cocquina
Bir az Zallaf Mbr	Zarzur Fm	<i>Fezzan-wide deflation event</i> Interbedded laminated Lmst and Ssts (ostracods, fish teeth)
Sifar Mbr		Aeolian and fluvial sandstones locally with ostracod & gastropod fauna
Nahiyah Mbr		Nahiyah Mbr = Conglomerate in N. Awbari Sand Sea
Sayl Mbr		Sayl Mbr = mudstone dominated unit
Brak Fm		<i>Deflation event forming ancestral Wadi ash Shati</i> Calcretised-palustrine, oversteps onto basement
Kunayr Mbr	Shabirinah Fm	Jabal al Sawda lavas [12 to 10 Ma] Clastic units, palustrine limestones & calcretes
Tmassah Mbr		Fluvial channel and other clastic units with palaeosols. Channels draining ESE and SE into Sirte Basin
Stromatolite Mbr		Stromatolitic limestone overlain by red mudstones
Maharshim Mbr		Palaeosols and clastics
Palaeozoic-Paleogene basement		<i>Erosion event forming Miocene drainage systems into Sirte Basin</i>

fig3.pdf

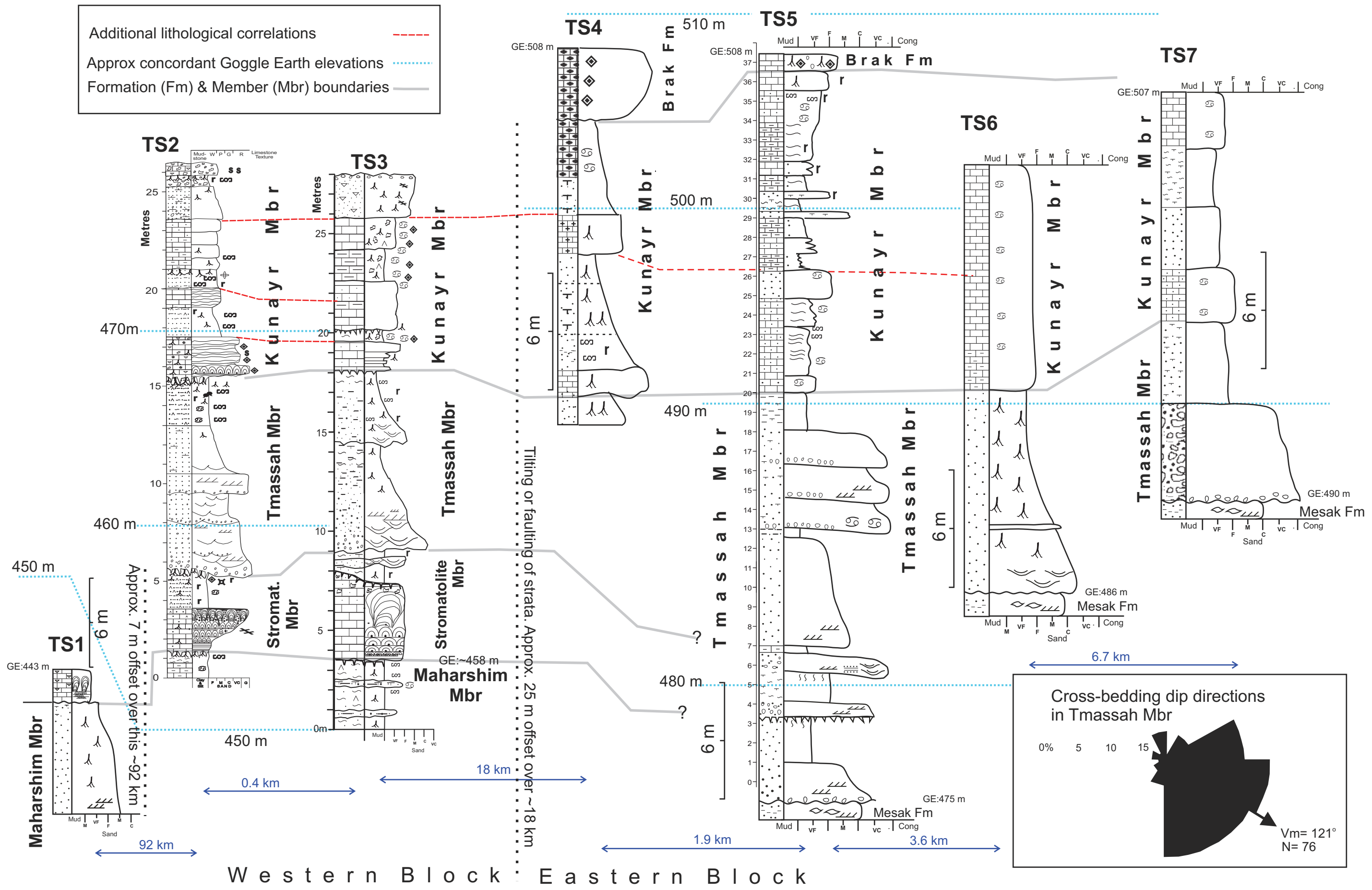


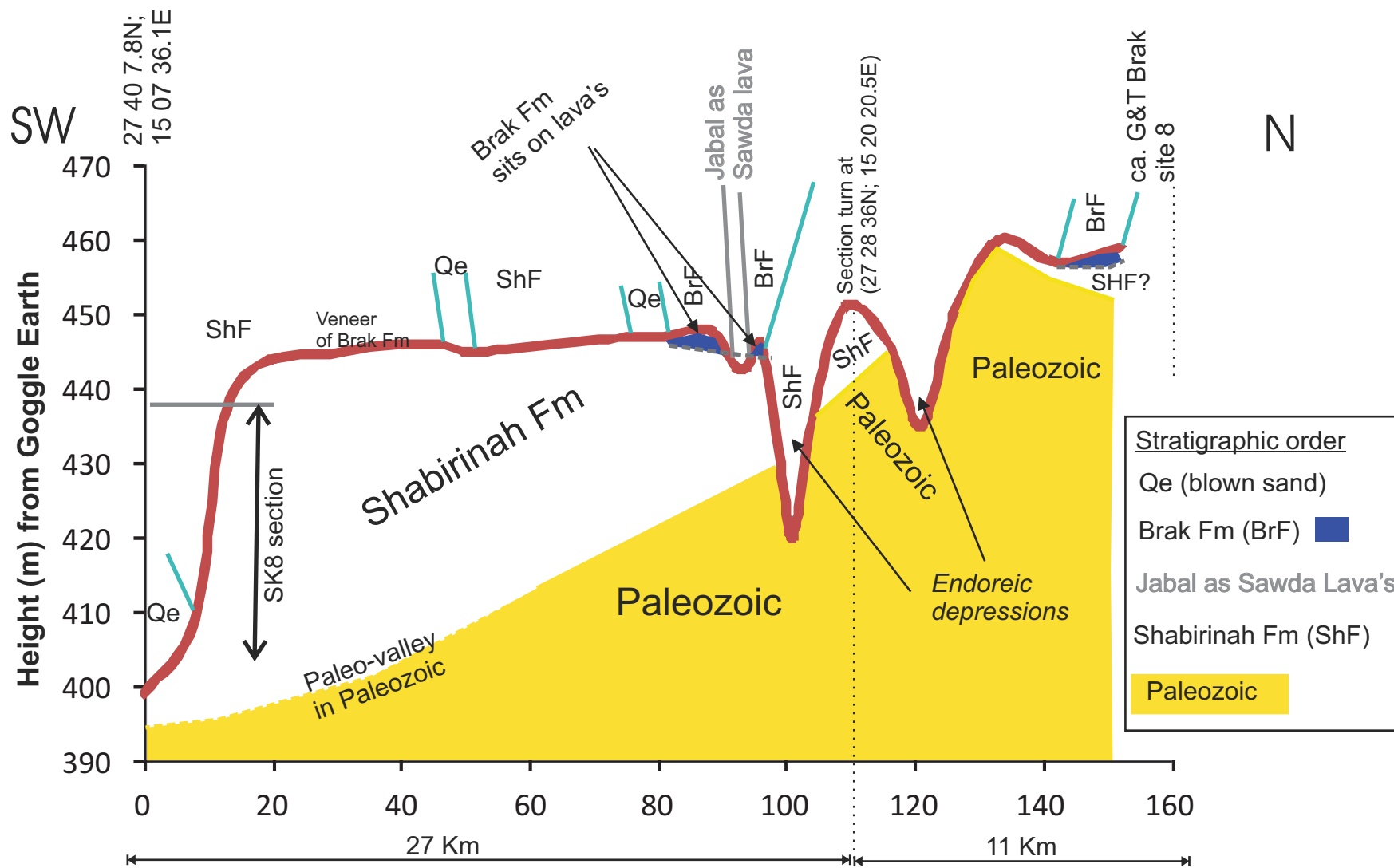


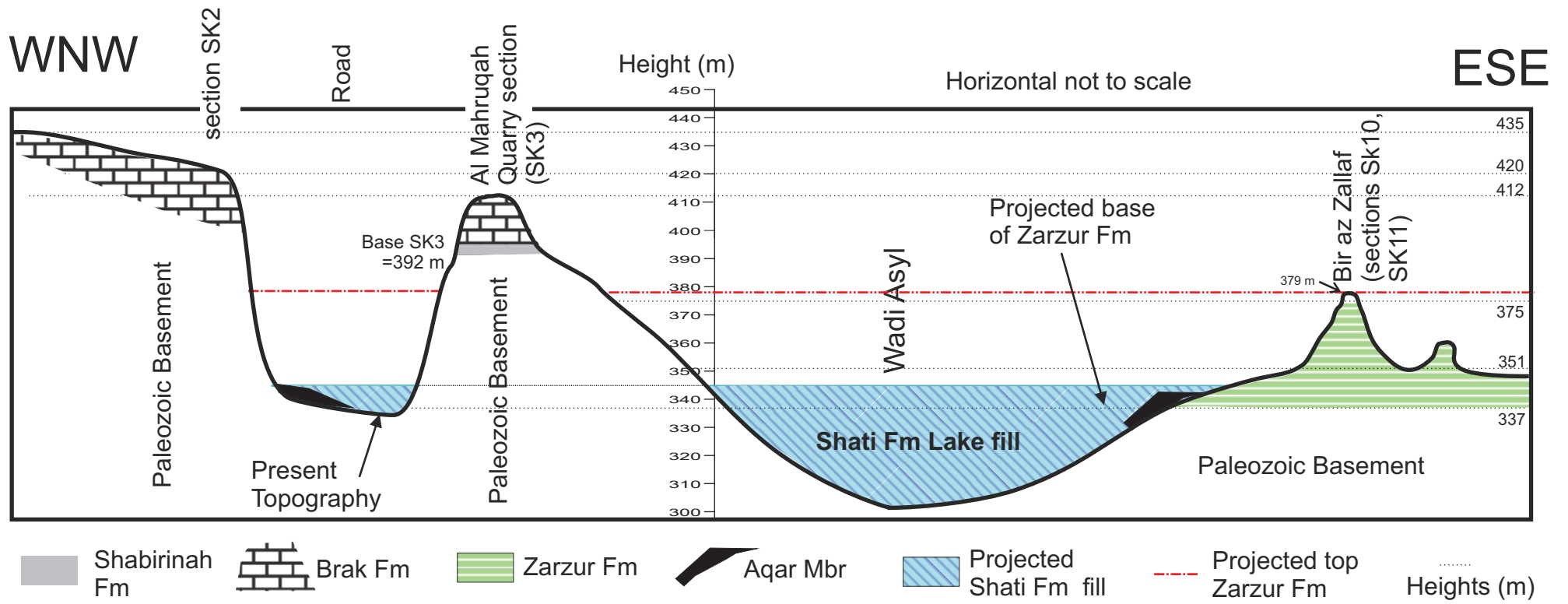


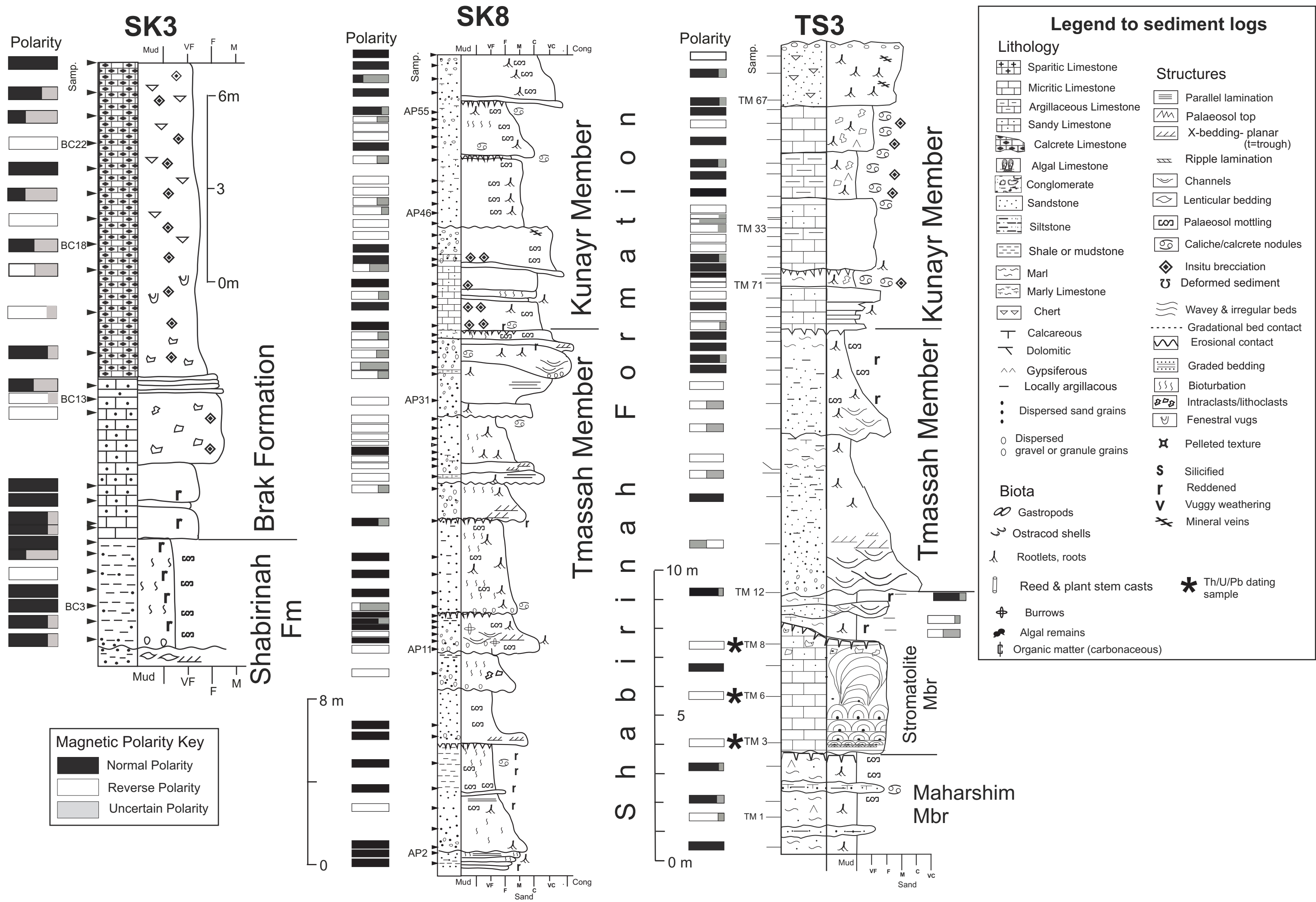
○ Observed and inferred outcrop boundary or trend of the Stromatolite Mbr

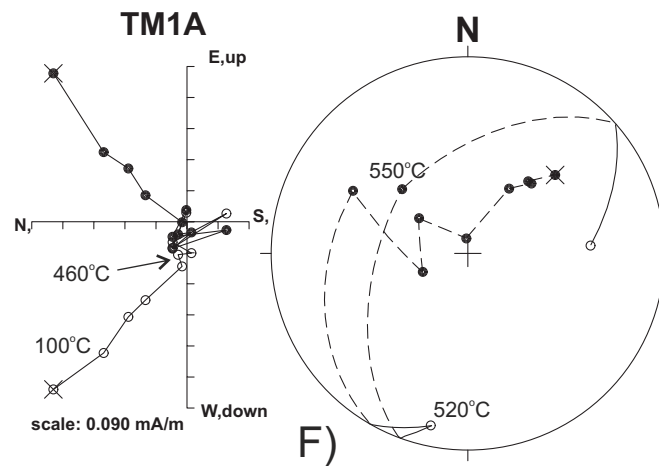
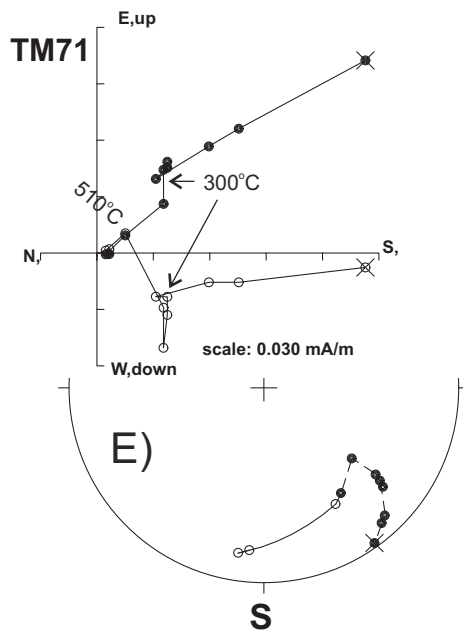
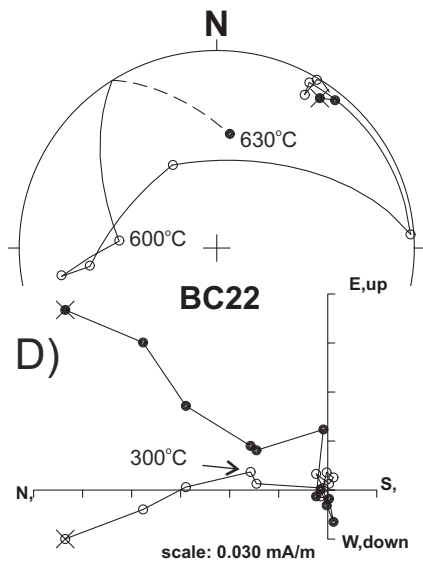
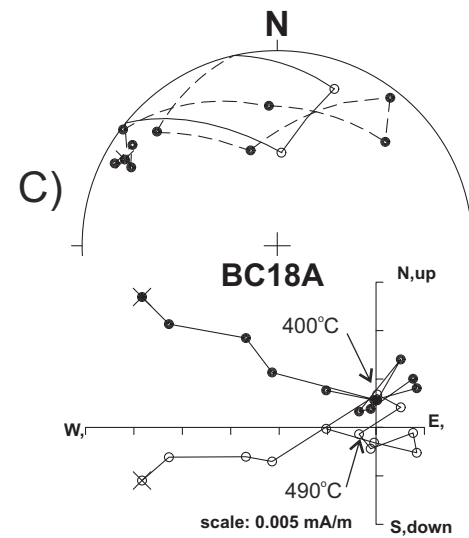
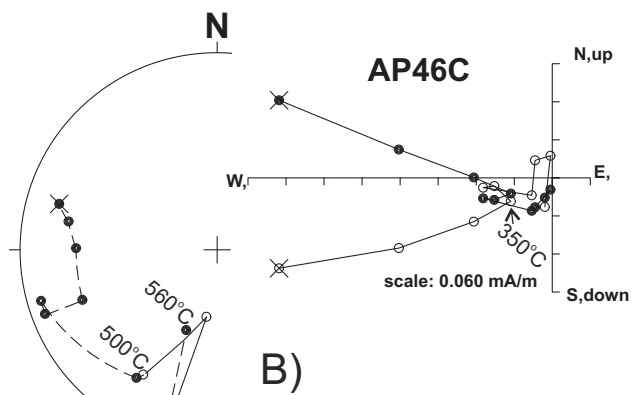
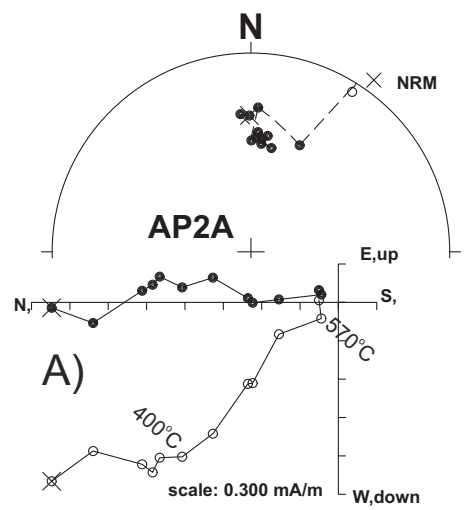
⋯ Observed and inferred outcrop of the Brak Fm

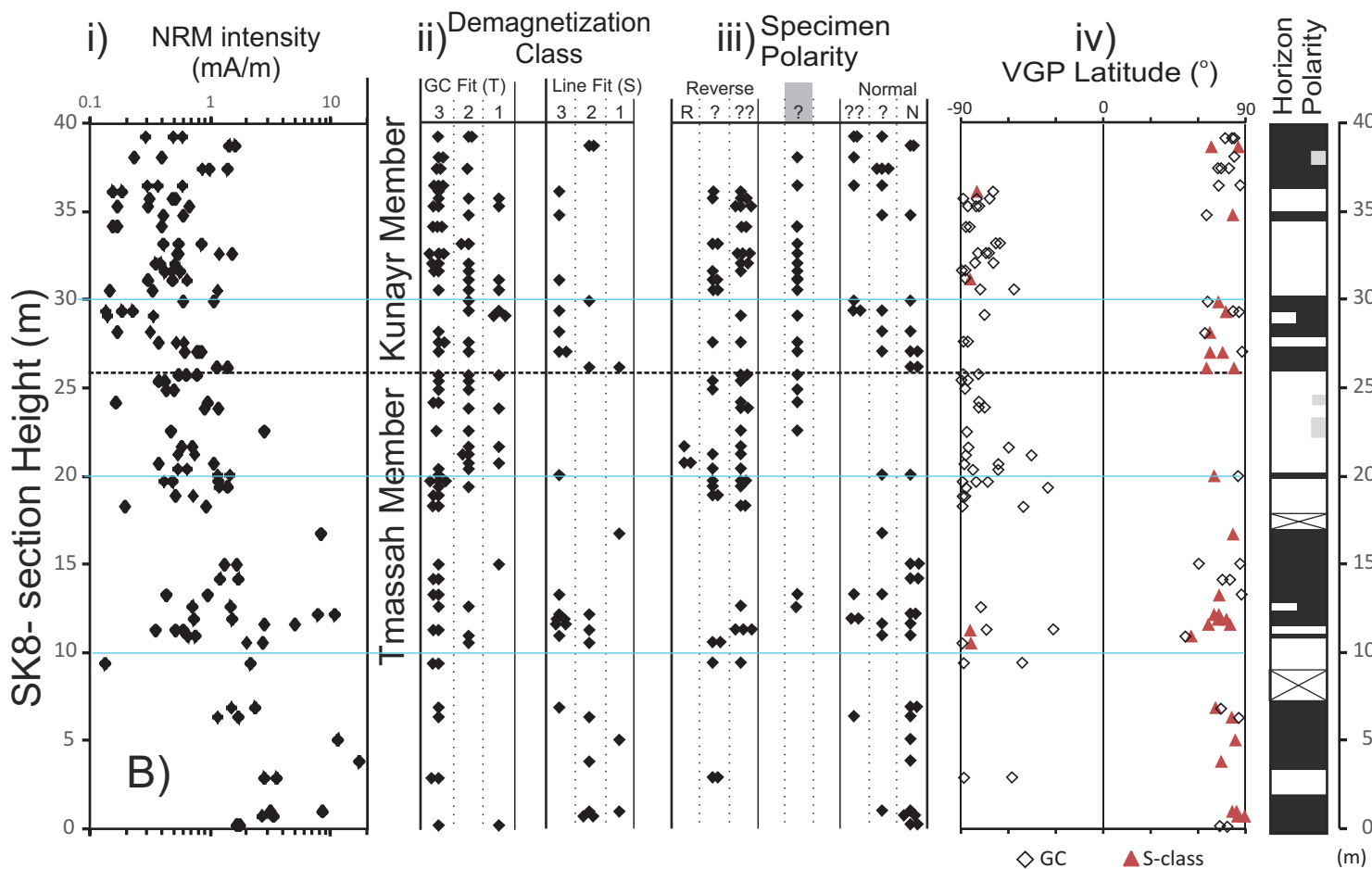
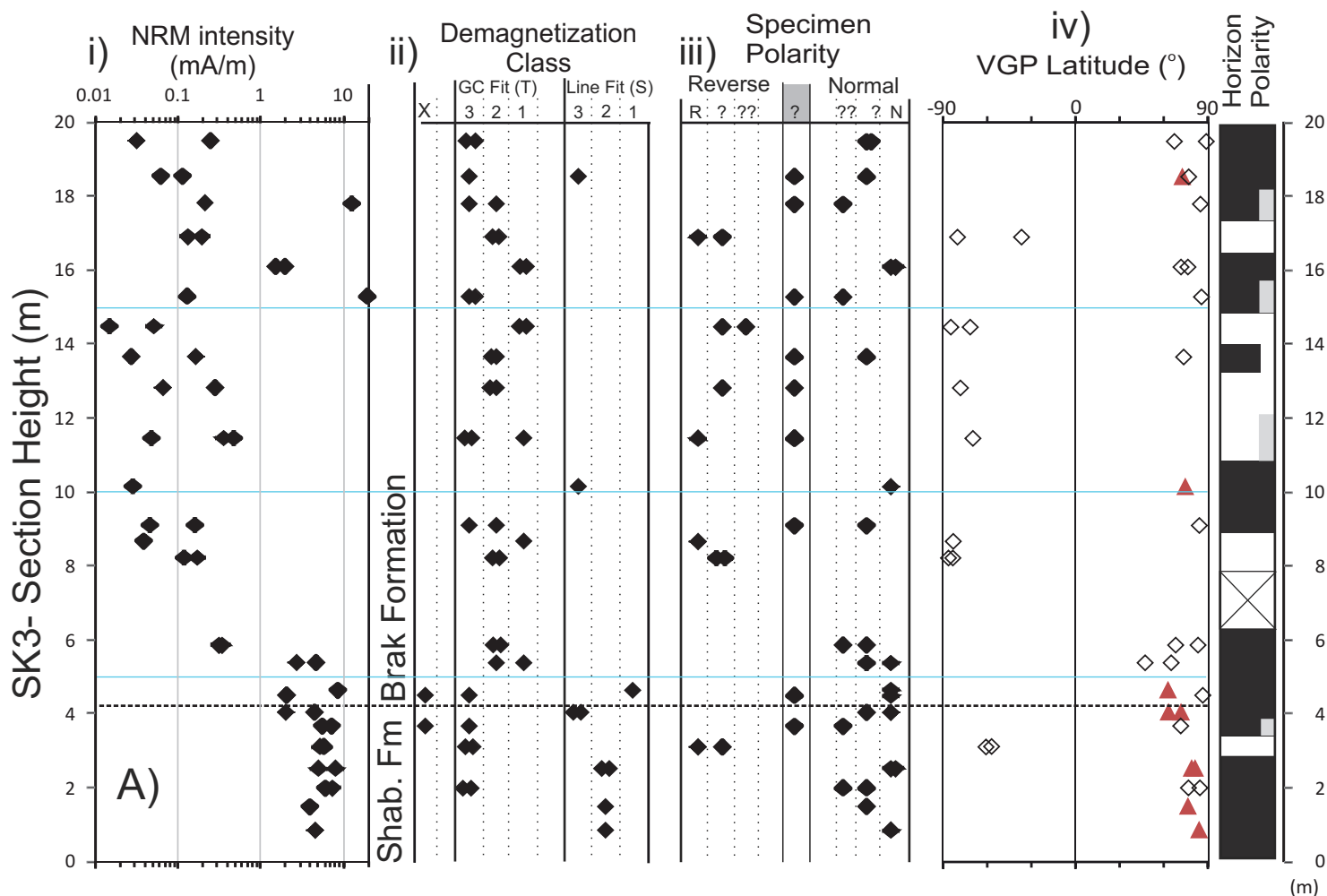












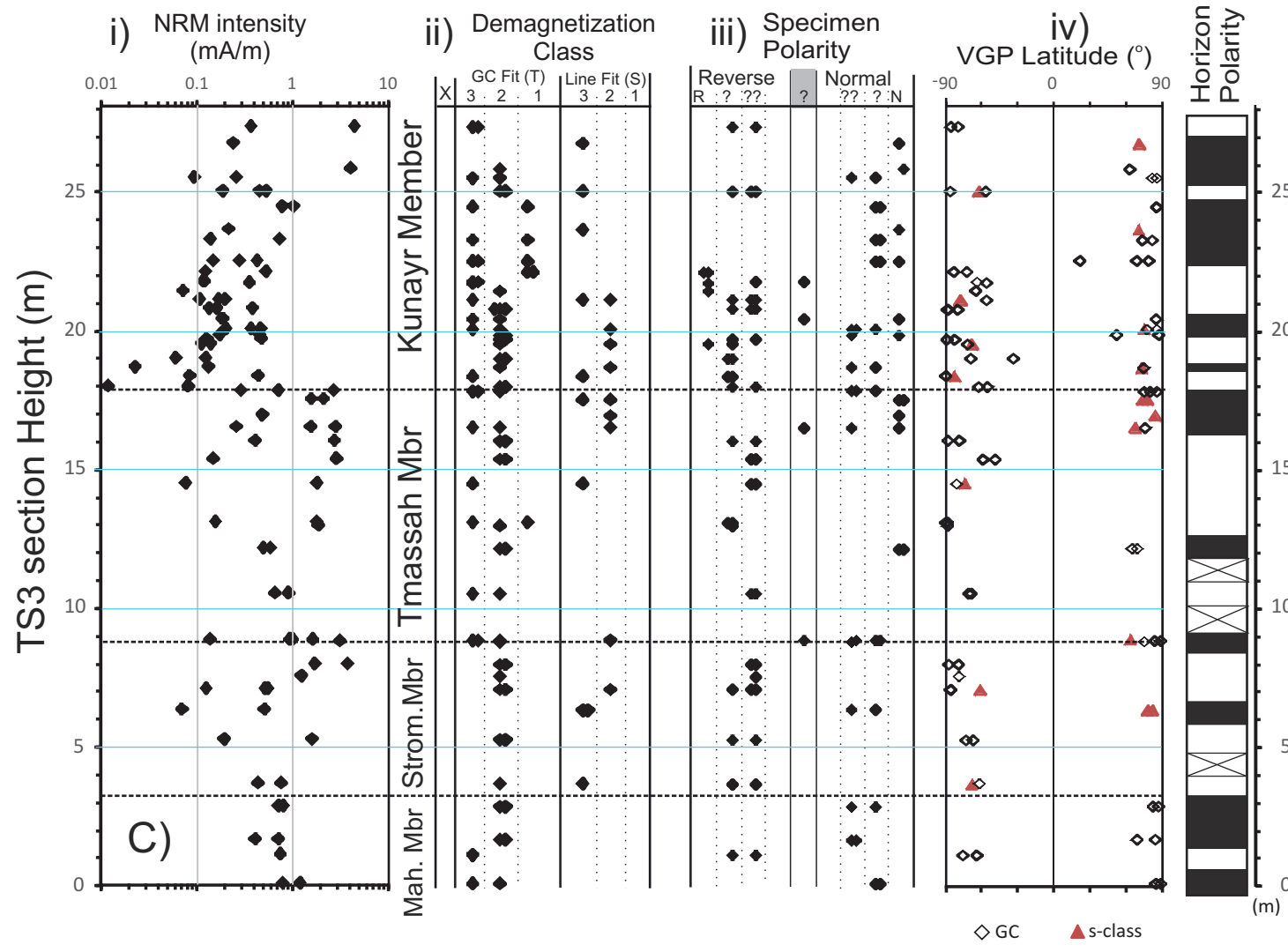


fig13.pdf

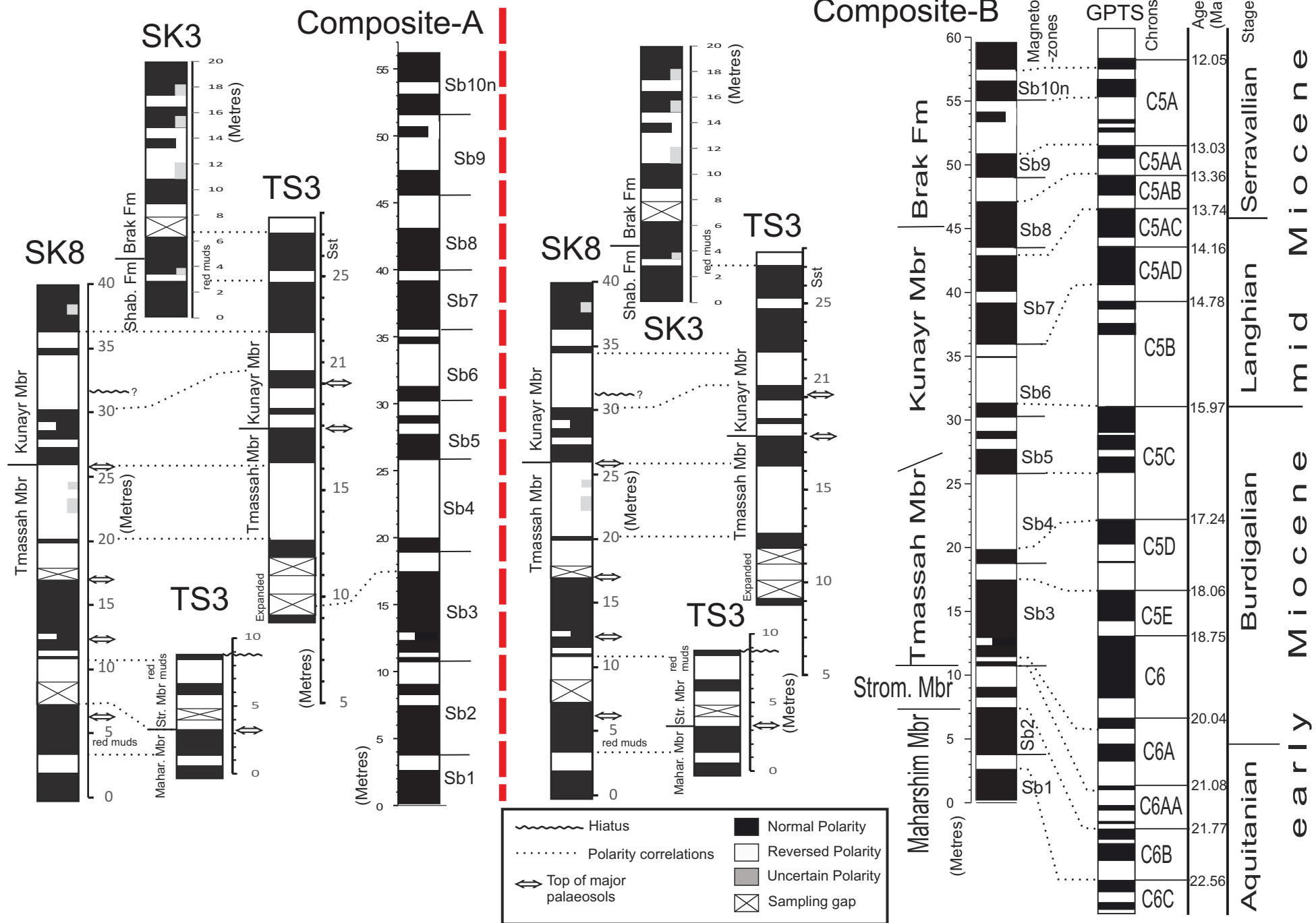
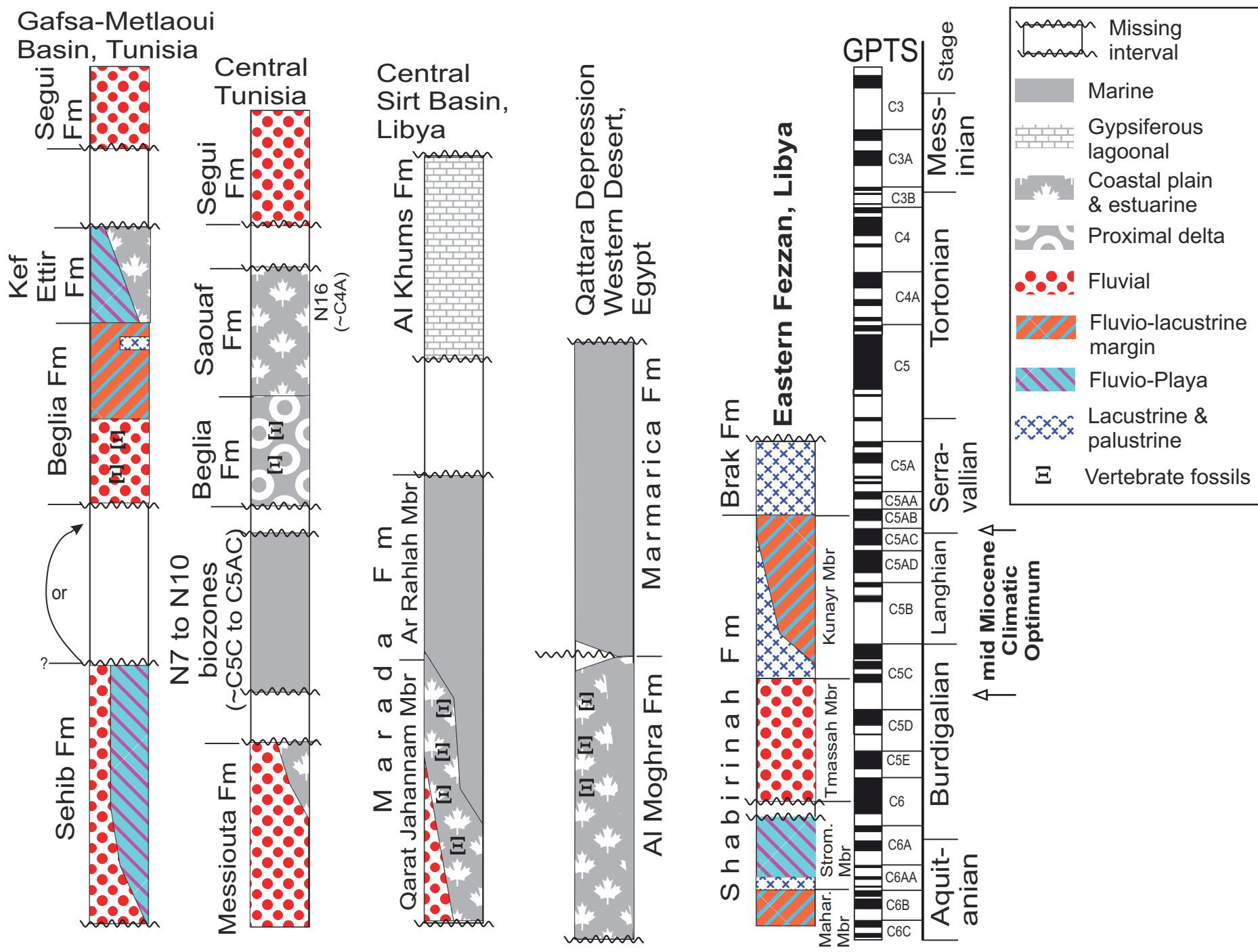


fig14.pdf



Supplementary Data

[Click here to download e-component: Supplementary Information_v7_2_.pdf](#)

Raw research data (under CC BY license; see above)

[Click here to download Raw research data \(under CC BY license; see above\): Pmag data for the SD.xlsx](#)

Raw research data (under CC BY license; see above)

[Click here to download Raw research data \(under CC BY license; see above\): Seq_Slotting_files.zip](#)

Interactive Map file (.kml or .kmz)

[Click here to download Interactive Map file \(.kml or .kmz\): Hounslow etal-gondwana_res_Places.kmz](#)

Supplementary Data

Supplementary Data (SD) includes:

1. **Part 1:** Formal definition of the new lithostratigraphy, illustrated with photos (SD Fig. S1) and detailed descriptions, tied to logs (SD Fig. S2). Locations of all sections discussed in this work are in SD Table S1, and listed in the Google Earth .kmz file, with this Supplementary Data. Part 1 includes sedimentary logs and locations for the sections in the northern Awbari sand sea area, which help define the lithostratigraphy in the Zarzur Fm, but are not the main focus of this work (SD Figs. S3, S4).
2. **Part 2:** Additional magnetic data illustrating the magnetic mineralogy measurements (SD Figs. S5, S6), nature of the magnetic overprints (SD Fig. S7), and the virtual geomagnetic pole data (SD Fig. S8).
3. **Part 3:** Methodology and results for attempted U-Th-Pb geochronology (SD Fig. S9 and SD Table S2).
4. **Part 4:** Additional figures and text which explain the alternative correlation models (SD Fig. S10) and discussion of the output from the sequence slotting procedures (SD Figs. S11, S12 and SD Table S3). The files related to the slotting procedures and the CPLSlot windows slotting program are contained in the additional .zip file with this SD.

1. Description and type sections of the new lithostratigraphic units

We outline the sources for the naming of the lithostratigraphic units, and a brief lithologic description of the units, approach used to define bases and tops, and suggested type sections. We do not provide a comprehensive assessment here of late Quaternary-Holocene age units which belong to the Shati Formation, instead our focus here is largely the pre- late Quaternary units, particularly focussing on the Brak and Shabirinah formations. The Shati Formation units are described by Petit-Maire et al. (1980), Armitage et al. (2007) and Drake et al. (2006). Place name spellings are taken from the IRC geology maps of Libya (Roncevic, 1984; Parizek et al., 1984; Berendeyev, 1985; Gundobin, 1985).

1.1 *Al Mahruqah Group*

We have upgraded the formation name, first used by Seidl and Röhlich (1984). They used Al Mahruqah to refer to the limestone units resting on basement on the northern side of Wadi ash Shati (i.e. our Brak Formation). Al Mahruqah is a village west of Brak, in Wadi ash Shati (Fig. 4). The name was later modified and expanded by Theidig et al. (2000) and Geyh and Theidig (2008) to include all the Miocene (?) and younger units on the fringes of the Awbari and Murzuq Sand Seas. We maintain this expansion of stratigraphic coverage, but upgrade the unit to group status to accommodate the new formations. Locations of all sections mentioned are detailed in SD Table S1.

1.2 *Shabirinah Formation*

Name from Wadi ash Shabirinah, the main E-W oriented wadi, east of Tmassah with extensive (over some 35 km distance) south-facing bluffs of the Shabirinah Formation on the North side of the wadi. Al Mahruqah Group sections in this area are also described by Koráb (1984). The formation is unfossiliferous except for ostracods seen in thin section in the limestone part of the Stromatolite Member.

Type sections: TS2 and nearby section TS3 (Fig. 6). TS5 is a good section which covers a larger stratigraphic thickness (Fig. 6) but it has no representatives of the Stromatolite or Maharshim members. An Al Mahruqah type section described by Koráb (1984) is present further south in the Wadi ash Shabirinah area and is there exposed in inselbergs. In both of the geological maps of the Wadi Kunayr and Wadi ash Shabirinah areas (Goudarzi, 1970; Koráb

1984; Wooley, 1984), this formation (and the Brak Formation) is erroneously combined with the late Cretaceous (Masstrichtian) Bin Affin Member. However, both ourselves and Thedig et al.

Our field Seasons	Sect. ID	Location, Area	Palaeomag . sampled	Mbr/Fm present	Goggle Earth location	Ref. sources [Pmag code]
	Sk1	West of Al Mahruqah	no	Brak	27°, 29', 20"N; 13°, 51', 6"E	G&T sites 5b,c,e; Abdullah (2010) site A
	Sk2	East of Al Mahruqah	no	Brak	27°, 31', 52"N; 14°, 4', 9"E to 27°, 34', 60"N; 14°, 1', 60"E	G&T site 6, Abdullah (2010) site B
2009	SK3	Quarry south of Al Marhruqah	yes	Brak, Shabirinah	27°, 30', 20.1"N; 14°, 04', 5.0"E	Here, G&T site 6b,c; [BC]
2011	Sk4	Road side sections in Brak	no	Brak	27°, 31', 55.1"N; 14°, 17', 54.5"E	Here
	Sk5	Ashkidah	no	Brak	27°, 37', 22.0"N; 14°, 31', 59.5"E	Here
	Sk6	East of Ashkidah	no	Brak	27°, 38', 51.3"N; 14°, 20', 23.1"E	Abdullah (2010) site C, G&T site 7D
2005, 2009	Sk7	Lower part is cave in north Side of Wadi Kunayr	no	Kunayr, Shabirinah	27°, 40', 47.1"N; 15°, 06', 49.0"E	Here
2009	Sk8	North Side of Wadi Kunayr	yes	Kunayr, Shabirinah	27°, 40', 47.07"N; 15°, 08', 10.7"E	Here; [AP]
	Sk9	33 km NNE of SK8	no	Brak	27°, 55', 8"N; 15°, 19', 46"E	G&T site 8
2007,2011	SK10	Bir az Zallaf, Wadi ash Shati	yes	Bir az Zallaf, Sifar Top of Sayl	27°, 26', 0.9"N, 14°, 23', 37.1"E to 27°, 26', 0.9"N, 14°, 23', 37.1"E	Here and Abdullah (2010) section C, G&T site 2b; [BZ,AL]
2011	SK11	Bir az Zallaf section in west side of hill. Sub-section to NE	yes	Bir az Zallaf, Sifar, top of Sayl	27°, 25', 47.5"N 14°, 23', 12.2"E; to 27°, 25', 50"N; 14°, 23', 15.7"E	Here; [BZ]
2007,2011	SK12	Washkat Zarzur, near Bir az Zallaf	yes	Sifar, top Sayl	27°, 24', 34.8"N; 14°, 21', 35.0"E	Here; [ALA, BZ]
2011	SK13	NW of Bir az Zallaf, Washkat Zarzur	yes	Aqar, Base of Sayl,	27°, 25', 29.09"N; 14°, 20', 54.2"E	Here; [BZ]
	NU1a	W. Awbari Sand Sea	no	Bir az Zallaf, Sifar	27°, 59', 21"N; 10°, 49', 49"E	Roncevic (1984), Fig.13
2008	NU1b	Al Kuthbanyar Ramliya, W Awbari Sand Sea	yes	Sifar	27°, 59', 47.9"N; 10°, 50', 12.5"E	Here [M,V]
2007,2008	NU1c	Al Kuthbanyar Ramliya, W Awbari Sand Sea	No	Bir az Zallaf, Sifar	27°, 59', 34.8"N; 10°, 49', 48.2"E	Here
2008	NU2a	Wadi Taharat, N. Awbari Sand	no	Bir az Zallaf, Sifar	28°, 38', 57.6"N; 11°, 21', 13.07"E	Here

		Sea				
2008	NU2b	Wadi Taharat, N. Awbari Sand Sea	no	Nahiyah, Shabirinah(?)	28°, 41', 1.2"N; 11°, 22', 45.12"E	Here
	NU2c	Wadi Taharat, N. Awbari Sand Sea	no	Nahiyah, Sifar	28°, 42'N; 11°, 12'E	Berandeyev (1985) fig. 14
2010	NU3a	Wadi as Sifar, N. Awbari Sand Sea	yes	Sifar, top Sayl	28°, 23', 22.1"N; 12°, 27', 19.5"E	[QM2]
2010	NU3b	Wadi as Sifar, N. Awbari Sand Sea	yes	Bir az Zallaf, Sifar	28°, 23', 5.42"N; 12°, 27', 44.97"E	[QM5]
2010	NU3c	Wadi as Sifar, N. Awbari Sand Sea	yes	Bir az Zallaf, Sifar	28°, 22', 51.7"N; 12°, 29', 55.2"E	[QM4]
2010	NU3d	Wadi as Sifar, N. Awbari Sand Sea	yes	Bir az Zallaf, Sifar	28°, 24', 29.3"N; 12°, 27', 53.2"E	[QM3]
2008	NUS3e	Wadi as Sifar, N. Awbari Sand Sea	yes	Bir az Zallaf, Sifar	28°, 18', 11.09"N; 12°, 39', 59.60"E	[QM1]
2009	TS1	Sarir al Qattusah, NW of Tmassah	no	Stromatolite, Maharshim	26°, 43', 27.9"N; 15°, 36', 40.1"E	Here
2009	TS2	N. side of Wadi Ash Shabirinah East of Tmassah	no	Kunayr, Tmassah, Stromatolite, Maharshim	26°30'51.90"N; 16°29'50.40"E	Here
2009	TS3	N. side of Wadi Ash Shabirinah East of Tmassah	yes	Kunayr, Tmassah, Stromatolite, Maharshim	26°, 30', 54.20"N; 16°, 30', 20.6"E to 26°, 30', 45.10"N; 16°, 30', 3.10"E	[TM]
2009	TS4	N. side of Wadi Ash Shabirinah East of Tmassah	no	Brak, Kunayr, Tmassah,	26°, 29', 45.9"N; 16°, 40', 37.5"E	Here
2009	TS5	N. side of Wadi Ash Shabirinah East of Tmassah	no	Brak, Kunayr, Tmassah,	26°, 29', 25.6"N; 16°, 41', 42.5"E	Here
2009	TS6	N. side of Wadi Ash Shabirinah East of Tmassah	no	Kunayr, Tmassah,	26°, 30', 53.4"N; 16°, 43', 5.1"E	Here
2009	TS7	N. side of Wadi Ash Shabirinah East of Tmassah	no	Brak?, Kunayr, Tmassah	26°, 32', 59.1"N; 16°, 39', 48.2"E	Here

Supplementary Table. S1. Locations of sections figured in this work, and sections mentioned in text, but not figured here. G&T= section location from Geyh and Theidig (2008).

(2000) consider the clastic units here to belong to the Al Mahruqah. In the Wadi Kunayr area the older geological map of Collomb (1961), like us, assigns these units to the 'Miocene', also associating them with units in Wadi ash Shati, that we now call the Al Mahruqah Group. The numerous magnetozones from these strata clearly show they are not Masstrician in age, as the Masstrician has a much simpler magnetic polarity pattern.

Age: Aquitanian to earliest Serravallian, chrons C6C to C5AAr

1.2.1 Maharshim Member

From the NNW-SSE oriented Wadi al Maharshim, 28 km to the NW of Tmassah (as marked on Tmassah Geology map). To the west and NW of this wadi there are good exposures of the lower two members of the Shabirinah Fm. Outcrops young towards the east in the Wadi al Maharshim to Tmassah area. This member can also be seen at section TS3 (SD Fig. S1B).

Base not seen. Top defined by base of overlying Stromatolitic Member (SD Fig. S1B). Thickness ~7 m or more (at section TS1, Fig. 6).

Description: Clastic unit with well-developed palaeosols, chalky groundwater calcretes, extensive rootletting and some cross-bedded sandstones.

Type section: at TS1.

Age: mid Aquitanian, chrons C6C to C6Bn.

1.2.2 Stromatolite Member

Name from the dramatic and distinctive stromatolite mounds which occur in the upper part of limestone bed that forms the lower part of this member (SD Fig. S1A, S1C). Theidig et al. (2000) has probably previously figured the stromatolites from the limestone unit in this member as their Plates 1e, 1f (and possibly Plate 5c), but assigned them to their 'Bir az Zallaf Member'

Base defined by the base of the distinctive white, stromatolitic limestone forming the lower part of this member (SD Fig. S1B). Top defined by base of overlying Tmassah Mbr (SD Fig. S1D). Thickness up to ~8 m at section TS2 and TS3 (Fig. 6).

Description: A lower white limestone unit, with weakly developed stromatolitic textures and occasional mounds on the upper surface, overlain by red, to locally green smectitic mudstones (SD Fig. S2). The limestone bed locally displays large stromatolitic mounds on the upper surface (e.g. at 26°31',47.9"N; 16°24',31.7"E and 27°26',2.8"N; 15°34',15.6"E and 26°30',55.3"N; 16°31',57.6"E), when the overlying red mudstone is eroded. The mudstone displays extensive pedogenic mottling (SD Fig. S1D). The mudstone may contain sandstone beds. The limestone bed contains ostracods. In thin section the limestones are micritic, with scattered fragments of micritised ostracods. Textures are strongly peloidal.

Type section: TS3. Auxiliary sections occur in the vicinity of TS2 and TS5 and up to ca. 10 km to the east (Fig. 6).

Age: late Aquitanian, chrons C6AAr to C6Ar.

1.2.3 Tmassah Member

Name from the town south of Sabha. To the east of Tmassah scattered outcrops of the Tmassah Member occur (and other units of the Shabirinah Formation) as far east as the NE end of Wadi ash Shabirinah (SD Fig. S1E). The fluvial-dominated units below the Kunayr Member in the Wadi Kunayr area are also assigned to the Tmassah Member.

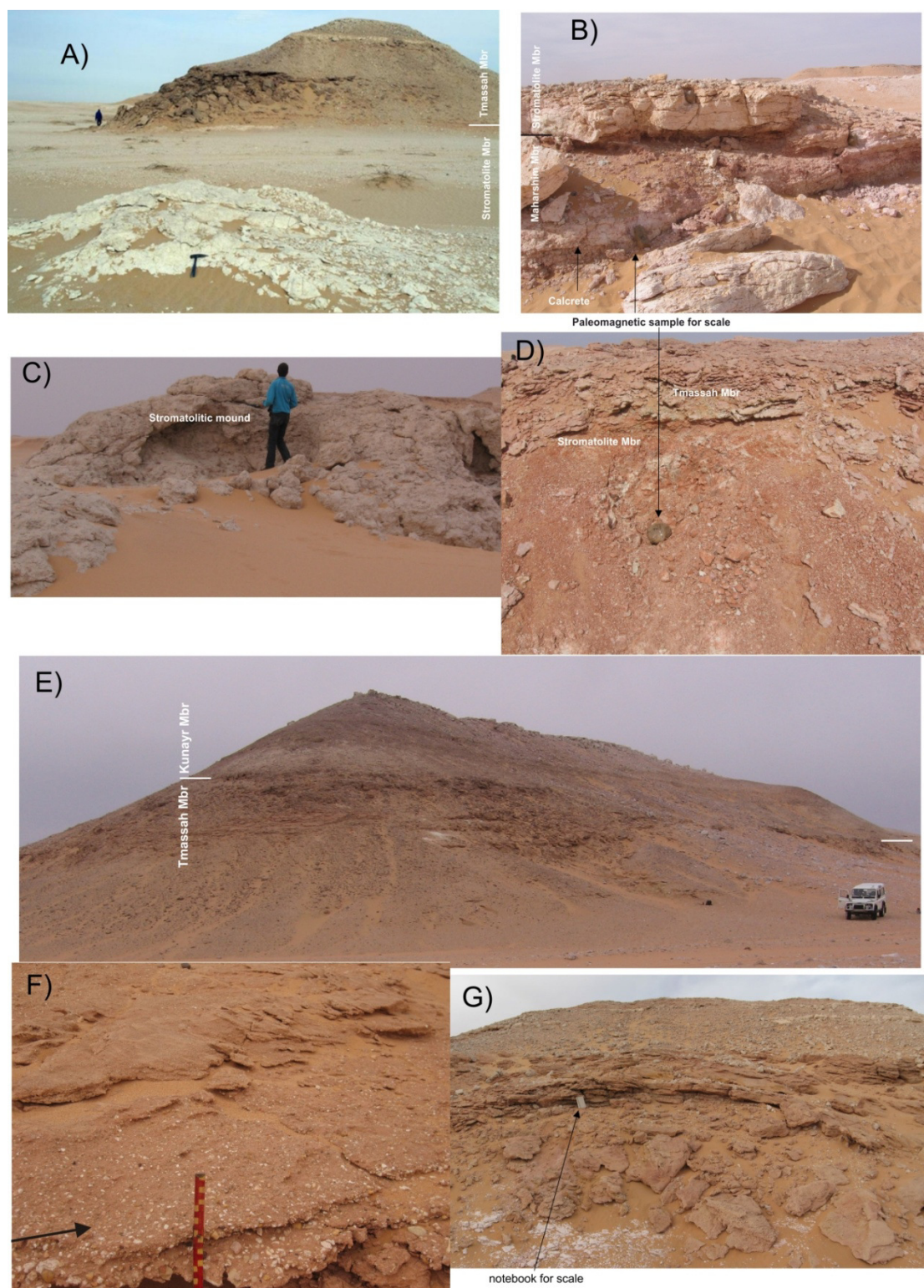


Fig. S1. Photographs illustrating the new lithostratigraphy, and key features of these units. A) Stromatolitic mound (in foreground) in the limestone part of the Stromatolite Member overlain by all the Tmassah Member in this small hill, which at this location is composed of coarse-grained cross bedded sandstone (section TS3). B) Base of the Stromatolite Member (white limestone in upper part of photo) overlying the mottled upper part of the Maharshim Member. The lower part of the outcrop shows a layer of calcrete (at ca. 2.5m in the TS3 log in Fig. 6). C) Stromatolitic mounds in the top of the limestone bed in the Stromatolite Member ca. 9 Km west of section TS2 (Fig. 5). D) Base of the Tmassah Member (top of outcrop), overlying red mudstones forming the top of the Stromatolite Member (Section TS3). Sample TM10 is shown. E) Tmassah Member underlying the Kunayr Member at section TS5, in which the Kunayr Member has no well-bedded limestones, but is shown by the presence of rubbly calcrite nodules throughout. F) Pebbly sandstone in the base of the Tmassah Member (arrowed), photo from section TS2. G) Cross-bedding in the lower part of the Tmassah Member (scale shown by notebook), photo from section TS2.



Fig. S1. continued. H) View of the prominent limestone beds in the Kunayr Member (from section TS2), overlying the Tmassah Member in the lower part of the photo, with the upper-most part of the Kunayr Member shown in the distance. I) Close-up of the heavily rootletted sandstone, and overlying darker, reddish palaeosol (top of photo). Height shown in photo ~ 2.5 m in SK8 log (Fig. 10). J) The lower parts of the Shabirinah Formation in the SK8 section (Wadi Kunayr), showing the darker-coloured palaeosols behind the person, and the channelled nature of the sandstone beds in the upper part of the section. Photo starts from the ca. 7 m level of the log in Fig. 10. K) Gypsum with chicken-wire texture in the top-most part of the Tmassah Member (arrowed), immediately below the base of the Kunayr Member, section TS3. L) Desiccation cracks with upstanding ridges picked out by more carbonate-rich parts in a mudstone-rich layer in the lowest limestone of the Kunayr Member (section TS2). M) Termite burrow pod (adjacent to knife) in an extensively rootletted and burrowed silty sandstone in the Tmassah Member from section SK7.

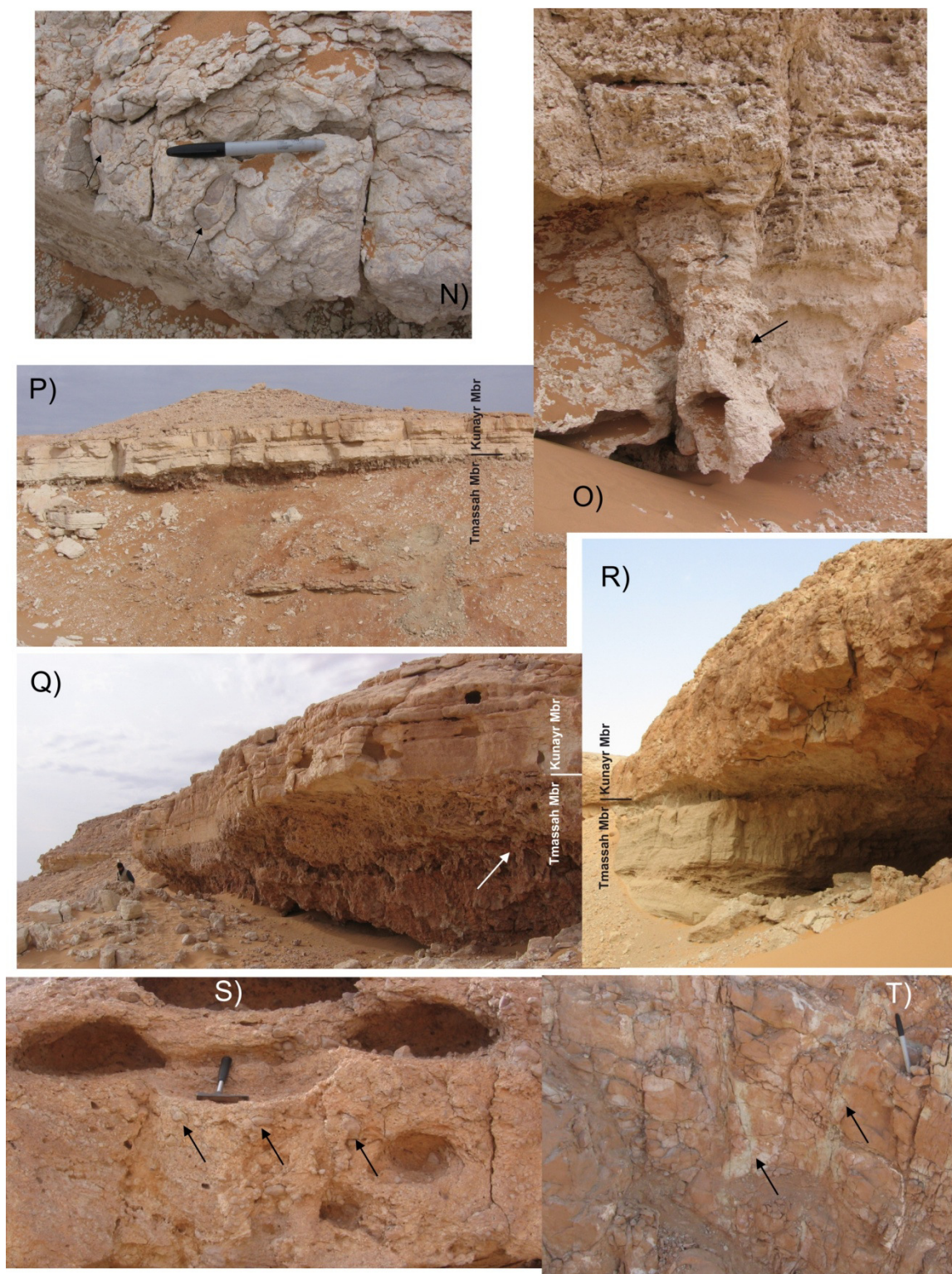


Fig. S1. continued. N) Pseudo-breccia developed in the base of the Kunayr Member ca. 100m east of the TS5 section in the Wadi ash Shabirinah area (Fig. 6). O) A large rhizoconcretion (arrowed) developed in the base of the Kunayr Member (ca. 200 m east of the TS5 section in the Wadi ash Shabirinah area; Fig. 6); pen for scale. P) upper-most clastic units of the Tmassah Member underlying the well-bedded lacustrine limestones in the base of the Kunayr Member (section TS3). Q) base of the Kunayr Member seen in the TS3 section in the Wadi ash Shabirinah area (Fig. 6), displaying the well-bedded lacustrine limestones, overlying the heavily rootletted top of the Tmassah Member (arrowed). R) Base of the Kunayr Member in the Wadi Kunayr area in section SK-7 (Fig. 7), displaying heavily calcretised and brecciated limestones overlying locally cross-bedded clastics. Section height shown ca. 10 m. T) Red mottled mudstones from the upper most part of the Shabirinah Formation, in the lower part of section SK3, Wadi ash Shati (Fig. 7). The mudstones display vertical mottling structures (arrowed) that may be ghosts of rootlet structures. S) Brak Formation in the Wadi ash Shabirinah area (some ca. 6.5 km NW of section TS7; Fig.6), displaying pseudo-breccia (arrowed) due to extensive calcretisation.

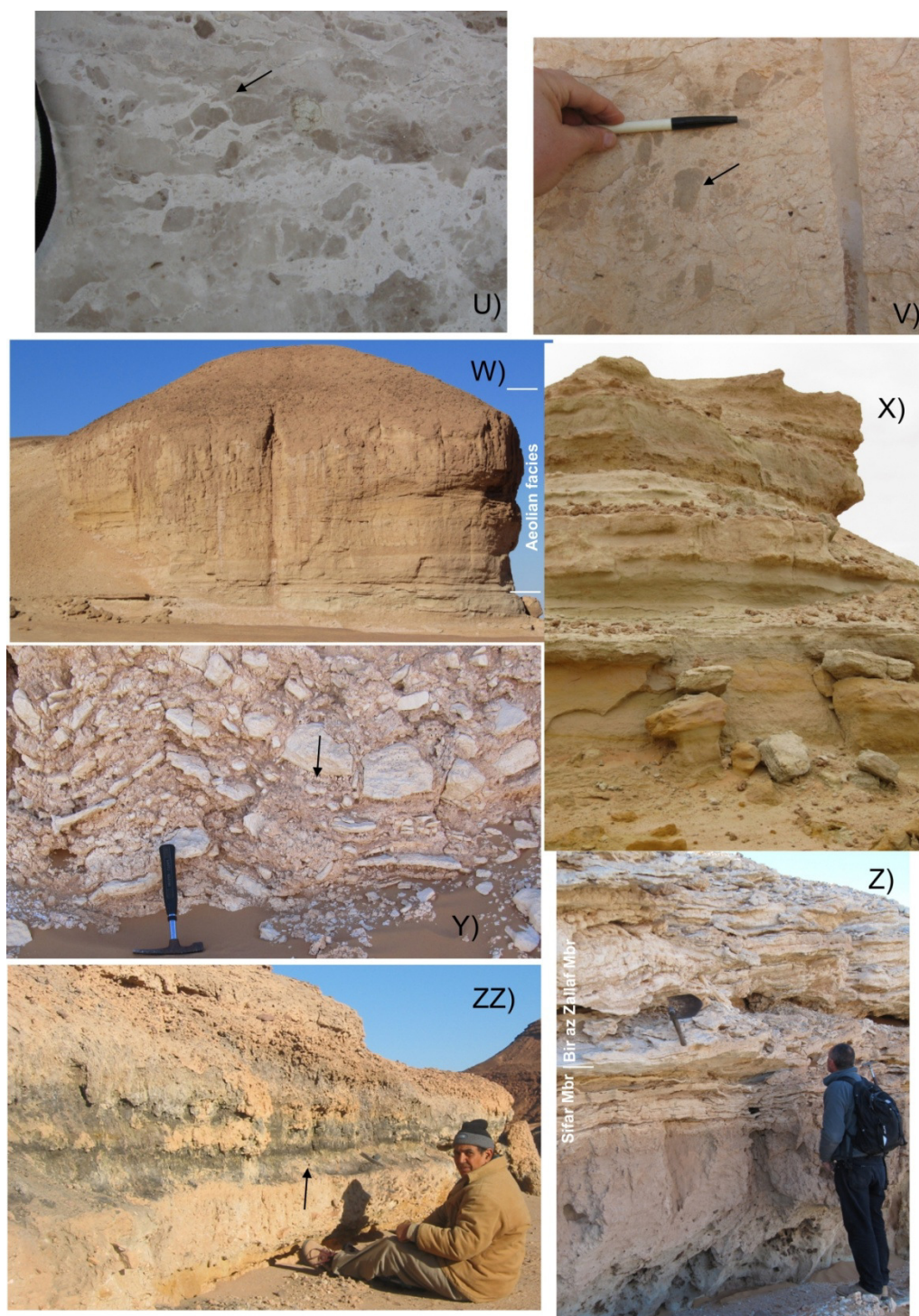


Fig. S1. continued. U) Pseudo-breccias with veinlets (arrowed), typical of the mid and upper parts of the Brak Formation, with several generations of cement, and colour density of breccias pods, probably related to the relative dolomite and silica content (on a polished block). V) Similar textures to U) seen in the type section, SK3 of the Brak Formation (near Al Marhuqah in Wadi ash Shati), in the quarried face. W) Aeolian cross-bedded facies of the Sifar Member in section NU3a, occupying the mid part of this cliff (shown on log in SD Fig. S4 starting in the photo at ca.6 m level). X) Typical outcrop of the Sifar Member of the Zarzur Formation, with harder more calcareous ribs of sandstone (sometimes gastropod or ostracod rich) interbedded with softer green and brown sandstones, mostly lacking sedimentary structures. Height of section ca. 17 m (section SK12), Washkat Zarzur near Bir az Zallaf. Y) Gypsum-facies in the Bir az Zallaf Member consisting of inter-bedded layers of gypsum (darker, arrowed) and micritic white limestone, in this case deformed by a tepee structure. Section NU3b Northern Awbari sand Sea (SD Fig. S3). Z) Typical limestone facies of the base of the Bir az Zallaf Member, consisting of laminated, crinkly-bedded limestones interbedded with friable sandstone and sandy limestone layers, resting on the underlying sandstones of the Sifar Member (Section NU3-d, Northern Awbari sand Sea; SD Fig. S3). ZZ) Outcrop of the Bir al Hasy Member of the Shati Formation, displaying typical fossil rich dark silts (arrowed) interbedded between fine-medium sand layers above and below. El Grafya 25 km east of Jarma.

Base defined by first major fluvial sandstone unit (often cross-bedded; SD Fig. S1G), erosively based (SD Fig. S1F), cutting into the underlying red mudstones of the Stromatolite Member (if underlying member is seen). Top defined by base of overlying Kunayr Member. Thickness up to ~21 m (at section TS5, SD Fig. S1E).

Description: Variety of fluvial clastics (SD Figs. S1F, S1G; S2), often displaying well developed channel features (SD Fig. S1J) and cross-bedding. Pebbly sandstone (SD Fig. S1F), to sandstone, to sandy-mudstone intervals. May contain dark humid palaeosol levels (SD Fig. S1i). May contain minor limestone intervals, and intervals of mudstone. Intervals may be reddened and contain pedogenic mottling. Finer grained sandstone to siltstone intervals may be heavily rootleted (SD Fig. S1i), these may be more frequent at basin margin locations (e.g. section TS6, Fig. 6). In the Wadi Kunayr area termite-nests (SD Fig. S1M) occur like those described by Bown (1982). The boundary with the overlying Kunayr Member may show evidence of erosion, or more typically well-developed rootletting, and palaeosol development (SD Fig. S1K, S1O, S1Q). Away from basin-centre locations the lower part of the Tmassah Member probably laterally interdigitates with the Stromatolite and Maharshim members, to rest on basement. Thin sections show large well-rounded quartz clasts in a matrix of angular to sub-angular particles. Carbonate cements are similar to those in the Kunayr Member (see below).

Type section: TS3, with auxiliary type section at TS5 (Fig. 6), where the Tmassah Member sits on basement.

Age: earliest Burdigalian to latest Burdigalian, chrons C6An.1n to C5Cn.

1.2.4 Kunayr Member

From Wadi Kunayr, east of Wadi ash Shati, an E-W oriented wadi with extensive outcrops on its northern flank of the Tmassah and Kunayr members (the wadi houses the irrigation circles of the Areal Agricultural Project).

Base defined by first major calcareous bed (palustrine limestone; SD Figs. S1P, S1Q, S1R) following the Tmassah Member clastics. Top defined by base of overlying Brak Formation. Thickness up to ~16 m.

Description: Complex interdigitation of carbonates and clastics (SD Fig. S1H). Clastics may be of mixed lacustrine/fluvial and possibly of aeolian origin (SD Figs. S1T, S2). Carbonates range from variably calcretised palustrine limestones from thin to thick bedded. The carbonates may contain pseudo-brecciated units (SD Fig. S1N) grading into more nodular calcretes within the clastics. In the area east of Tmassah, the base may locally contain either a thickly-bedded, brecciated palustrine limestone (to east of section TS5, SD Fig. S1O, S1R), or laminated palustrine limestone's (e.g. sections TS2 and TS3, SD Figs. S1P, S1Q). These represent lateral equivalents, with the more better developed palustrine limestone's closer to the basin centre to the west. Weak pedogenic mottling is common throughout the clastics, as is rootlet development at a variety of scales from small (mm) to big (metres). The clastics may at some levels have well developed palaeosols shown by nodular calcrete development. In the Wadi ash Shabirinah area the units may contain a massive, well-cemented, rootleted sandstone bed in its upper part (26-28 m in section TS3; Fig. 10). The upper part of the member may laterally interdigitate with the Brak Formation. In thin section limestones tend to be more spar-rich than the Brak Fm, with complex cementation phases in heavily rootleted intervals. No fossils were seen at outcrop or in thin sections.

Type section: TS5 with auxiliary sections at SK8, TS3 and TS2 (Figs. 6,7). Section TS2 is re-drawn from that shown as Fig. 13 of Drake et al. (2008).

Age: latest Burdigalian to early Serravallian, chrons C5Cn to C5AAr.

1.3 Brak Formation

Upgraded from the 'Brak member' used in some literature to refer to this dominantly carbonate unit (Theidig et al., 2000; Abdullah, 2010), with type area around Brak, and resting on the Paleozoic basement outcrops on the north side of Wadi ash Shati. Formerly the "Calcarei di Murzuch" (Murzuq Limestone; Desio, 1971) and the 'Al Mahruqah formation' of Seidl and Rohlich (1984). Theidig et al. (2000) suggested the Brak also occurs in the region Murzuq to Tmassah, although we have not seen these Brak Formation outcrops.

Base defined by well cemented, often fairly pure limestone, with main part of unit showing distinct brecciated texture (SD Figs. S1U, S1V). Top is a major unconformity surface, often heavily karstified (dolines locally important). Thickness variable, but up to 15 m is seen in Wadi ash Shati; although often thinner than this. Contact with underlying Shabirinah Formation seen in the area east and NE of Tmassah (Fig. 5), and inferred in the area north of Wadi Kunayr (Figs. 4, 8).

Description: Well cemented white dolomitic palustrine limestones, often massive and poorly bedded, and variably mottled on flat fresh surfaces (SD Figs. S1S, S1V, S1U, S2). Showing pedogenic brecciation with rare vadose vugs, reddish wispy clots, and occasionally with pisoids and oncoids (Plates 1g, 1h in Theidig et al., 2000). Often seen resting on heavily brecciated basement rocks in Wadi ash Shati area, which may be several metres thick (Plate 1b in Theidig et al., 2000). In Wadi ash Shati, Abdullah (2010) has described a deformed clastic rich unit at the base, which clearly rests on basement, which from his photographs appears to be heavy calcretised and brecciated basement rocks. The upper surface of the Brak Formation often forms extensive dolines and major karst surface features and plateaus, which are probably relict from the time of unconformity formation before deposition of the Zarzur Formation. The formation may contain minor interbedded siliciclastic units. No fossils have been seen in thin section or outcrop. In the type section, thin sections of the palustrine limestones are typically pedoidal with apparent intraclasts, occasional pisoids and coated grains, with multiple phases of cementation (SD Fig. S1U). More sparry cements occur as veins and veinlets. Frequency of spar cements and peloids increase up through the Brak Fm.

Type section: SK3, a location previously suggested by Theidig et al. (2000) and Geyh and Theidig (2008).

Age: early to late Serravallian, chrons C5AAr to C5An.

1.4 Zarzur Formation

Name from Washkat Zarzur region (marked on Sabha geology map), in which extensive outcrops of the Zarzur Formation occur in Wadi ash Shati, to the south of Brak.

Top defined by the youngest part of the Bir az Zallaf Member, which is normally a silicretised limestone on the plateau tops. Base defined by the unconformity on various underlying Mesozoic and Palaeozoic units. Unconformity may be marked by pedogenic structures such as mottling, and rootletting developed in the underlying unit (e.g. section SK12), a basal calcrete-rich palaeosol (section NU1b; SD Figs. S3), conglomerate (e.g. section NU2b; SD Fig. S3) or occasionally a sharp erosional boundary.

Type section: Bir az Zallaf, section SK10 to SK11 (SD Table S21), which cover the Bir az Zallaf Member. Auxiliary sections at SK12 and NU3a (SD Fig. S3).

Age: younger than Serravallian and older than 420 ka.

1.4.1 Sayl Member

Name from Wadi Sayl to the North of major Zarzur Formation outcrops in Wadi ash Shati, south of Brak (Fig. 4).

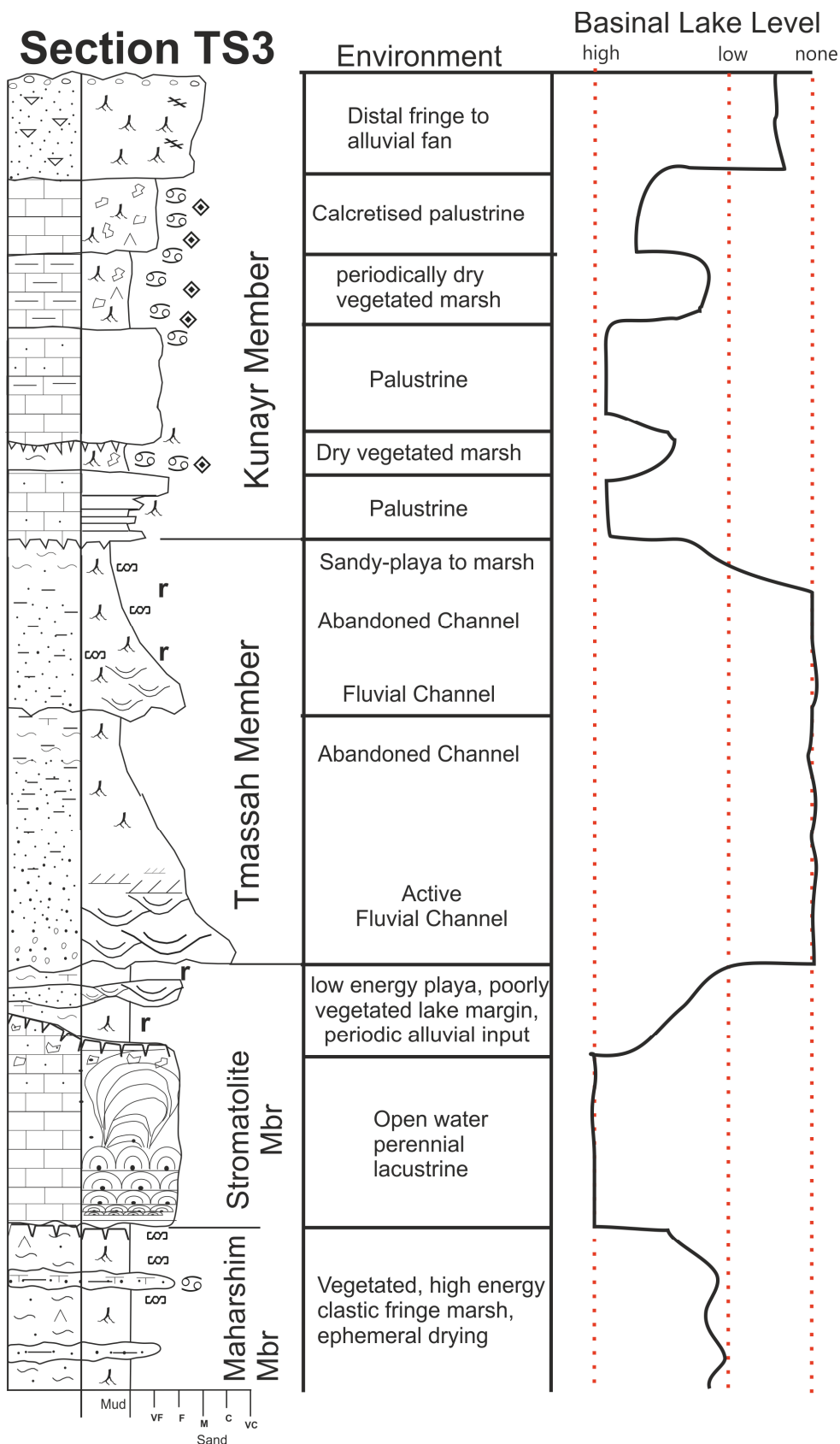


Fig. S2. Environmental model of the Shabirinah Formation, based on section TS3. The fluvial systems of the Tmassah Member probably bypassed or overrode the lacustrine system which developed during the Stromatolite Member. The low energy lacustrine system associated with the upper part of the Stromatolite Member was more saline (i.e. gypsiferous) than the palustrine systems of the Kunayr Member. The palustrine lake margin systems of the Kunayr and Maharshim members were more coarse-clastic dominated, and may have had an element of aeolian input in addition to the fluvial/alluvial inputs. The lake level interpretation assumes that a permanent lake (the main 'basin') existed W and SW of this section at all times, other than during the Tmassah Member.



Fig. S3. The figured sections and locations in the northern Awbari Sand Sea, discussed in the supplementary Data. Image from www.bing.co.uk.

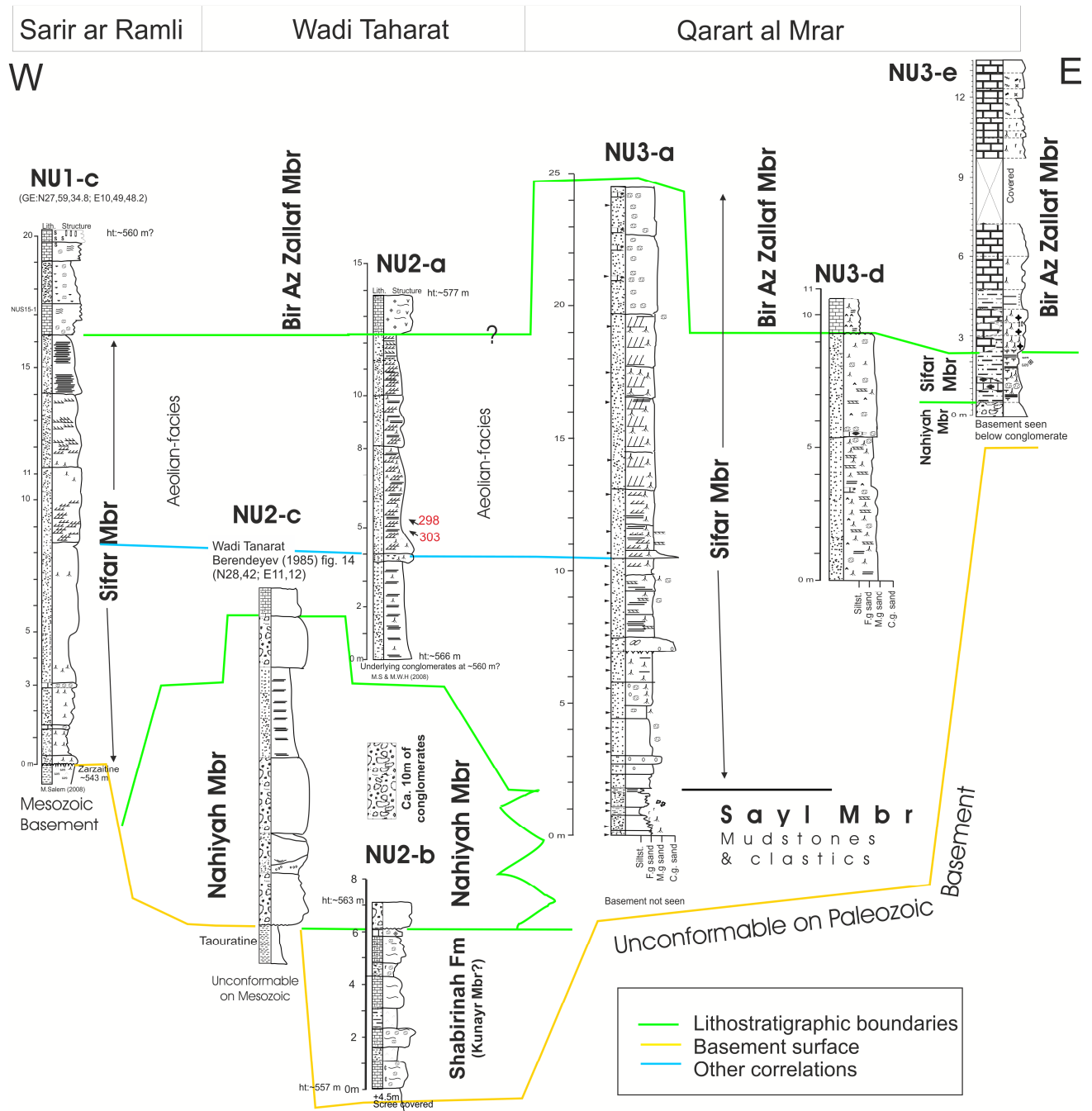


Fig. S4. Schematic relationships of Northern Awbari Sand Sea sections, mostly in the Zarzur Formation (location code=NU). See SD Fig. S1 and SD Table S3 for locations. Cross bedding directions shown in red. Section NU2-c is redrawn from Berendeyev (1985), all others from this study. Same scale for all logs.

Top defined by first incoming of major mudstone units in the lower parts of the Zarzur Formation (SD Fig. S4). Base when seen is base of Zarzur Formation. Thickness of the order of 10-12m at Bir az Zallaf.

Description: Interbedded grey to green to rare red mudstones and fine to course sandstones. No complete section has been seen, since in Wadi ash Shati the Aqar Member cuts into this unit. Of fluvial-lacustrine origin.

Type section: One not seen. There may be one ~30 km west of Bir az Zallaf or at or slightly west or SW of location 28,23,48.6N; 12,26,27.9E; SK12, SK13 include upper and lower boundaries of this member respectively (SD table S1).

Age: Younger than Serravallian and older than 420ka.

1.4.2 Nahiyah Member

Region and named well on south side of Wadi Taharat (SD Fig. S3), with good exposures of the Nahiyah Member conglomerate, and its contact with the underlying Shabirinah Formation, and overlying exposures of the Sifar Member (SD Fig. S4).

Top defined by last conglomerate bed. Base is base of Zarzur Formation. Thickness about 10-15 m.

Description: Assorted clast-supported conglomerates with interbedded sandstone layers, with clasts derived from the underlying basement units (SD Fig. S4). Clasts of black chertified wood common in the Hamadat Tanghirt region.

Type section: No complete section seen, but upper and lower boundaries of this unit seen at sections NU2a and NU2b. Member is exposed along the escarpment ca. 2 km to the NW and 2 to 5 km to the ESE from NU2a. Berendeyev (1985) has also figured (his Fig. 14) a similar section (NU2c; SD Fig.S4), which may equate with this unit, and could serve as a type section.

Age: Younger than Serravallian and older than 420 ka.

1.4.3 Sifar Member

Origin of name is Wadi as Sifar marked on geology map to the south of major outcrops in the Qararat al Marar area (N. Awbari Sand Sea) in which major well exposed outcrops of the Zarzur Formation occur (SD Fig. S3).

Top and based defined by overlying member units. Up to 22 m thick.

Description: Well sorted sandstone, fine to coarse grained, occasionally pebbly, often rootleted or with other bioturbation structures destroying most original sedimentary structures (SD Fig. S1X). Rootlets may be preserved as gypsum casts. Rootletting systems may be several metres long vertically. Parts may be cross-bedded and or well laminated, if rootletting is not too severe. Large-scale aeolian cross-bedding more common in its upper parts (SD Fig. S1W). May contain nodular or groundwater chalky calcretes, or impersistent layers of ostracod or gastropod rich sandstone (as in Wadi ash Shati; SD Fig. S1X). Environment is of mixed fluvial (lower parts) to aeolian origin in upper parts. In thin section the sandstones are quartz-rich with minor feldspar, containing well rounded larger grains within a matrix of sub-angular smaller sand particles. Fossiliferous horizons of ostracods and gastropods and may contain rare ooids and coated grains. Less consolidated intervals are cemented by micritic rims. Chalky calcrete horizons (in western Ubari Sand Sea area) are composed of dense micrite.

Type section: NU3a (SD Fig. S3, S1W), with auxiliary section at SK12 (SD Table S1).

Age: younger than Serravallian and older than 420ka.

1.4.4 Bir az Zallaf Member

Name from the prominent inselberg south of Brak (Fig. 4). A prominent limestone bearing unit at the top of the Zarzur Formation (SD Figs. S1Y, S1Z). A similar usage was largely implied by Theidig et al. (2000) and Geyh and Theidig (2008), since their focus was on the carbonate units, largely ignoring the dominant underlying siliciclastic units, which make up 90% of the Zarzur Formation.

Base defined by the oldest major laminated limestone unit (SD Fig. S1Z). Up to 6.5 m thick.

Description: Interbedded laminated limestones (Plates 3c, 3d in Theidig et al., 2000), and green or orange rootletted sandstones (Fig. 2 in Armitage et al., 2007). Sandstones are often poorly consolidated. Limestones typically have undulose bedding, and may show sharp, erosional contact onto the underlying sandstone. Limestones may contain ostracods, fossil fish, fossilised phragmites, or tepee structures (SD Fig. S1Y) or interbedded gypsum (Plates 3e, 3f in Theidig et al., 2000). Limestone's may grade laterally into nodular palustrine limestones or rarely nodular calcretes. Massive calcrete beds, having brecciated texture may occur where this unit sits on basement (e.g. section NU3e; SD Fig. S4), or at basin margin locations. In thin sections, limestones tend to be Fe-poor micrites, with occasional ostracods, peloidal intervals and intraclasts. At basin margin sections (e.g. NU3e) calcretisation has produced heavily micritised fossils (ostracods, algal fragments) in peloidal palustrine limestones, with sparry cements.

Type section: SK10 with auxiliary section at NU3c (SD Fig. S1Z). SK10 is the same type area (their site 2b) as proposed by Geyh and Thiedig (2008).

Age: Pliocene(?) to possibly as young as 420 ± 37 ka (OSL sample FZ5 in sand near the top of member; Armitage et al., 2007). Other OSL dated samples from this member were all saturated, casting some doubt on the reliability of the one near-saturated OSL date. Dating of the limestone beds using $^{230}\text{Th}/\text{U}$ suggests ages of 206-259 ka (Geyh and Thiedig, 2008) in conflict with the OSL date.

1.5 Shati Formation

Named after Wadi ash Shati in which this formation has many small outcrops (Drake et al., 2006) of Quaternary-Holocene lake deposits.

Base defined by unconformity onto various Palaeozoic strata and Zarzur Formation in Wadi ash Shati and Qararat al Marar (Fig. 9). Top defined by overlying modern dune sands, Wadi deposits and interdune lake deposits.

Description: Includes various deposits including shell rich deposits (Aqar Member) to gastropod rich silts and mudstones, sometime organic rich (Bir al Hasy Member) to various kinds of sandy and pebbly-sand deposits, some of which may be fluvial in origin (and contain bivalves) and probably some units may be aeolian.

Age: In Wadi ash Shati 150 ka (from uranium-series dates from the Aqar M Member; Petit Maire et al., 1980) to 3.5 ka from OSL dates (Armitage et al., 2007; Drake, et al., 2004).

1.5.1 Aqar Member:

Already, widely used in the literature derived from Petit-Maire et al. (1980), described in detail by them and Theidig et al. (2000), Geyh and Theidig (2008).

Description: Cross-bedded, shell-rich shore line deposit, often interbedded with variable amounts of sandstone (see Plates 4a to 4d, 2c in Theidig et al., 2000, Fig. 3 in Armitage et al., 2007).

Type section: 10 km east of Quttah and 0.6 km south of the main road ($27^{\circ}28',40''\text{N}$; $13^{\circ}53',10''\text{E}$, sample locality Xv of Petit-Maire, 1982), as suggested by Theidig et al. (2000). Additional auxiliary sections at $27^{\circ}31',26''\text{N}$; $14^{\circ}06',08''\text{E}$ and $27^{\circ}29',30''\text{N}$; $14^{\circ}00',39''\text{E}$ as suggested by Petit Maire et al. (1980) and Geyh and Thiedig (2008).

Age: OSL dates give ages 97.7 ± 6.5 ka to 108 ± 9 ka (Armitage et al., 2007). TIMS uranium-series dates suggest an age of 128 ka (Thiedig et al., 2000) to ~ 135 ka from 21 uranium-series ages obtained by Petit-Maire et al. (1980) using shells from the coquina. $^{230}\text{Th}/\text{U}$ dates from the Aqar Member suggest median ages of 136 ± 5 ka (Geyh and Thiedig, 2008).

1.5.2 *Bir al Hasy Member* :

From a well near the Qararat al Marar NU3-e section (SD Fig. S3). Section NU3-e shows excellent exposures of fossil-rich mudstones and siltstones resting unconformably on the upper parts of the Zarzur Formation. Gundobin (1985) outlines this area figured in his Fig. 27, but their description and interpretation is erroneous. He failed to recognise the significant topography on the basal unconformity of the Shati Formation at this location, in which fragments of the gastropod-bearing Bir al Hasy Member are spread-out down the wadi, on top of the Zarzur Formation, filling shallow depressions and cracks in the underlying unit. Hence, Gundobin's Fig. 27 log, is a random mix of the two formations. Some of the other map sheets in the northern Awbari Sand Sea area have used Gundobin's Fig. 27 as a kind of type-section to infer fossil-content into Zarzur Formation type units further west, which is again erroneous, since the visibly abundant gastropods occur in the overlying Bir al Hasy Member only. In this immediate area, the Bir al Hasy Member locally has a conglomerate at its base.

Description: Dark coloured silts and mudstones containing gastropods (*Melanoides* sp., *Bulinus* sp.), locally with sandy or gravelly interbeds (SD Fig. S1ZZ). Poorly consolidated. Described also by White et al. (2000, 2006) and Drake et al. (2006) from Wadi al Ajal, and Petit Maire et al. (1980) from Wadi ash Shati.

Type section: NU3f (28° 18', 16.62"N; 12° 40', 22.2"E). Auxiliary key location at el Ghrayfah 25 km east of Awbari (SD Fig. S1ZZ and Plate 5b in Theidig et al., 2000), dated by Armitage et al. (2007) from 53 ± 6.3 ka to 11 ka.

Age: OSL dates from 52.8 ± 6.3 ka at the base to as young as 9.2 ± 0.6ka (Brooks et al., 2003; Armitage et al., 2007). Older in Wadi al Ajal (Drake et al., 2006).

1.6 *Comments about other proposed lithostratigraphic units*

Geyh and Theidig (2008) have described the Antalkhata Member from outcrops in the Awbari Sand Sea. We have not seen the location figured by them, but have seen similar outcrops in interdune depressions which we have considered to be Holocene or late Quaternary interdune lake deposits, composed of limestones, that are typically fossil-rich, and occasionally stromatolitic. The fossil rich nature of their unit is unlike the Shabirinah or Brak formations, but much more like a unit of the Shati Formation (or perhaps Bir az Zallaf Member), so we consider their Antalkhata member to be likely younger than the Brak Formation.

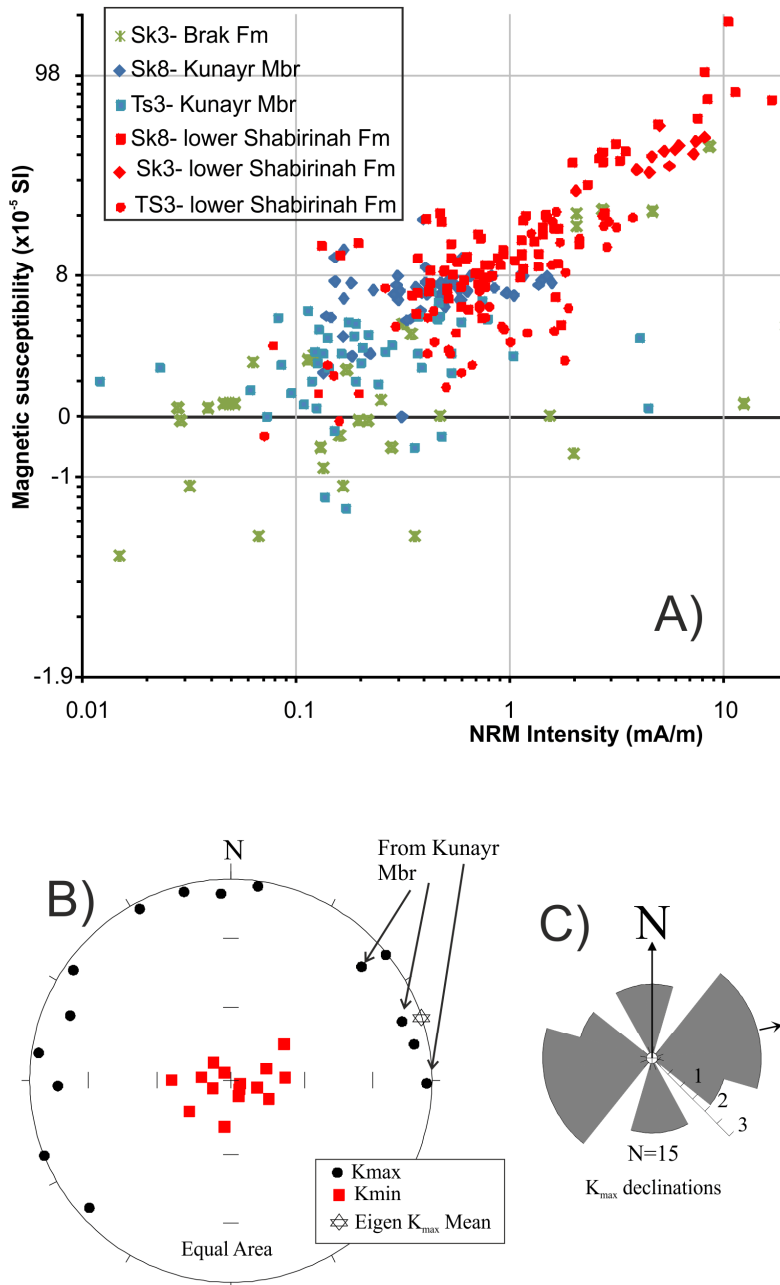


Fig. S5. a) NRM intensity and magnetic susceptibility of all specimens from the Shabirinah and Brak formations (magnetic susceptibility values have 2.0 added to value to plot on the log scale). B), C) Anisotropy of magnetic susceptibility of specimens from the SK8 section, with shown in C), the declinations of the K_{\max} axes (reflected about 0-180°), and mean direction indicated with an arrow (all specimens from Tmassah Member, except three specimens from the Kunayr Member, indicated by their flagged K_{\max} directions in B).

2. Additional magnetic data

The natural remanence intensity and magnetic susceptibility are strongly related to the lithology and formations, with much of this variation controlled by either the carbonate content, or the degree of reddening (SD Fig. S5a). The anisotropy of magnetic susceptibility of specimens displays a depositional fabric (Fig. S5B), with the K_{\max} axes appearing to reflect scant paleocurrent orientations (SD Fig. S5C). Rock magnetic data indicates both magnetite and haematite as the source of the ferrimagnetic properties (SD Fig. S6), likely contributing to the rather complex palaeomagnetic behaviour of these samples (SD Fig. S7). Existing paleopole data for the African Miocene is very scattered (SD Fig. S8), but our data is rather more tightly grouped along the 0-30 Ma segment of the African apparent polar wander path, which shows relatively little pole movement in the last 50 Ma.

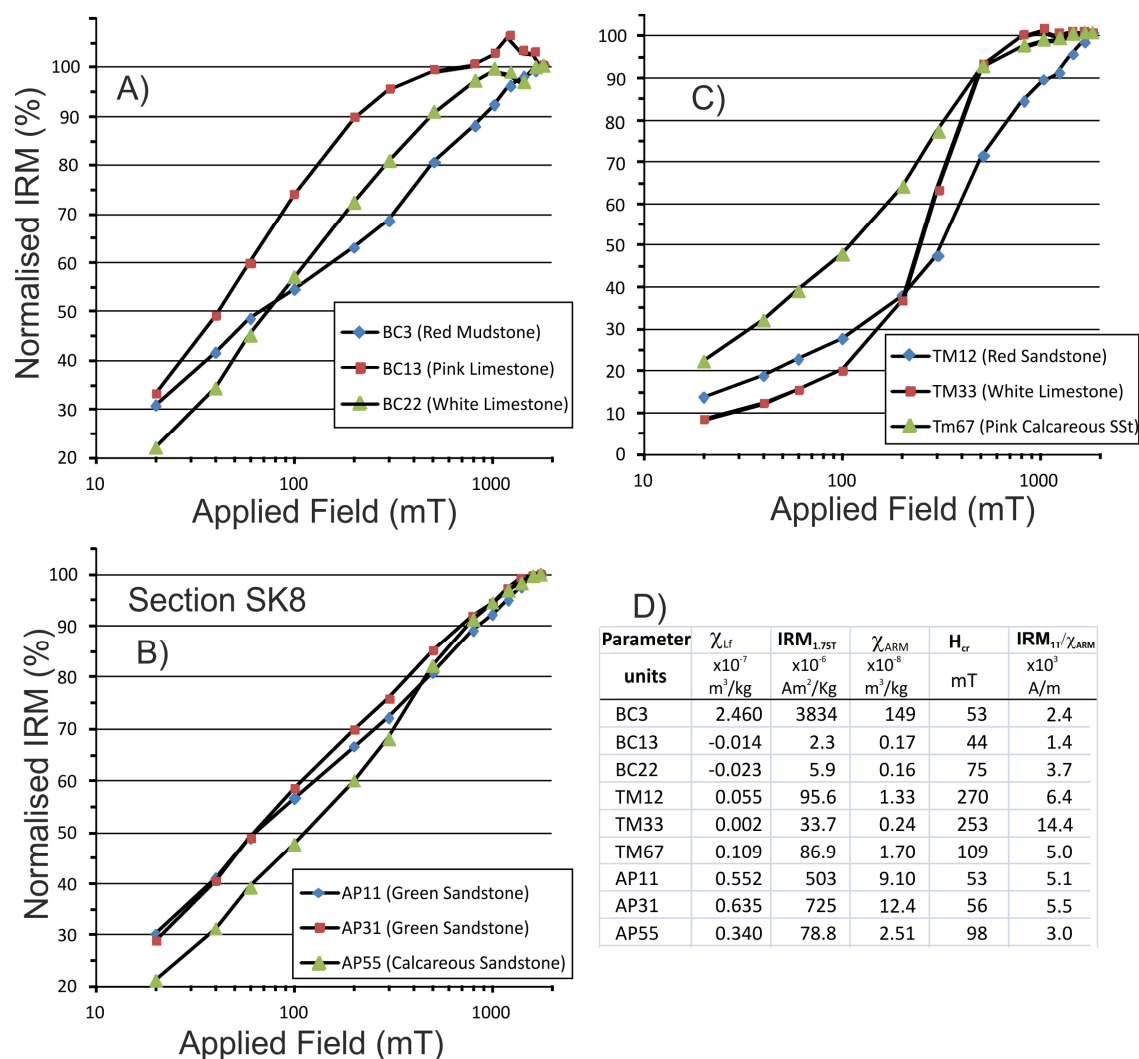
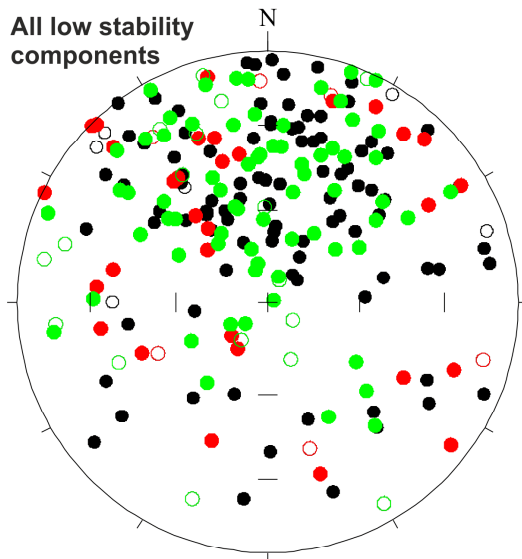


Fig. S6. Rock magnetic data for representative specimens from the Shabirinah and Brak formations. A, B and C show normalised isothermal remanent magnetisation data with respect to the (backfield) magnetic field applied, and type of specimen lithology. D) Summary magnetic properties of mineral abundance parameters of low frequency magnetic susceptibility (χ_{LF}), saturation magnetisation at 1.75T (IRM 1.75T) and susceptibility of anhysteretic magnetisation (χ_{ARM}). The coercivity of remanence (H_{cr}) and the magnetite granulometry proxy IRM_{1T}/χ_{ARM} are shown.

3. U-Th and U-Pb dating, methods and details

3.1 Sample preparation

Fourteen carbonate samples from the TS2 and TS3 sections were sub-sampled for assessment of suitability for U series geochronology. Sub-sample slabs containing relatively unaltered carbonate were obtained using a Dremel tool fitted with a diamond cutting disk and ultrasonically cleaned in water. These slabs were mounted in 25 mm diameter epoxy mounts that were polished flat and the top surface sliced off for preparation of 100 μm -thick petrographic sections for microscopy. The petrographic sections permit transmitted light microscopy but were thick enough to facilitate SEM imaging (e.g. cathodoluminescence) without burning the surface due to charge build-up and also to facilitate potential follow-up laser ablation ICP-MS analysis. The remaining mount was re-ground with diamond paste to yield a flat and highly polished surface suitable for laser ablation ICP mass spectrometry (LA-ICP-MS) and reflected light microscopy. Sub-sample slabs for solution-mode U-Th isotope analysis were obtained adjacent to the petrographic sample locations.

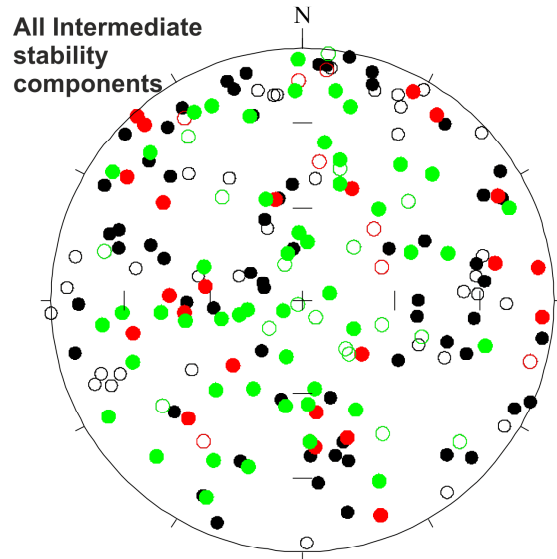


Eigen mean= Declination =356.2°, Inclination = 43.4° R= 133.419, n=225. Type:Bipolar, Rotational Symmetry of Bipolar distribution accepted at 95% probability, 95% Circular confidence Cone: 8.3°

Fisher Mean. Normal Polarity Directions: Dec= 354.9°, Incl.= 45.0°, Alpha(95%)= 6.2°, k= 3.63, n= 198, R= 143.7628, R-bar= 0.7261,

Fisher Mean, Reverse Polarity Directions: Dec.= 174.4°, Incl.= -17.7°, Alpha(95%)= 32.7°, k= 1.71, n= 27, R= 11.7576, R-bar= 0.4355,

All directions converted to Normal Polarity: Dec.= 354.8°, Inc.= 43.0°, Alpha(95%)= 6.4°, k= 3.17, n= 225, R= 154.3089, R-bar= 0.6858,

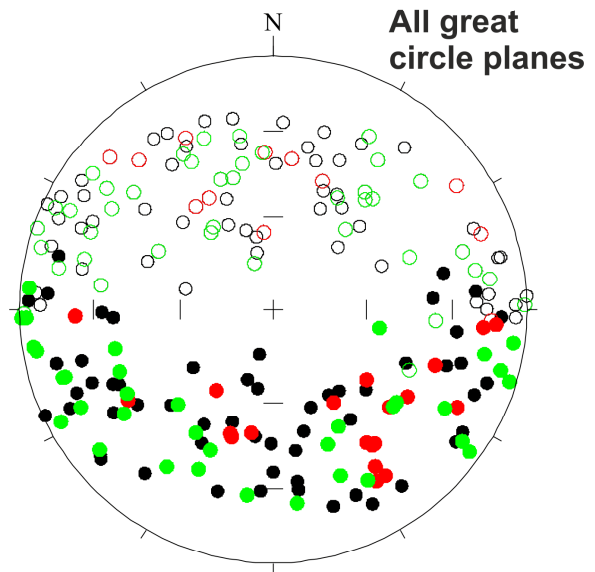
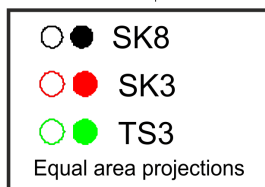
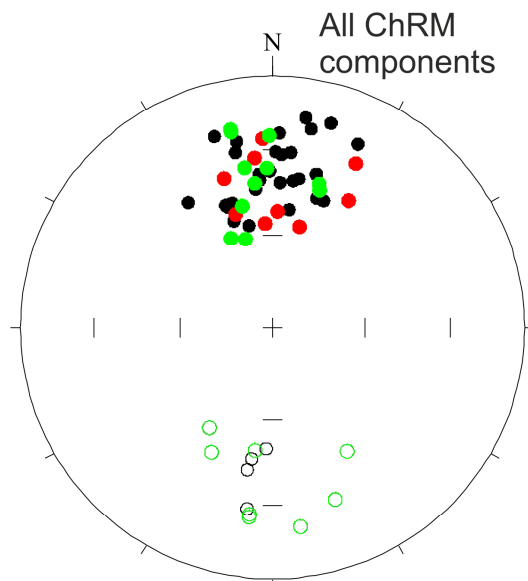


Intermediate stability components

Eigen Mean statistics

Tao	1	2	3
Declination	62.8°	326.1°	220.2°
Inclination	32.0°	10.6°	55.9°
EigenValue	57.5080,	65.5971,	73.8949

R= 46.886, n=197
Uniformity Hypothesis accepted- vectors apparently random



Eigen Mean Statistics

Tao	1	2	3
Declination	183.6°	256.9°	332.1°
Inclination	-44.3°	16.4°	-41.1°
EigenValue	10.7293,	90.7331,	112.5376

R= 9.499, n=214
Distribution Type: Girdle, with girdle plane spanned by Tao2 and Tao 3 with girdle pole at Tao1
Rotational Symmetry of Girdle distribution accepted at 95% probability
95% Circular confidence Cone: 3.8°

Fig. S7. Components extracted from demagnetisation data, and their statistical evaluation. The ChRM statistics are detailed in Table 2.

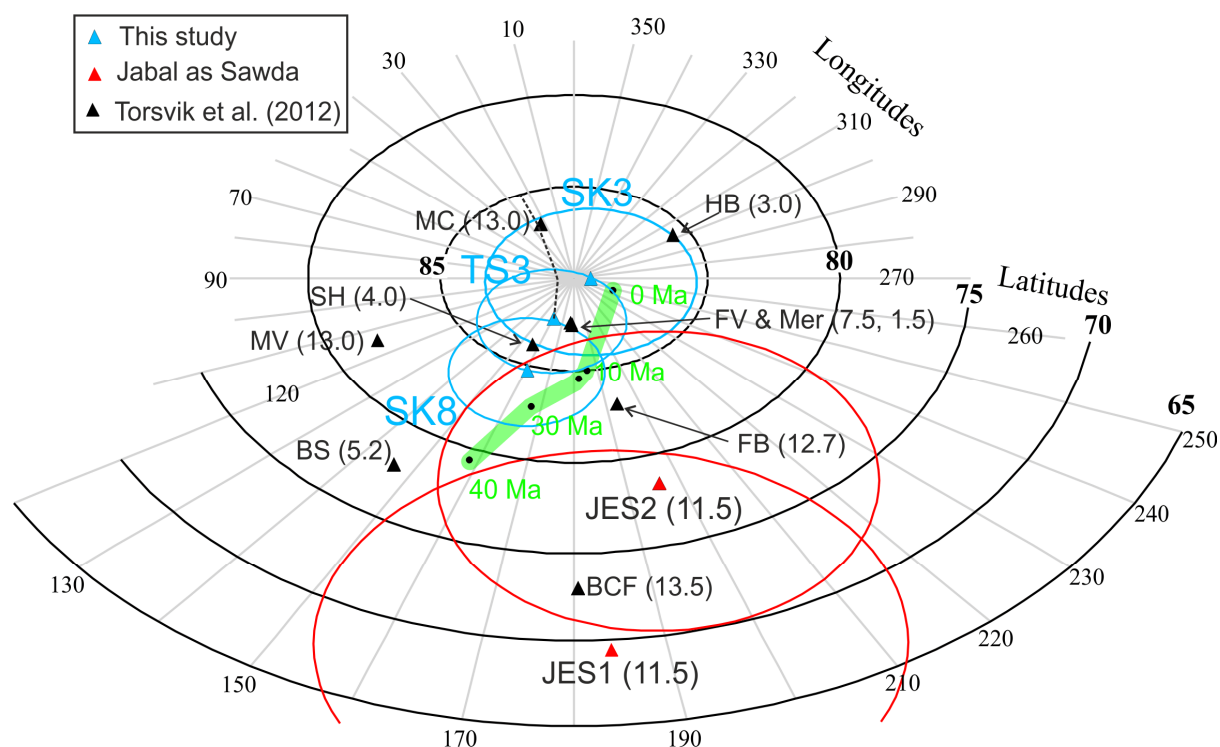


Fig. S8. Miocene to recent North African palaeopoles, with 95% confidence cones shown for the Libyan data. Blue are data from this study, red from Jebal as Sawda (JES1 = Ade-Hall et al. 1975; JES2 = Schultz & Soffel, 1973). Green is the Gondwana apparent polar wander path (APWP) from Torsvik et al. (2012; Table 7), labeled in 10 Ma increments. Other labels in black are poles (age in Ma), listed in Torsvik et al. (2012). FV=Famara Volcanics, Canary Islands (CI); BS= Basalt Series II, CI; MV= Miocene Volcanics, CI; MC=Basalt Series I, CI; Mer= main Ethiopian rift basalts; HB= Hadar Basin, Ethiopia; SH= South Holhol-Djibouti; BCF= Blue Clay Formation, Malta; FB=Ethiopian flood basalts. Dashed line from the TS3 pole is the expected trend in the pole position, if we undid $\sim 5^\circ$ of inclination shallowing. Similar trends are shown with the SK poles.

3.2 Petrography

Microscopy showed most of these samples contained significant silicate detritus rendering them unsuitable for U-Th geochronology. Generally, unsuitable samples possessed a uniform detritus distribution precluding an isochron approach, while a further sample (FEZZ/04/64/2) was unsuitable due to the presence of several carbonate generations that could not be isolated and individually sampled, due to their small physical dimensions. Samples that passed screening for detritus and considered the most likely to be successful for geochronology (SD Fig. S8; SD Table S2) included micritic limestones TM3, TM6, TM8, and FEZZ/04/64/5, and two coarser-grained limestones FEZZ/04/64/4 and FEZZ/04/64/6.

3.3 Laser ablation reconnaissance for in-situ U-Pb and U-Th analysis

LA-ICP-MS screening of these samples was done along line rasters on all chips using a New Wave Research 193 nm excimer UV laser fired at 10 Hz using a ca. 100 μm diameter laser spot at ca. 7 J/cm^2 fluence. All ablations employed He as the ablation cell carrier gas. Some samples were screened using a Nu Instruments MC-ICP-MS fitted with a U-Pb optimized detector block (Horstwood et al., 2003), while other samples were screened using a Nu single collector fast scanning sector field ICP-MS (SF-ICP-MS) following analytical protocols in Roberts and Walker (2016). Only semi-quantitative data were obtained, given the aim was to locate regions favourable for subsequent detailed analysis. Areas within a single sample chip that yielded a spread in U/Pb elemental and Pb isotope ratios for the chip as a whole were sought. Unfortunately, insignificant variation in U/Pb ratio, together with relatively uniform Pb isotope ratios of common Pb composition, were the norm, with the conclusion that the carbonate U and Pb contents and isotope characteristics

precluded their use for U-Pb geochronology. Additionally, the semi-quantitative uranium and thorium ion beam intensity data showed that while carbonates have ca. 0.1-2 ppm U contents, the amounts of accompanying ^{232}Th indicate their relative unsuitability for U series geochronology. Furthermore, direct determination of U series ages was impossible given ^{230}Th signals at or below the detection limit of the instrumentation.

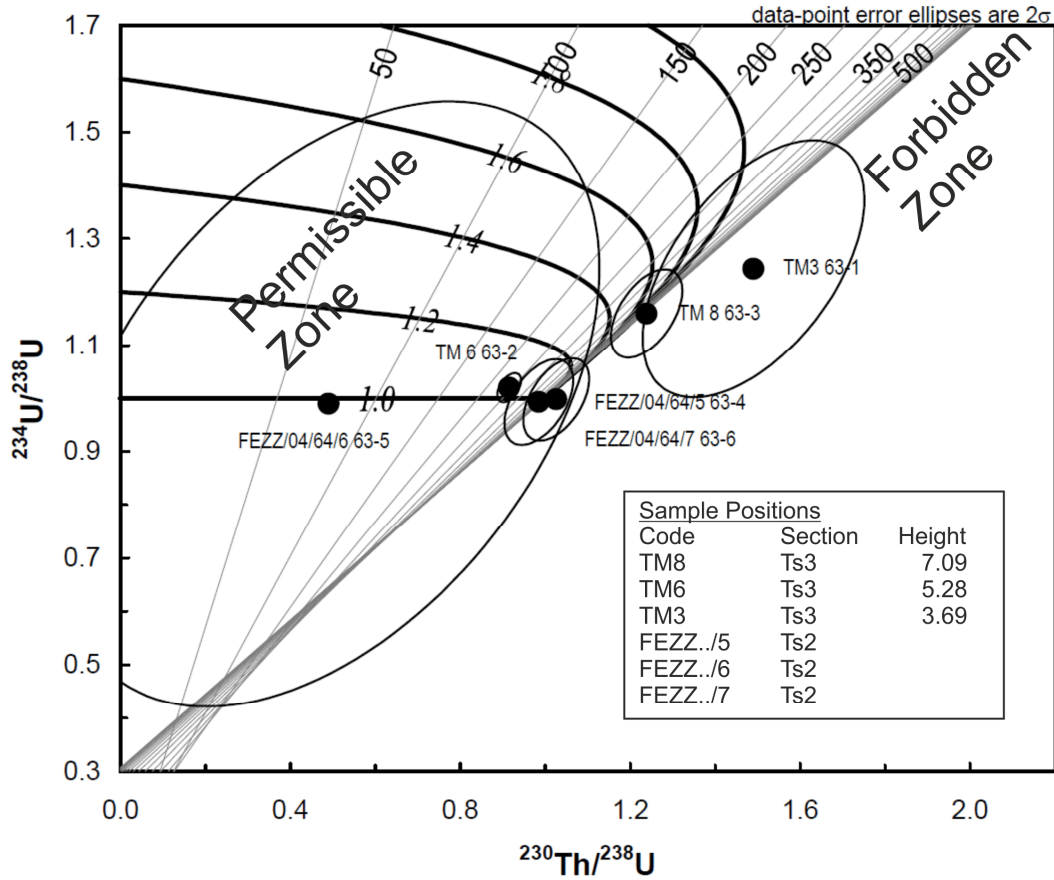


Fig. S9. The detrital Th-corrected $^{230}\text{Th}/^{238}\text{U}$ vs $^{234}\text{U}/^{238}\text{U}$ data. A series of sloping lines represent age contours (50 to 500 ka). Data points to the right of the 500 ka contour (approximate $^{230}\text{Th}/^{234}\text{U}$ secular equilibrium) plot in a 'forbidden zone' where the observed isotope compositions cannot be generated by normal U decay to Th. Such forbidden zone data are indicative of open-system conditions in samples and so no age can be determined because the main prerequisite condition required for application of the U-Th age equation is violated.

Sample	U (ppm)	^{232}Th (ppb)	$^{230}\text{Th}/^{232}\text{Th}$	$\pm 2\sigma$ (%)	$^{230}\text{Th}/^{238}\text{U}^*$	$\pm 2\sigma$ (%)	$^{234}\text{U}/^{238}\text{U}^*$	$\pm 2\sigma$ (%)	ρ_{08-48}	$\delta^{234}\text{U}_{\text{init}}$	$\pm 2\sigma$ (abs)	Age (ka, BP)	$\pm 2\sigma$ (abs)
TM 3	1.1	1.08	4.1	± 2.0	1.4900	± 14.3	1.243	± 15.8	0.54			>500	
TM 6	1.50	0.24	17.8	± 1.8	0.9149	± 2.5	1.020	± 2.2	0.49	1.0400	± 0.04	242.0	± 23.7
TM 8	1.28	0.55	8.6	± 1.8	1.2390	± 5.5	1.160	± 5.8	0.05			>500	
FEZZ/04/64/4	5.40	2.21	7.6	± 1.4	1.0260	± 6.2	0.998	± 6.3	0.50			>500	
FEZZ/04/64/5	0.51	0.90	1.3	± 1.7	0.4898	± 106.4	0.990	± 46.9	0.45	0.9870	± 0.57	74.4	± 101.6
FEZZ/04/64/6	3.25	1.38	7.0	± 2.5	0.9847	± 6.7	0.993	± 6.6	0.50	0.9670	± 0.44	>500	

Notes: * activity ratios corrected for detrital Th using average continental detritus U/Th and Th isotope composition; ** Age in ka (detrital Th-corrected), BP relative to 2016 AD; italics indicate activity ratios. Ages calculated using the decay constants of Cheng et al. (2013)

Supplementary Table S2. Solution-mode U-Th data summary. Corrections for detritus contributions assumed an average continental U and Th composition ($[\text{Th}/^{238}\text{U}] = 1.2 \pm 50\%$, $[\text{Th}/^{232}\text{U}] = 1 \pm 50\%$, and $[\text{U}/^{238}\text{U}] = 1 \pm 50\%$). For the samples that passed screening for detritus, and the estimated ages. All samples are from the carbonate bed in the Stromatolite Mbr. FEZZ/04/64/4- 6 samples from 26, 30, 51.1N; 16,29, 58.2E.

3.4 Solution-mode U-Th chronology

Six samples with the lowest content of silicate detritus from the TS2 and TS3 sections were analysed for U-Th, to further investigate the carbonate isotope systematics. The samples were subjected to total dissolution using a mixture of concentrated HNO₃-HClO₄-HF and U and Th separated by anion ion exchange chemistry. U and Th isotope data were obtained on a Neptune Plus multicollector ICP-MS. These analytical protocols are described in detail by Douarin et al. (2013). The U and Th decay constants of Cheng et al. (2013) were used in all activity ratio and age calculations. Raw data were processed using the Isoplot add-in (Ludwig, 2013) and in-house reduction engines employing Excel and Matlab.

3.5 U-series results

The best samples in terms of relatively low Si-detritus content were assessed for U-Pb by both laser ablation ICP-MS, and analysed for U-Th by solution-mode ICP-MS. However, the fairly homogeneous distribution and abundance of Si-detritus relative to host carbonate, indicated these samples were unsuitable for U-Th chronology (SD Fig. S9). This is since isochron methods only help where a large spread in the relative proportions of silicate detritus and carbonate occurs in the samples.

Sample TM3 is the worst case and is far enough to the right of the secular equilibrium age contour to suggest significant open-system U-Th behaviour (SD Fig. S9). Th is relatively immobile but in oxidizing environments uranium is very mobile and recrystallisation or major disturbance of the carbonate at any time can cause uranium to be redistributed. Uranium loss would explain the measured isotope composition of TM3. TM8 and FEZZ/04/64/5 and FEZZ/04/64/7 also plot slightly in the forbidden zone, albeit sufficiently close to the secular equilibrium isotope composition so as to indicate only limited open-system behaviour or a slight inaccuracy in the Th isotope composition assumed for the detritus that is used to correct the raw isotope data. If the latter is the case then these samples record closed systems that are at least 500 ka old. Two analyses plot in the permissible zone for closed isotope systems (SD Fig. S9). TM6 had the highest [²³⁰Th/²³²Th] of all the samples and yielded an age of 242 ± 24 ka (SD Table S2). The validity of this age would depend upon it being in correct stratigraphic order relative to TM8 (which it is not). Sample TM3 plots so far into the forbidden zone (not shown) that it can be dismissed from consideration when interpreting the significance of the data for the other two TM samples. The other sample in the permissible zone is FEZZ/04/64/5 which has such a low [²³⁰Th/²³²Th] as to render corrected isotope ratios and calculated “age” highly suspect given that the other FEZZ samples suggest true ages >500 ka. Given that open system behaviour is possible in some of these samples, the same may apply here and this young “age” could easily be accounted for by uranium influx.

Given the general unsuitability of the rocks that were analysed, and those that were eliminated during the initial screening, we can say emphatically that they are unsuited to U-Th analysis. The chronology of these rocks needs to be investigated with other methods, unless much cleaner carbonates can be found.

4. Details of the sequence slotting and age models

A graphical expression of the two best fitting sequence slotting correlations is shown in SD Fig. S10, for the two magnetostratigraphic composites A and B. In a visual sense, it is clear that both the Serravallian correlation models show a better match to the GPTS, particularly for the interval younger than chron C6. The Tortonian correlation models tend to show a poor match over the chron interval C5AD to C5A.

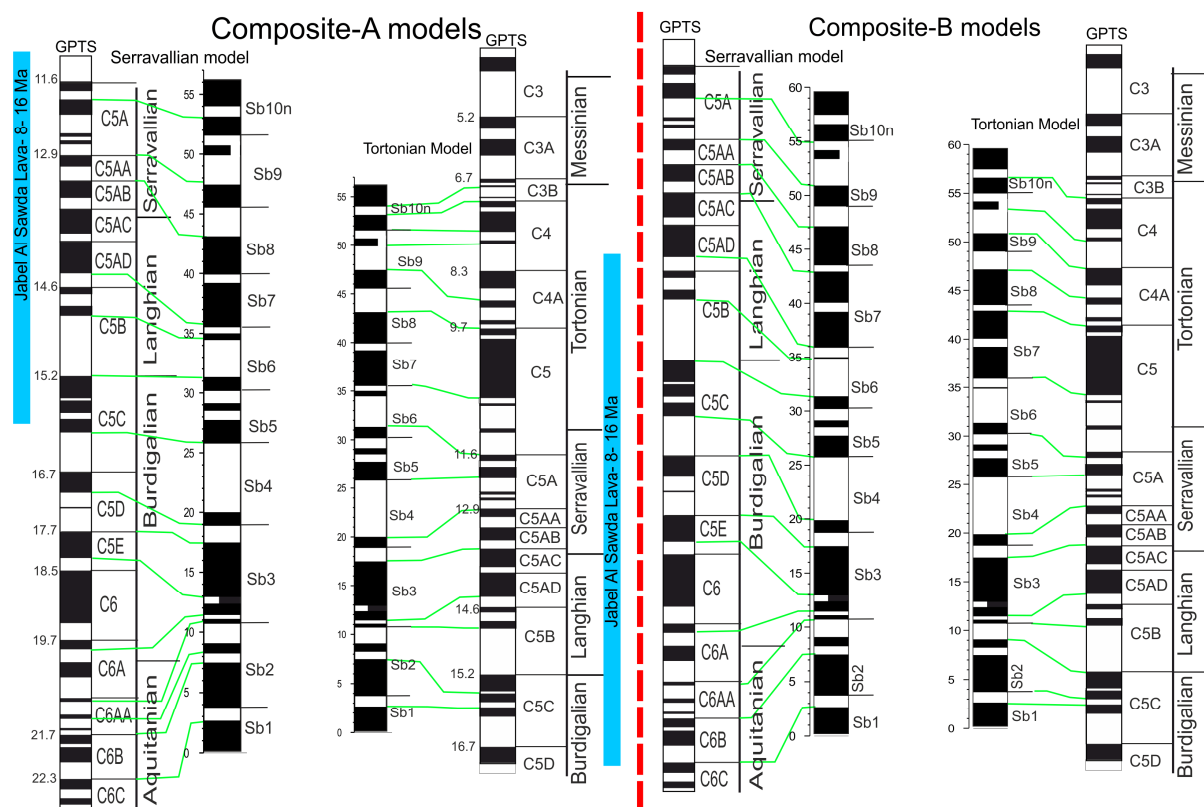


Fig. S10. The two composite magnetic polarity sections (A and B models on left and right). For each composite model the two most likely correlations to either of the intervals is shown which begin in the Serravallian and the latest Tortonian. Correlation lines shown in green derived from the sequence slotting.

Since the sequence slotting does not 'know' that normal polarity should correlate with normal polarity, we force it into this, by weighting the polarity variable (set at either -1 or +1 value) with a value of 5 times the base value of 1.

The alternative correlation models can clearly be seen in the H-matrix plots (SD Figs. S11b, S11b), by the brighter bands inclined down to the right across the plot. The values shown on the H-matrix plots are the ratio of the constrained path (i.e. as the matched composite polarity data is incrementally slid past the GPTS) relative to the (optimum) minimum CPL, with brighter values indicating path-length values near the CPL optimum (Gordon et al 1988). These give a visual clue to the search paths (i.e. somewhat similar to similarity matrix plots in Gary et al., 2005) sought by the sequence slotting, which in a simple sense find the path with the 'brightest response' through this matrix.

The Oligocene correlation model (Composite B, SD Fig. S12a) actually gives the lowest Δ value, only marginally lower than the composite B Serravallian model. This is also the case for the N-CSTAT value. However, the high degree of inter-chron variability in the parameters (see description of Δ value in SD Table S3) makes these slotting parameters less useful for considering the best overall fit. In terms of the RV association parameters, and the individual parameter correlations (i.e. Spearman R_s , SD Fig. S12a) between matched chrons and magnetozone, the Oligocene age model is the worst fitting (SD Fig. S12a).

The key output from the sequence slotting procedures is given in separate pages in the Excel spreadsheet with this SD, where the age models discussed are shown. The source data for the sequence slotting (GPTS, composites A and B) are in the additional zip file with this SD. The zip file also contains the Windows CPLSlot program, with examples of how to use the program and a Windows help file (extension .hlp). Additional information about this is in a text file in the zip file. Updates of the CPLSlot program may be available on Mark Hounslow web page.

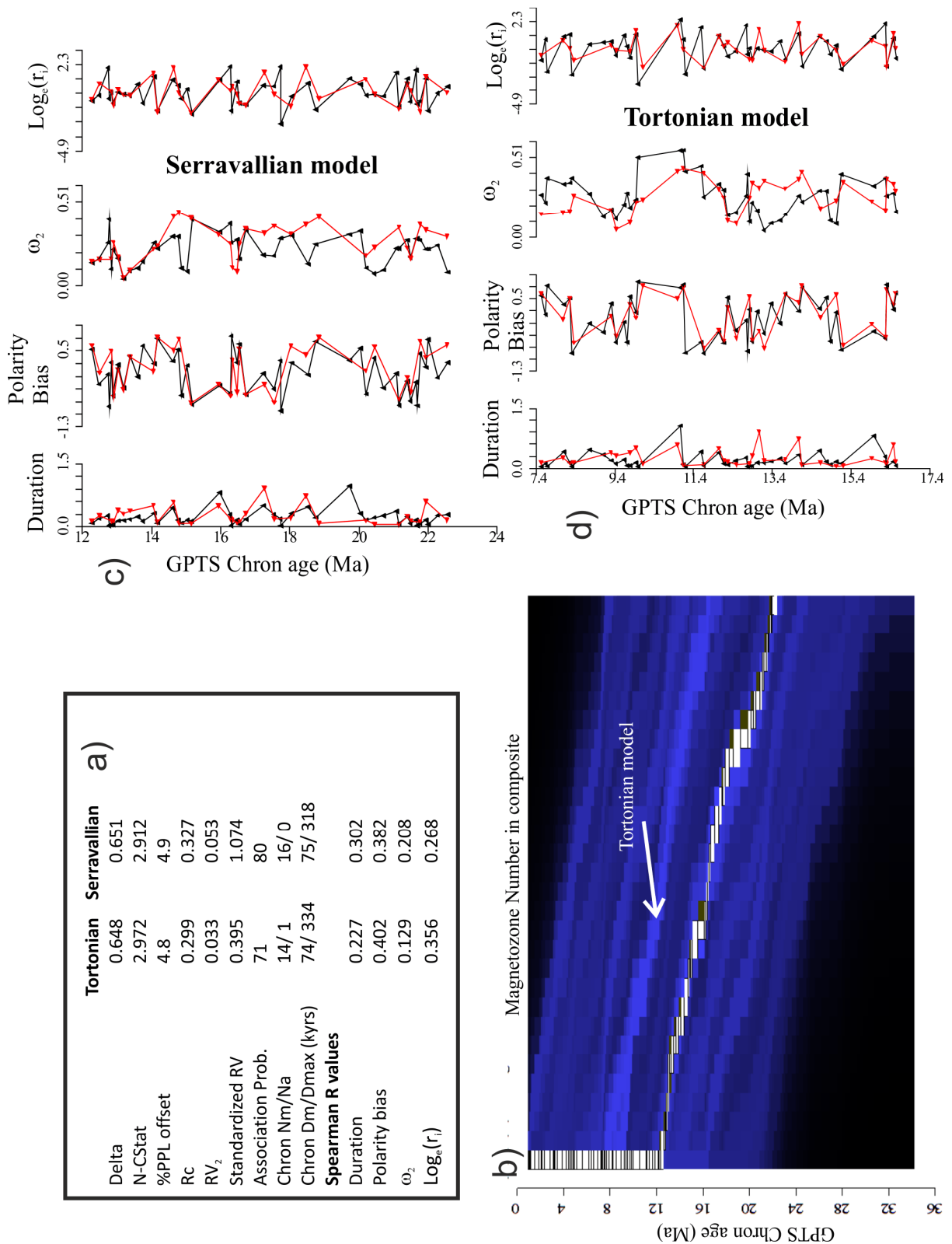


Fig. S11. Sequence slotting model output for the magnetic polarity composite-A, shown on the left panel in SD Fig. S10. a) the statistical summary of the Tortonian and Serravallian correlation models (see SD Table S3 for parameter description). b) The H-matrix plot, where the brighter blue bands correspond to alternative correlation models. The mostly likely model (ending in Serravallian) is shown as the white boxes across the plot, with y-axis height (of the boxes) corresponding to GPTS chron duration. The band corresponding to the Tortonian model is arrowed. The x-axis on this plot is the magnetozone number. Green boxes indicate alternative 'slots' the same as the optimum. c) and d) The input data to the slotting model, plotted against chron age for the two correlation options (shown in left panel in Fig. 10), derived from the sequence slotting. GPTS chron data in red, section data in black. Parameters described in SD Table S3.

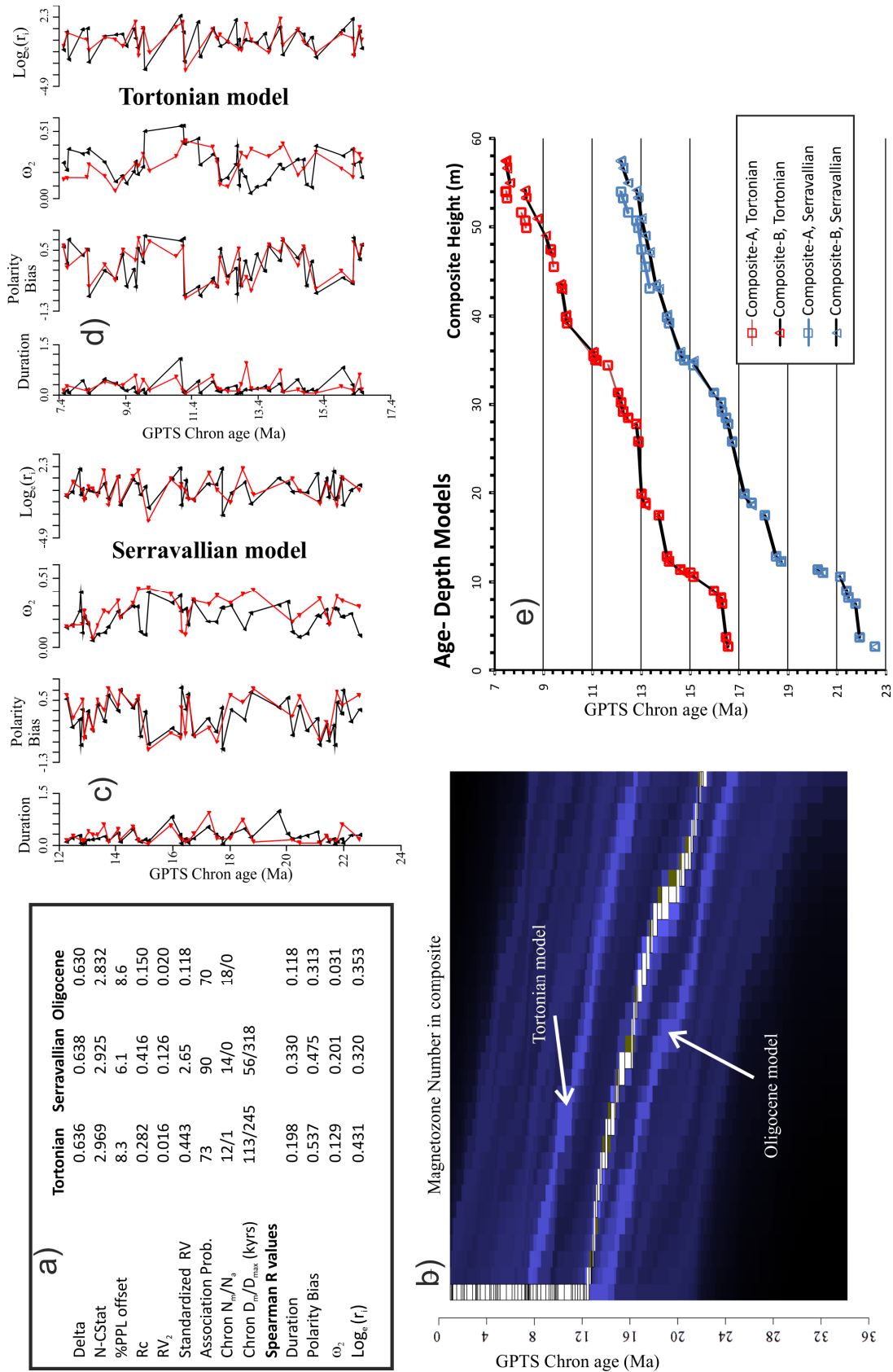


Fig. S12. Sequence slotting model output for the magnetic polarity composite-B (right panel in SD Fig. S10), showing data for the three mostly likely correlation models. a) to d) details as in SD Fig. S11 (parameters shown in A) detailed in SD Table S3). e) Depth-age models for the two polarity composites A and B, and the Tortonian and Serravallian age models. The age-depth relationships for the two age models are similar for composite A and B apart from the upper part of the composite sections. Parameters described in SD Table S3.

Statistic	Description and comments
Delta (Δ)	$\Delta = (2 * \min(\text{CPL})) / (\text{APL} + \text{BPL}) - 1$ where CPL is the combined path length, or the total discordance between the start and end of the matched points (in multivariate space) when slotted together. APL is the individual path length through the GPTS chrons, and BPL is the individual path length through the matched data. The value of the CPL is controlled by the type of scaling and distance measure used, since this will control the magnitude of the discordance measured by CPL (see Thompson and Clark, 1989). The best slotting model of the many considered for each slotting run is that with the minimum CPL (hence $\min(\text{CPL})$), where the <i>min</i> indicates the search criteria. Δ is a goodness of match statistic independent of the chosen distance measure and the units of measurements used, and measures of the 'local-fit' of the two sequences. If correctly scaled, Δ generally lies between zero and somewhere around 1.0; a small value of Δ (less than ca. 0.5) indicates that Sequences A and B are interleaved or slotted together very well (Thompson and Clark, 1989; Thompson et al., 2012). Generally the Δ value expresses the goodness of fit well with datasets which have a low degree of inter-level variability (i.e. smoothly varying wiggles). In contrast, the parameterisation of the GPTS tends to give high variability between the chrons, since chron durations have a near random distribution (Lowrie and Kent, 2004).
N-CSTAT	The normalised CSTAT. A measure of the robustness of the fit, base on a sensitivity analysis (Gordon et al., 1988). Generally smaller N-CSTAT values are associated with better, more robust slotting. The CSTAT value is a sensitivity statistic, which is the reduction in the CPL when a particular chron in the GPTS is omitted (i.e. a test of the sensitivity of the model to missing chrons in the GPTS). i.e. each GPTS chron has a CSTAT value. The N-CSTAT value is the average CSTAT value divided by the average PPL.
%PPL offset	The PPL is the partial path length, or the discordance between adjacent points or (path length of sub-segments of the total CPL). %PPL is simply the sum of the absolute discordance between those matched chrons and magnetozones in the GPTS and matching sequence, expressed as a percentage of the CPL. Better match's should have lower %PPL in any set of slotted models. The Serravallian model for composite B has the lowest %PPL value, whereas for the polarity composite A the two age models have similar values.
R_c	The congruence coefficient a measure of the similarity (or association) of the two datasets. It measures the similarity of two configurations by computing a cosine between matrices of observations. R_c has a range like regression coefficients (i.e. up to +1 for positive association), but is not a regression coefficient (see Abdi, 2010). The largest R_c value is the Serravallian age model for composite B. Broadbooks and Elmore (1987) provide a method to test if R_c is significantly different from zero.
RV_2	The RV coefficient is a measure of the similarity (or association) of the two datasets. It is a matrix correlation coefficient. It corresponds to a squared cosine and therefore the RV coefficient takes values between 0 and 1 (Abdi, 2010). The RV_2 coefficient is a modification of the RV coefficient (taking values -1 to +1) according to Smilde et al. (2009) and is a more robust measure of common information contained in the two datasets. The largest RV_2 value is from the Serravallian age model for composite B.

RV _{std}	This is the standardized RV coefficient of Josse et al. (2008) (and Z _{RV} statistic of Abdi 2007) which allows an approximate evaluation if the RV coefficient is significantly different from zero. Values of RV _{std} >1.65 suggest the RV value reflects a significant association between the two datasets. However, the tests in Josse et al. (2008) suggest RV _{std} should be >~2 for an approximate 95% confidence value. Only the Serravallian age model for composite B has RV _{std} >1.65 (SD Fig. S12a).
Association probability, P _a	This is derived from the log-transformed Z statistic in Josse et al. (2008), which is tested against a standard normal distribution (SD Figs. S10a, S12a). This approximation evaluates the probability (p=1-P _a) that the RV coefficient is significantly different from zero. i.e. Larger values of the association probability, P _a indicate a better match between the datasets. The Serravallian age model for composite B has the largest P _a value (SD Fig. S12a). RV _{std} and P _a do not indicate the 'significance of the match', but only the probability of some association between the datasets.
N _m /N _a	N _m = number of chrons missing from the GPTS in the magnetostratigraphic match. N _a = number of additional magnetozone in the matched succession not present in the GPTS. These numbers should be at a minimum for a good match, but will depend on the sampling rate of the GPTS. N _a values >=1 imply spurious magnetozones in the section not present in the GPTS. Both of the Tortonian models have spurious magnetozones present in C5An (SD Fig. S10).
D _m /D _{max}	D _m = mean duration (in kyrs) of chrons missing from the GPTS in the match. D _{max} = duration of longest chron missing from the GPTS in the match (in kyrs). These give an idea of the missing time represented in the match. The longest chron missing is C6r for the Serravallian models, and C4An or C5ABn for the Tortonian models.
Spearman coefficients (R _s)	These are the rank correlation coefficients between the values of the two dataset of the duration, polarity bias, ω ₂ and Log _e (r _i) used in the sequence slotting procedure (using the correlation model given by the sequence slotting). Clearly larger values of R _s would be expected for better matches. The R _s allows a comparison of which are the stronger control variables in the matching process. In this case, for both composite models the polarity bias, and Log _e (r _i) seem to be generally stronger than duration and ω ₂ (SD Figs. S11a, S12a). This can be seen by inspecting the dataset co-plots with GPTS age in SD Fig. S11c,d and SD Fig. S12c,d.
Polarity Bias parameter	For chron/magnetozone i, the polarity bias= $\sum_{j=i-1}^{j=i+1} d_j p_j / \sum_{j=i-1}^{j=i+1} d_j$, where d _j is the duration of the chron or magnetozone, and p _j is the polarity (values -1 or +1) of the chron or magnetozone. It ranges from intervals in which reverse polarity dominates (bias <-0.5) to intervals in which normal polarity dominates (bias >+0.5).
Shearmans spacing statistic ω ₂	$\omega_2 = \frac{0.5 * \sum_{j=i-1}^{j=i+1} abs(\bar{d} - d_j)}{\sum_{j=i-1}^{j=i+1} d_j}$, where d _j is the chron or magnetozone duration, and \bar{d} is the mean duration in the interval i-1 to i+1 (see Olson et al., 2014). i.e. ω is a measure of how much the durations deviate from their average length.

Supplementary Table S3. Explanation of statistics derived from sequence slotting, and parameters used in the sequence slotting and shown in SD Figs. S11 and S12.

References

- Abdi, H., 2007. RV coefficient and Congruence coefficient. In: Salkind, N. (Ed.), *Encyclopaedia of measurement and statistics*. Thousand Oaks, CA, Sage, pp. 850-856.
- Abdi, H., 2010. Congruence: Congruence coefficient, RV -coefficient, and Mantel coefficient. In: Salkind, N. (Ed.), *Encyclopaedia of Research Design*. Thousand Oaks, CA, Sage, pp. 223-230.
- Abdullah, M., 2010. Petrography and Facies of the Al- Mahruqah Formation in the Murzuq Basin, SW Libya. (PhD. Thesis), Universität Hamburg.
- Ade-Hall, J. M., Reynolds, P. H., Dagley, P., Mussett, A. E., Hubbard, T. P., 1975. Geophysical studies of North African Cenozoic volcanic areas: II. Jebel Soda, Libya. *Canadian Journal of Earth Sciences*, 12, 1257-1263.
- Armitage, S.J., Drake, N.A., Stokes, S., El-Hawat, A., Salem, M.J., White, K., Turner, P., McLaren, S.J., 2007 Multiple phases of North African humidity recorded in lacustrine sediments from the Fezzan Basin, Libyan Sahara. *Quaternary Geochronology*, 2, 181–186.
- Berendeyev, N.S., 1985. Geological map of Libya 1:250,000, Sheet: Hamadat Tanghirt (NH 32-16) Explanatory Booklet. Industrial Research Centre, Tripoli.
- Broadbooks, W. J., Elmore, P. B., 1987. A Monte Carlo study of the sampling distribution of the congruence coefficient. *Educational and Psychological Measurement* 47, 1–11.
- Bown, T. M., 1982. Ichnofossils and rhizoliths of the nearshore fluvial Jebel Qatrani Formation (Oligocene), Fayum Province, Egypt. *Palaeogeography, Palaeoclimatology, Palaeoecology*, 40, 255-309.
- Brooks, N., Drake, N., McLaren, S.J., White, K., 2003. Studies in Geography, Geomorphology, Environment and Climate. In: Mattingly, D.J., Dore, J., Wilson, A.I. (Eds.), *The Archaeology of Fazzan: Synthesis*, Society for Libyan Studies, London, pp. 37–74.
- Cheng, H., Edwards, R.L., Shen, C.-C., Polyak, V.J., Asmerom, Y., Woodhead, J., Hellstrom, J., Wang, Y., Kong, X., Spötl, C., Wang, X., Alexander, E.C. Jr., 2013. Improvements in ^{230}Th dating, ^{230}Th and ^{234}U half-life values, and U-Th isotopic measurements by multi-collector inductively coupled plasma mass spectrometry. *Earth and Planetary Science Letters*, 371-372, 82-91.
- Collomb, G.R., 1962. E`tude geologique du Jabal Fezzan et de sa bordure Paléozoïque. *Notes Mémoires, Compagnie Française des Pétroles*, 1, pp. 35-36.
- Desio, A., 1971. Outlines and problems of the geomorphological evolution of Libya from the Tertiary to the present day. In: Gray, C. (Ed.), *1st symposium on the geology of Libya*. Fac. Sci. Univ. Libya, Tripoli, pp. 11-37.
- Drake, N.A., Wilson, A., Pelling, R., White, K.H., Mattingly, D., Black, S. 2004 Water Table Decline, Springline Desiccation and the Early Development of Irrigated Agriculture in the Wādī al-Ajāl , Libyan Fazzan. *Libyan Studies*, 35, 95-112.
- Drake, N.A, White, K. McLaren, S., 2006. Quaternary climate change in the Germa region of the Fezzan, Libya. In: Mattingly, D., McLaren, S.J., Savage, E. al-Fasatwi, Y., Gadgood, K. (Eds.), *The Libyan desert: nature resources and cultural heritage*. Society for Libyan Studies, pp. 133-144.
- Drake , N.A, El-Hawat, A.S., Turner, P., Armitage, S.J., Salem, M.J., White, K.H., McLaren, S.J., 2008. Palaeohydrology of the Fezzan Basin and surrounding regions: the last 7 million years. *Palaeogeography, Palaeoclimatology, Palaeoecology*, 263, 131-145.
- Douarin, M., Elliot, M., Noble, S.R., Sinclair, D., Henry, L.-A., Long, D., Moreton, S.G., Roberts, J.M., 2013. Growth of north-east Atlantic cold-water coral reefs and mounds during the Holocene: A high resolution U-series and ^{14}C chronology. *Earth and Planetary Science Letters*, 375, 176-187.
- Gary, A.C, Johnson, G.W. Ekart, D.D., Platon E., Wakefield, M.I., 2005. A method for two-well correlation using multivariate biostratigraphical data. In: Powell, A. J., Riding, J.

- B. (Eds.), *Recent Developments in Applied Biostratigraphy*. The Micropalaeontological Society, Special Publications, pp. 205–217.
- Geyh, M.A., Thiedig, F., 2008. The Middle Pleistocene Al Mahruqah Formation in the Murzuq Basin, northern Sahara, Libya evidence for orbitally-forced humid episodes during the last 500,000 years. *Palaeogeography, Palaeoclimatology, Palaeoecology*, 257, 1-21.
- Gordon, A.D., Clark, R.M. Thompson, R., 1988. The use of constraints in sequence slotting. In: Diday, E. (Ed.), *Data analysis and informatics*, V. North Holland Publishing, Amsterdam, pp. 353-364.
- Goudarzi, G.H., 1970. *Geology and mineral resources of Libya — a reconnaissance*. U.S. Geological Survey Professional Paper, 660, 104p
- Gundobin, V.M., 1985. Geological map of Libya 1:250,000, Sheet: Qararat al Marar (NH 33-13) Explanatory Booklet. Industrial Research Centre, Tripoli.
- Horstwood, M.S.A., Foster, G.L., Parrish, R.R., Noble, S.R., Nowell, G.M., 2003. Common-Pb corrected in situ U-Pb accessory mineral geochronology by LA-MC-ICP-MS. *Journal of Analytical Atomic Spectrometry*, 18, 837-846.
- Koráb, T., 1984. Geological Map of Libya 1: 250 000. Sheet: Tmassah NG 33-7. Explanatory Booklet. Industrial Research Centre, Tripoli.
- Lowrie, W., Kent, D.V., 2004. Geomagnetic polarity timescales and reversal frequency regimes, In: Channell, J.E.T., Kent, D.V., Lowrie, W., Meert, J. (Eds.), *Timescales of the palaeomagnetic field*, America Geophysical Union, pp. 117-129.
- Ludwig, K.R., 2012. *Isoplot 3.75: A geochronology toolkit for Microsoft Excel*, Berkeley Geochronology Center Special Publication 5, 75p.
- Parizek, A., Klen, L., Rohlich, P., 1984 Geological map of Libya 1:250,000, Sheet: Idri (NG 33-1) Explanatory Booklet. Industrial Research Centre, Tripoli.
- Petit-Maire, N., Delibrias, G., Gaven, C., 1980. Pleistocene lakes in the Shati area, Fezzan (27, 30°N). *Palaeoecology of Africa*, 12, 289-295.
- Josse, J. Pages, J., Husson, F., 2008. Testing the significance of the RV Coefficient. *Computational Statistics and Data Analysis*, 53, 82-91.
- Olson, P., Hinnov, L., Driscoll, P., 2014. Nonrandom geomagnetic reversal times and geodynamo evolution. *Earth Planetary Science Letters*, 388, 9–17.
- Roberts, N.M.W., Walker, R.J., 2016. U-Pb geochronology of calcite-mineralized faults: Absolute timing of rift-related fault events on the northeast Atlantic margin. *Geology* (published on-line June 2016, DOI: 10.1130/G37868.1).
- Roncevic, N.S., 1984. Geological map of Libya 1:250,000, Sheet: Hasi Anjiwal (NG 32-4) Explanatory Booklet. Industrial Research Centre, Tripoli.
- Seidl, K., Röhlich, P., 1984. Geological map of Libya, 1: 250 000. Sheet Sabhá (NG 33-2), Explanatory Booklet, Industrial Research Centre, Tripoli.
- Schultz A., Soffel H.C., 1973 Paleomagnetism of Tertiary basalts from Libya. *Geophysical Journal of the Royal Astronomical Society*, 32, 373–380.
- Smilde, A. K., Kiers, H.A.L., Bijlsma S., Rubingh C.M., van Erk, M.J., 2009. Matrix correlations for high-dimensional data: the modified RV-coefficient. *Bioinformatics*, 25, 401–405.
- Thiedig, F.M., Oezen, D., El-Chair, M., Geyh, M.A., 2000. The absolute age of the Quaternary lacustrine limestone of the Al Mahruqah Formation - Murzuq Basin, Libya. In: Sola, M.A., Worsley, D. (Eds.), *Geological Exploration in the Murzuq Basin*. Elsevier, Amsterdam, pp. 89–116.
- Thompson, R., Clark, R.M., 1989. Sequence slotting for stratigraphic correlation between cores: theory and practice. *Journal of Paleolimnology*, 2, 173–184.
- Thompson, R., Clark, R.M., Boulton, G.S., 2012. Core correlation. In: Birks, H.J.B., Lotter, A.F. Juggins, S., Smol, J.P. (Eds.), *Tracking Environmental Change Using Lake Sediments: Data Handling and Numerical Techniques*, *Developments in Paleoenvironmental Research*, Vol. 5, pp. 415–430.
- Torsvik, T. H., Van der Voo, R., Preeden, U., Mac Niocaill, C., Steinberger, B., Doubrovine, P. V., van Hinsbergen D.J.J., Domeiere, M., Gaina, C., Tohver, E. , Meert, J.G.,

- McCausland, P. J.A., Cocks, L. R. M., 2012. Phanerozoic polar wander, palaeogeography and dynamics. *Earth-Science Reviews*, 114, 325-368.
- White, K., McLaren, S., Black, S., Parker, A., 2000. Evaporite minerals and organic horizons in sedimentary sequences in the Libyan Fezzan: implications for palaeoenvironmental reconstruction. In: McLaren, S.J., Kniveton, D.R. (Eds.), *Linking Climate Change to Land Surface Change*. Kluwer Academic Press, Amsterdam, pp. 193–208.
- White, K., Charlton, M., Drake, N., McLaren, S., Mattingly, D., Brooks, N., 2006. Lakes of the Edeyen Awbari and the Wadi al-Hayat. In: Mattingly, D., McLaren, S. J., Savage, E., al-Fasatwi, Y. & Gadgood, K. (Eds.), *The Libyan Desert, Natural Resources and Cultural Heritage*. The Society for Libyan Studies, London, pp. 123–130.
- Woller, F., 1984. Geological Map of Libya 1: 250 000. Sheet: Al Fuqaha (NG 33-3). Explanatory Booklet. Industrial Research Center, Tripoli.